Earth-Science Reviews 281 (2026) 105603

Contents lists available at ScienceDirect

Earth-Science Reviews

journal homepage: www.elsevier.com/locate/earscirev

Review Article

Occurrence and petrogenesis of diamondiferous lamprophyres: Insights into mantle metasomatism and diamond formation

Francesca Innocenzi [a,*], Maxwell C. Day [a], Fabrizio Nestola [a], Davide Novella [a], Mattia La Fortezza [a], Kristina Kublik [b], D. Graham Pearson [b], Martha G. Pamato [a]

[a] Dipartimento di Geoscienze, Università degli Studi di Padova, Via Gradenigo 6, 35131 Padova, Italy.
[b] Department of Earth & Atmospheric Sciences, University of Alberta, Edmonton, Alberta, Canada

ARTICLE INFO

Keywords:
Mantle metasomatism
Diamonds
Lamprophyres
Lamproites

ABSTRACT

Lamprophyres are a rare rock-type that include different lithologies, classified mineralogically (abundance of mica, amphibole, feldspathoids) rather than geochemically (enrichment in alkalis and volatiles). Despite the attention that these rocks have attracted, due to their possible economic interest, their sources, petrogenesis and classification remain a matter of debate. One of the most intriguing aspects is the relationship of some lamprophyre sub-types with diamonds, especially because diamondiferous lamprophyres are the rarest diamond-bearing rock-types. The reason for this association and their potential genetic relationship remain poorly understood. Previous studies on lamprophyres (diamond-bearing and barren) are reviewed to improve our knowledge of peculiar mantle paragenesis, fertilization events, metasomatic agents and the relationship between lamprophyres and diamonds. *Calc-alkaline lamprophyres* (CALs) are often emplaced in subduction-related settings, where slab dehydration and crustal recycling can stabilize hydrous phases (amphibole/phlogopite). Low degree partial melting of shallow metasomatized sources may explain CALs petrogenesis. To reconcile this shallow formation depth with the presence of diamonds, we propose a lithospheric stacking model, that results in a highly transient geotherm during the initial phases of craton formation. *Ultramatic lamprophyres* (UMLs) mostly crop out along rifts and are related to a veined lithospheric and/or asthenospheric source. A direct genetic link between diamonds and UMLs can be excluded. Instead, the presence of diamondiferous UMLs relies on spatial and temporal connections (e.g., mantle domains enriched in C-H-phases). Lamprophyric melts are hostile for diamonds, due to their high fO_2, H_2O and CO_2, along with a longer lag time and a lower volume of emplaced magma.

Contents

1. . Introduction 1
1.1. Linking the source of lamprophyres with mantle metasomatism 2
1.2. Mantle xenoliths and xenocrysts 2
2. Classification and nomenclature of diamond-bearing magmatic rocks 3
3. Diamondiferous lamprophyres 6
3.1. Australia 6
3.1.1. Petrographic and geochemical data 6
3.1.2. Diamonds 8
3.2. Greenland 8
3.2.1. Petrographic and geochemical data 9
3.2.2. Diamonds 9
3.3. Japan 9
3.3.1. Petrographic and geochemical data 9

* Corresponding author at: Dipartimento di Geoscienze, Università degli Studi di Padova, Via Gradenigo 6, 35131 Padova, Italy.
E-mail address: francesca.innocenzi@unipd.it (F. Innocenzi).

https://doi.org/10.1016/j.earscirev.2026.105603
Received 9 December 2025; Received in revised form 24 June 2026; Accepted 26 June 2026
Available online 29 June 2026
0012-8252/© 2026 The Author(s). Published by Elsevier B.V. This is an open access article under the CC BY license (http://creativecommons.org/licenses/by/4.0/).

3.4. India . . . 10
3.4.1. Petrographic and geochemical data . . . 11
3.4.2. Diamonds . . . 11
3.5. North America . . . 11
3.5.1. Petrographic and geochemical data . . . 13
3.5.2. Diamonds . . . 13
3.6. South America . . . 14
3.6.1. Petrographic and geochemical data . . . 14
3.6.2. Diamonds . . . 14
4. Discussion . . . 14
4.1. Constraints on CAL petrogenesis . . . 14
4.1.1. Constraints from mantle xenoliths in CALs . . . 15
4.2. Implications for diamond genesis and CAL formation . . . 15
4.2.1. Insights from Fourier-Transform infrared (FTIR) spectroscopy . . . 16
4.3. The diamond-CALs connection . . . 18
4.4. Constraints on aillikites petrogenesis . . . 18
4.4.1. Constraints from mantle xenoliths in aillikites . . . 19
4.4.2. Petrogenetic constraints from similar UMLs (alnöite) . . . 19
4.4.3. Implications for diamond genesis and aillikite formation . . . 19
4.5. The kimberlite-aillikite connection . . . 20
4.6. The diamond-aillikites association . . . 20
5. Conclusions . . . 22
Declaration of competing interest . . . 23
Acknowledgements . . . 23
Supplementary data . . . 23
Data availability . . . 23
References . . . 23

1. . Introduction

There are three principal volcanic host-rocks for natural diamonds: kimberlites, lamproites and lamprophyres. Kimberlites are ultramafic, silica-poor and CO_2-rich rocks and, by far, are the most abundant and commonly mined diamondiferous rock-type (Kjarsgaard et al., 2022; Giuliani et al., 2024), followed by olivine lamproites (i.e., ultrapotassic, peralkaline and ultramafic rocks, with low CaO; Mitchell, 2020).

The term lamprophyre was coined by Gumbel (1874) to describe some dikes cropping out in Germany, characterized by large phenocrysts of brown mica. A fundamental contribution to the understanding of lamprophyres was made by Nickolas Rock, who published many works focused on the origin of such rocks (e.g., Rock, 1984, 1986, 1987, 1990). Initially, in 1977, Rock stated that '*lamprophyres lack any coherent terminological framework at present: there are agreed definitions neither of the term lamprophyre itself, nor of its varieties; the genetic connotations of lamprophyre names also remain contentious*'. In an effort to resolve such ambiguities, Rock conducted follow-up work, first on alkaline lamprophyres (e.g., Rock, 1979), then on calc-alkaline lamprophyres (e.g., Rock, 1984). The term "ultramafic lamprophyre" was later proposed by Rock in 1986, to group together hypabyssal products, characterized by low silica and high MgO, CaO, K_2O and trace element contents. This group described rocks previously termed *melilitic lamprophyres* (proposed by Streckeisen, 1979) which did not consider the carbonate-bearing compositions that lack melilite (i.e., aillikites and polzenites) and that could not be classified using the Streckeisen diagram (Rock, 1986). As first pointed out by Rock in 1986, many ultramafic lamprophyres have been erroneously classified as kimberlite, leading to a paucity of literature data for such rocks. Finally, based on previous works, he proposed the first classification scheme for lamprophyres (Rock, 1987).

For many years, lamprophyres, kimberlites and lamproites were grouped together in the "lamprophyre clan" (e.g., Rock, 1987), until Mitchell (1994) highlighted how, even if all these rock-types are characterized by similar volatile-rich magmas, their petrological evolution may differ significantly. In the current IUGS classification (Le Maitre, 2002), lamprophyres are differentiated from kimberlites and lamproites, but this classification has been strongly criticised as it does not include ultramafic lamprophyres (e.g., Tappe et al., 2005; Ulrych et al., 2011). Moreover, melilite-bearing ultramafic lamprophyres (i.e., polzenite and alnöite) are recommended to be classified following the rules applied to other melilite-bearing rocks, increasing the potential for contradictory and ambiguous classification.

Overall, lamprophyres are generally defined as primary-exotic rocks which represent <1% of igneous products on Earth (e.g., Rock, 1986, 1987, 1991; Mitchell, 1994; Tappe et al., 2005). Lamprophyres are characterized by extreme mineralogical and geochemical variability. Typically, lamprophyres have mafic to ultramafic compositions, enriched in alkalis and volatiles (both H_2O and CO_2), and have highly variable silica contents (e.g., Le Maitre, 2002). Lamprophyres should also contain phenocrysts of hydrous mafic silicates (mica and/or amphibole), and feldspar and feldspathoids should be restricted to the groundmass (e.g., Rock, 1987; Le Maitre, 2002). These features are related to a metasomatised mantle, affected by crustal recycling and/or mantle plumes (e.g., Chalapathi Rao et al., 2020). However, the relationship between such processes and the generation of lamprophyric melts remains poorly constrained.

1.1. Linking the source of lamprophyres with mantle metasomatism

Despite the economic importance of lamprophyres, their petrogenesis and evolution are not well constrained, but are often related to variably metasomatised mantle paragenesis, such as carbonated peridotites or lithologies enriched in pyroxene ± phlogopite ± amphibole ± oxides ± apatite (e.g., Foley, 2008; Giuliani et al., 2024; Foley et al., 2025).

Mantle metasomatism was first described as '*alteration which involves enrichment of the rock by new substances brought in from the outside*' (Goldschmidt, 1922; O'Reilly and Griffin, 2013). Our understanding of metasomatic processes greatly improved when alkali-rich igneous products began to be attributed to metasomatic processes (e.g., Lloyd, 1981; Dawson, 1984) (Bailey, 1970, 1972; Irving, 1980; Foley, 1992; Ionov et al., 1993; Griffin et al., 1999). These magmas could not be reconciled with derivation from a *normal* lherzolitic mantle, whose

melting produces *normal* basaltic melts, and required a different enriched mantle source (e.g., Green, 1971; Frey et al., 1978; Davis et al., 2011).

Today, the term mantle metasomatism is used to describe a process that causes a change in the original mantle. Metasomatism can be: i) *modal*, if new phases crystallize; ii) *cryptic*, if there is a change in major or trace elements composition, without the crystallization of any new mineral; and iii) *stealth*, if new minerals form, but they cannot be distinguished from the 'normal' peridotitic mantle (e.g., O'Reilly and Griffin, 2013; Kiseeva et al., 2017). Metasomatic processes are still highly debated, but the recycling of crustal material is undoubtedly a fundamental requirement in the formation of fertile mantle reservoirs (Plank, 2014; Foley and Pintér, 2018). The assimilation of subducted crustal lithologies, together with the fluids released by the slab, can initiate refertilization processes and subsequently produce mantle reservoirs characterized by a strong enrichment in both incompatible elements and in particular isotopic values. Recycling of compositions similar to GloSS (Global Subducting Sediments) or eclogites, which are commonly interpreted as subducted oceanic crust, is often invoked as an important mantle metasomatic agent. Nonetheless, the resultant source-compositions of the different metasomatic processes and the exact composition of the metasomatic fluids and/or melts required to produce specific lithologies are not yet well-constrained (e.g., Roden and Murthy, 1985; Huang et al., 2014; Kiseeva et al., 2017). Moreover, eclogites are often invoked as a viable source of metasomatic fluids, but they can also be metasomatised, often leading to a confusing framework (e.g., Kiseeva et al., 2017).

A clear petrogenetic understanding of exotic igneous rocks is fundamental to constrain the composition and evolution of the lithospheric mantle and the processes that affect it. Studying diamond-bearing magmatic lithologies, such as lamproites and lamprophyres, is particularly important as they are often related to strongly metasomatized and carbonated mantle sources. Lamprophyres, in particular, are understudied when compared to kimberlites (e.g., Giuliani and Pearson, 2019; Giuliani et al., 2023, 2024) and lamproites (e.g., Mitchell and Bergman, 1991; Scott Smith et al., 2018; Mitchell, 2020). Moreover, numerous complexities regarding the description of lamprophyres have resulted in a confusing and complicated classification scheme (e.g., Tappe et al., 2005; Lustrino et al., 2020). Consequently, the extent of geological information that can be extracted from lamprophyres is not completely understood. In this review, we aim to clarify the lamprophyre classification scheme, highlighting several unsolved questions regarding their genesis. To achieve this, a complete petrographic and geochemical characterization of each lamprophyre type, together with detailed insights about their petrogenetic evolution, associated with different geological settings, is provided.

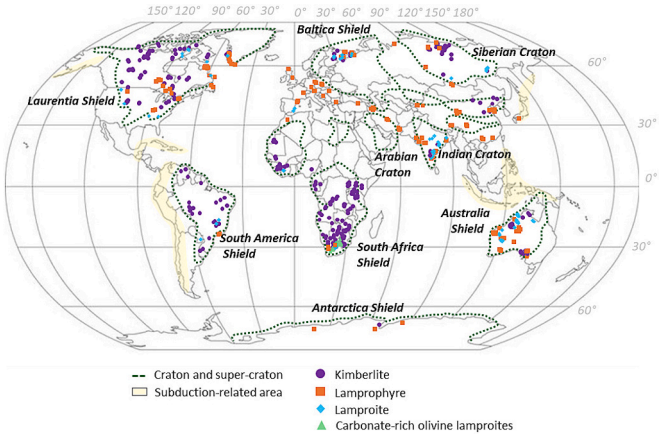


Fig. 1. Distribution of kimberlite, lamprophyre and lamproite occurrences. Different rock-type locations are from Giuliani et al. (2024) for kimberlite, olivine lamproites and carbonate-rich olivine lamproites (CROL). References for lamprophyres are reported in Supplementary Material 1. Cratons, supercratons and subduction related regions are from Pearson et al. (2021).

1.2. Mantle xenoliths and xenocrysts

Due to the inaccessibility of the continental lithospheric mantle, direct studies of the deeper regions of the Earth are based on: i) ophiolite sequences (e.g., Dilek, 2003; Dilek and Furnes, 2014; Bodinier and Godard, 2014; Hidas et al., 2021); ii) ultramafic massifs (e.g., in the Pyrenees and Betics, Downes, 2001); and iii) mantle xenoliths or xenocrysts (e.g., Nixon, 1987; Pearson et al., 2003). Even if most of the mantle xenoliths exhibit typical peridotitic compositions (olivine + clinopyroxene + orthopyroxene ± spinel ± garnet), in some cases less common minerals and parageneses have been observed, for example clinopyroxenite and glimmerite nodules (e.g., Lloyd, 1981; Pitcavage et al., 2021; Muravyeva and Senin, 2018; Innocenzi et al., 2024b), MARID, i.e., Mica + Amphibole + Rutile + Ilmenite + Diopside xenoliths (e.g., Fitzpayne et al., 2018), PIC, i.e., Phlogopite + Ilmenite + Clinopyroxene xenoliths (e.g., Fitzpayne et al., 2018) and eclogites (e.g., Jacob, 2004; Heaman et al., 2006). These samples have been a fundamental part of reconstructing the refertilization events, the metasomatic fluids and/or melts, and the metasomatic vein parageneses that characterize the lithospheric mantle.

One of the most useful types of mantle xenocrysts are diamonds, which form in the lithospheric mantle (120–200 km, at average conditions of 1160 °C and 5–6 GPa), or in the deeper sub-lithospheric mantle (300–800 km, at average conditions of 1200–1500 °C and 9–11 GPa; Day et al., 2023; Pearson et al., 2014). Diamonds provide crucial information about the Earth's mantle, as mineral and fluid inclusions can help to reconstruct different mantle paragenesis and associated thermobarometric conditions (e.g., Harris et al., 2022; Stachel et al., 2022; Rinaldi et al., 2023; Day et al., 2023; Curtolo et al., 2025). Diamonds also contain a variety of crystallographic point-defects (mainly nitrogen, hydrogen and boron) that provide information about the composition of

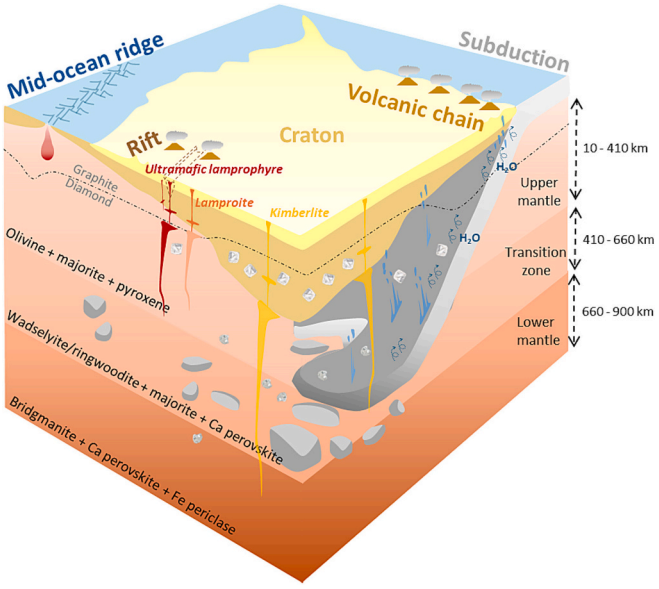


Fig. 2. Block diagram of different geodynamic environments: continental rift, craton and mantle keel, mid-ocean ridge, subduction system (with fluid release and mantle metasomatism, slab detachment and break off) and associated volcanic chain. Red upwelling melts represent ultramafic lamprophyres, yellow melts represent kimberlite while orange melts represent lamproites. Modified after Stachel and Harris (2008), Tappert and Tappert (2011), Zheng (2019) and Timmerman et al. (2023). (For interpretation of the references to colour in this figure legend, the reader is referred to the web version of this article.)

diamond-forming media (e.g., Regier et al., 2023), and about the residence time and temperature in the mantle (e.g., Harris et al., 2022; Nimis, 2022; Stachel et al., 2022; Day et al., 2023, 2024, 2025).

Diamonds are transported to the surface by different types of magma, but kimberlites are the principal diamond-bearing rock-type. Approximately 3500 kimberlite occurrences have been reported worldwide, and diamond exploration works have revealed the presence of ~3000 additional occurrences (Faure, 2010; Giuliani and Pearson, 2019). Diamonds have been identified in about one third of the known deposits (Faure, 2010; Giuliani and Pearson, 2019), though only a small number of deposits become economic mines.

Although diamond-kimberlite mines have been active since 1869 (Jagersfontein and Koffiefontein in South Africa, Kjarsgaard et al., 2022), it was only in 1976 that olivine lamproites were discovered to be diamondiferous, with the identification of diamonds in the Ellendale field (East Kimberly area, Western Australia; Atkinson et al., 1984; Jaques et al., 1986b). The Argyle olivine lamproite pipe represents the largest magmatic deposit for diamonds on Earth (Olierook et al., 2023). Later, diamondiferous ultramafic lamprophyres (in the Bulljah bodies; Yilgarn craton; Hamilton and Rock, 1990) were discovered in Western Australia. Less than 50 diamondiferous lamproite and lamprophyre fields have been described in the literature (Fig. 1, e.g., Atkinson et al., 1990; Jaques, 1994; Gurney et al., 2005; Faure, 2010; Kjarsgaard et al., 2022) but unlike lamproites, no lamprophyre localities have been mined for diamonds and the vast majority of lamprophyres contain microdiamonds <0.5 mm in size.

Although these diamondiferous rock-types are strictly associated with cratons, some important differences can be highlighted (Fig. 1). Kimberlites are mainly emplaced in Archean cratonic nuclei and the neighbouring orogenic belts (e.g., Kaminsky, 2007; Giuliani and Pearson, 2019), while lamproites are more commonly found towards the edges of cratons (Fig. 2; e.g., Skinner et al., 1992; Jaques and Milligan, 2004; Tappe et al., 2009). Different types of lamprophyres are emplaced in different settings, spanning from cratonic edges to collisional zones and arc systems (Jaques and Milligan, 2004; Aghazadeh et al., 2015; Belyaev et al., 2021; Liu et al., 2022).

All kimberlites dated thus far are older than 25 Ma (except for the Igwisi Hills pipe, Tanzania dated at 11.2 ± 7.8 and 12.4 ± 4.8 ka, Brown et al., 2012) and are younger than 2 Ga (e.g., Giuliani et al., 2024). However, more than half of the known kimberlites were emplaced between 250 and 50 Ma (Heaman et al., 2019). Cratonic lamproites have ages of 2 Ga (Pilbara lamproites, Western Australia; Sarkar et al., 2025) to 20 Ma (Ellendale, Western Australia; Mitchell, 2020; Kjarsgaard et al., 2022 and references therein), with the vast majority being emplaced after 50 Ma (Sarkar et al., 2025). Compared to kimberlites and lamproites, less detailed and systematic studies have been conducted on the emplacement age of lamprophyres, which ranges between 2.7 Ga (calc-alkaline lamprophyres in southern Ontario, Canada) to 10 Ma (calc-alkaline lamprophyres in northwestern Iran, e.g., De Stefano et al., 2006; Aghazadeh et al., 2015).

Due to the scarcity of diamond-bearing lamprophyres and their limited economic interest, especially when compared to kimberlites and lamproites, a detailed description of global diamondiferous lamprophyre deposits has yet to be completed. The petrogenesis of these rocks and their potential genetic link with diamonds are still poorly constrained.

This work aims to provide a deeper understanding of the relation between lamprophyres and diamonds. In particular, petrographic, geochemical and isotopic data are used to elucidate the types and sources of metasomatic agents required to form lamprophyres and how the diamond xenocrysts that they may contain can help to constrain the possible lamprophyre source regions.

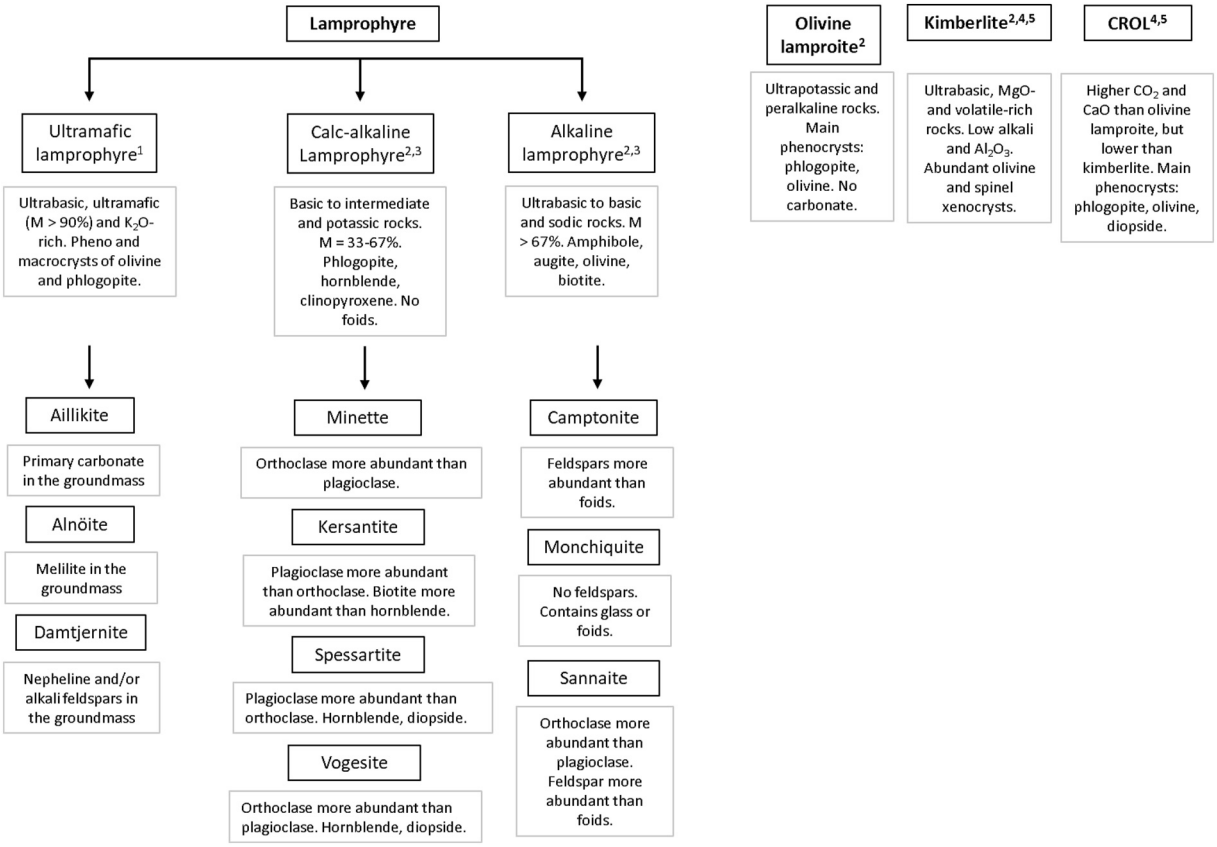


Fig. 3. Simplified flow-chart for classifying the various diamond-bearing magmatic rocks (kimberlite, carbonate-rich lamproite, lamproite and lamprophyre). M stands for mafic and related minerals. [1]Tappe et al. (2005), [2]Le Maitre (2002), [3]Rock (1987), [4]Pearson et al. (2019), [5]Kjarsgaard et al. (2022).

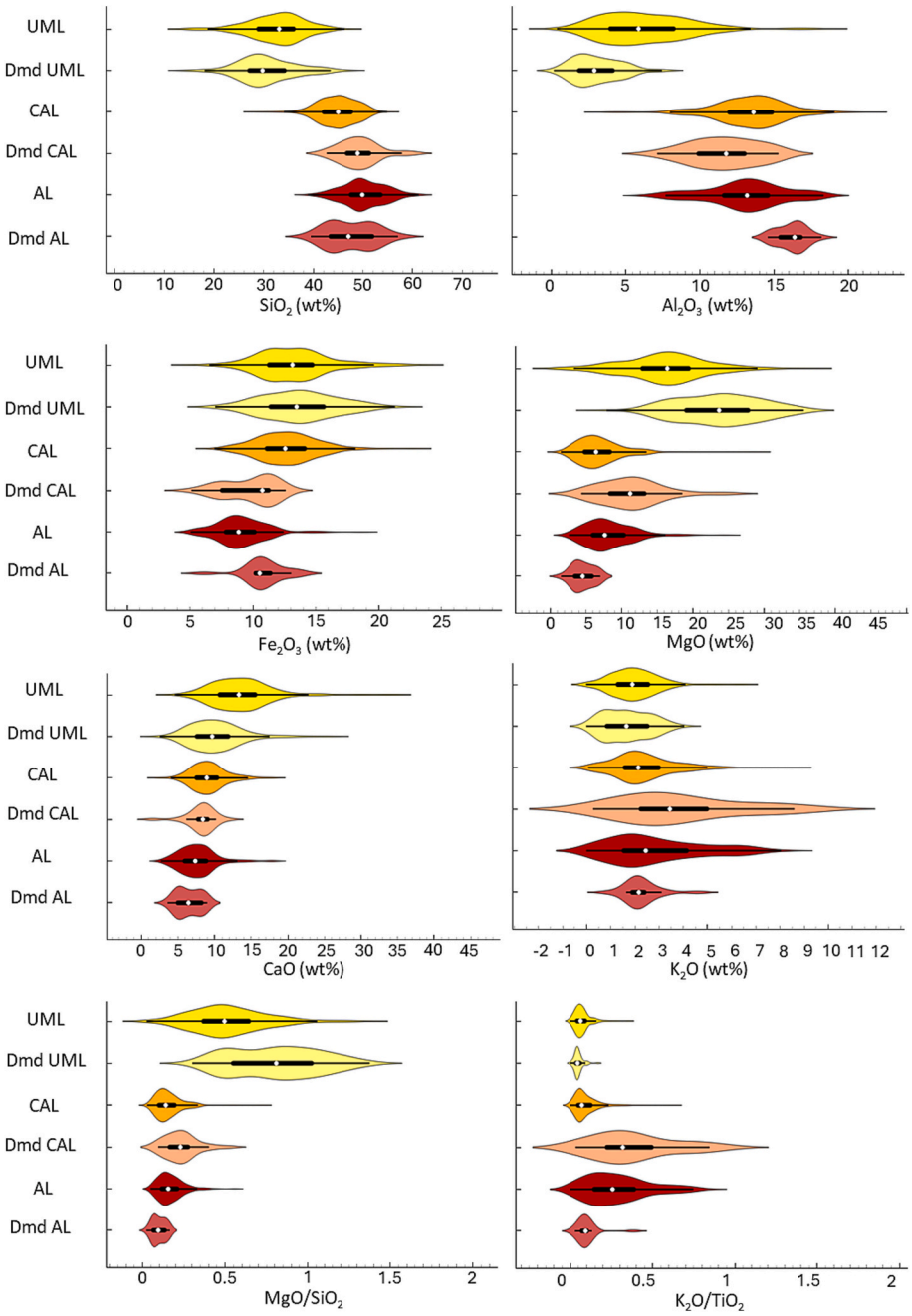


Fig. 4. Violin plots for selected major elements (SiO_2, Al_2O_3, Fe_2O_{3tot}, MgO, CaO and K2O) and their ratios (MgO/SiO_2 and K_2O/TiO_2) for the barren and diamond (dmd) bearing-rock types discussed in the paper (references are reported in Supplementary Material 1). CROL = carbonate-rich olivine lamproites, UML = ultramafic lamprophyre, CAL = calc-alkaline lamprophyre and AL = alkaline lamprophyre. The white dot is the median value, and the black rectangle is the interquartile range. A normal Kernel density estimate was used.

2. Classification and nomenclature of diamond-bearing magmatic rocks

Despite decades of scientific work, the classification schemes for diamond-bearing magmatic lithologies still lack rigorous guidelines, mainly because a comprehensive classification must include not only petrographic, mineralogical, geochemical and isotopic criteria, but also genetic aspects of each rock-type (Mitchell, 2020). In the following section, we describe the classification of the main diamond-bearing rocks, defining the principal features and the main differences for each group (see Fig. 3 for a simplified classification chart). More details can be found in Giuliani et al. (2024).

Traditionally, *kimberlites* have been classified as *Group I* or *Group II* (Smith, 1983). However, despite the continued use of these groups in the literature, the Group I and Group II terms are now considered obsolete, and Group II kimberlite has been recently reclassified as carbonate-rich olivine lamproites (CROL; Pearson et al., 2019). Uncontaminated and unaltered kimberlites are melts enriched in volatile elements (H_2O and CO_2) and MgO, but with low silica, Al_2O_3 and alkali contents (e.g., Kjarsgaard et al., 2009; Brett et al., 2015; Soltys et al., 2018; Pearson et al., 2019). Moreover, their altered nature, coupled with their abundant mantle and terrigenous xenolith cargo, makes the reconstruction of the parental magma compositions a difficult task (e.g., Scott Smith et al., 2013). Kimberlites contain macrocrysts and xenocrysts of olivine, MgO-rich ilmenite, pyrope, diopsidic clinopyroxene, phlogopite, enstatite and chromite, set in a groundmass mainly composed of olivine, monticellite,

Table 1
Major oxide compositions (wt%) for each type of diamond-bearing lamprophyre (the whole range and the interquartile range of each rock-type are reported). References are reported in Supplementary Material 1. UML = ultramafic lamprophyre, CAL = calc-alkaline lamprophyre and AL = alkaline lamprophyre.

	SiO_2	TiO_2	Al_2O_3	Fe_2O_3	MgO	CaO	Na_2O	K_2O	P_2O_5
CAL									
Whole range	39.30–61.04	0.47–4.85	6.61–18.27	5.11–18.59	2.72–24.37	1.60–18.04	0.06–7.55	0.03–9.27	0.04–3.10
Interquartile range	47.48–53.14	0.73–1.19	11.57–14.53	7.83–10.31	6.04–10.83	5.99–8.88	1.83–3.31	1.56–4.23	0.27–0.72
AL									
Whole range	28.50–54.70	0.36–12.32	3.82–21.00	6.99–22.65	1.57–28.83	2.41–18.10	0.15–8.24	0.10–8.50	n.d.-3.14
Interquartile range	42.07–47.54	2.21–3.50	11.96–14.82	11.13–14.10	4.83–8.35	7.5–10.357	2.41–4.15	1.59–2.98	0.41–0.90
UML									
Whole range	14.34–46.15	0.67–9.42	0.23–17.99	5.37–23.30	0.15–35.75	2.64–24.19	0.01–16.95	n.d.-6.46	0.03–6.85
Interquartile range	28.30–35.80	2.21–4.10	3.08–7.39	11.30–14.90	14.25–23.08	9.66–15.08	0.21–1.42	1.12–2.53	0.47–1.11

phlogopite, perovskite, spinel, apatite, carbonate and serpentine (Le Maitre, 2002).

Carbonate-rich olivine lamproites (CROL), previously referred to as Group II kimberlites or orangeites are ultrapotassic (K_2O and MgO > 3 wt%; K_2O/Na_2O > 2; Foley et al., 1987), peralkaline and H_2O-bearing magmas (Fig. 4). By definition, CROL should also have high K_2O/TiO_2 and K_2O (0.1–6.7 wt%) compared to kimberlites (Fig. 4 and Table 1), and a CO_2 content higher than 2 wt% (Giuliani et al., 2024). CROL show rare megacrysts, abundant phlogopite pheno- and microphenocrysts and primary carbonates (Kjarsgaard et al., 2022). Rocks of the CROL group are characterized by macrocrysts and/or phenocrysts of phlogopite and olivine, hosted in a groundmass composed of diopside, spinel, perovskite, apatite and accessory phases such as monazite, titanate and ilmenite (Le Maitre, 2002). The presence of primary carbonate phases, such as calcite and dolomite, and higher CO_2 contents than in other lamproites, are distinguishing features of these rocks (Pearson et al., 2019; Mitchell, 2020).

Lamproites include many varieties characterized by different mineralogical compositions (see Mitchell, 2020 and Sarkar et al., 2025 for a review of lamproites). According to Le Maitre (2002), the main phases that characterize lamproites are Ti-rich phlogopite (phenocryst and groundmass phase), Ti- and K_2O-rich richterite, diopside, leucite and/or sanidine (e.g., Mitchell and Bergman, 1991). The identification of minerals such as melilite, kalsilite, nepheline, plagioclase, schorlomite and kimzeyite rule out classification as a lamproite (e.g., Mitchell, 2020).

Lamproites are divided into cratonic (e.g., those from Leucite Hills, USA) and orogenic (e.g., those from the circum-Mediterranean region) types (Mitchell, 2020). Cratonic (or anorogenic) lamproites, which also include CROL, are characterized by an ultrapotassic and peralkaline composition, with variable SiO_2 (from ultrabasic to intermediate), CaO and MgO contents, coupled with high LILE and LREE (Sarkar et al., 2025).

Lamprophyre is a collective name that groups together various rock-types related to different parental melts which may share similar features and conditions of formation, such as high volatile contents (Scott Smith et al., 2018; Lustrino et al., 2020). However, following Rock (1987, 1991), many authors suggest a genetic link (magma evolution and fractionation) between different lamprophyre compositions (e.g., Kamvisis and Phani, 2022, 2024). According to the current IUGS classification (Le Maitre, 2002), lamprophyres are defined as alkaline and volatile-rich rocks, which are commonly found as porphyritic dykes, ranging from mesocratic (M = 35–65%, where M stands for mafic and related minerals) to melanocratic (M = 65–90%) and, only in few cases, to holomelanocratic terms (M > 90%). Lamprophyres can be divided into the following subgroups according to their mineralogical compositions (Rock, 1987) as follows:

1) feldspar-bearing rocks with amphibole ± biotite ± clinopyroxene ± olivine, such as *minette* and *spessartite* (i.e., the *calc-alkaline lamprophyre* – CAL).

2) feldspathoid- and feldspar-bearing rocks with brown amphibole + augite + olivine + brown mica, such as *monchiquite* and *camptonite* (i.e., the *alkaline lamprophyre* – AL).

3) ultramafic, potassic or ultrapotassic and silica-undersaturated compositions ranging from melanocratic to holomelanocratic, containing phenocrysts and macrophenocrysts of olivine and phlogopite (i.e., the *ultramafic lamprophyre* - UML - Tappe et al., 2005; Table 1).

The following end-members are used to subdivide the UML group: 1) *alnöite*, containing melilite; 2) *damtjernite*, containing alkali feldspars and feldspathoids; 3) *aillikite*, relatively enriched in primary carbonate (Tappe et al., 2005; Ulrych et al., 2011). From a geochemical perspective, CALs are enriched in silica (39.3–61.0 wt%) and K_2O (0.0–9.3 wt%) when compared with ALs (SiO_2 = 28.5–54.7 wt% and K_2O = 0.1–8.5 wt %) and UMLs (SiO_2 = 14.3–46.2 wt% and K_2O = 0.0–6.46 wt%), but they have lower TiO_2 (= 0.5–4.9 wt% vs. 0.4–12.3 wt% for ALs and 0.7–9.4 wt% for UMLs) and CaO contents (= 1.6–18.0 wt% vs. 2.4–18.1 wt% for ALs and 2.6–24.2 wt% for UMLs; Fig. 4 and Table 1).

In general, the different petrogenetic models for kimberlites, lamproites and lamprophyres can be explained with variable mantle source compositions, i.e., lithosphere versus asthenosphere and different degrees of partial melting. Moreover, complex aspects of melt evolution, including stagnation, fractionation and magma mixing, have been used to differentiate these rock-types (e.g., Xu et al., 2007; Prelević, 2004). Kimberlite compositions are usually related to very deep sources (peridotites enriched in H_2O and CO_2), as deep as the lower mantle (e.g., Torsvik et al., 2010), and to a later (i.e., *en route* to surface) interaction with the lithospheric mantle and crustal wall-rock (e.g., Pearson et al., 2019; Pilbeam et al., 2023; Giuliani et al., 2024).

Cratonic lamproites are often enriched in incompatible elements and have radiogenic Sr and unradiogenic Nd—Hf which points to mixing of enriched (and probably veined) lithospheric and asthenospheric mantle components. The three types of lamprophyres require different mantle assemblages (see section 4. Discussions), where the formation of CALs is typically associated with shallower depths (commonly at pressures ≤3/4 GPa) and UMLs are attributed to deeper source environments (e.g., Hari et al., 2000; Foley et al., 2002; Pandey et al., 2018). In all cases, a metasomatized source, affected by volatile- and alkali-rich melts/fluids, as evidenced by the occurrence of hydrous minerals (e.g., amphibole and/or phlogopite) ± carbonate phases, is needed to produce these compositions (e.g., Tappe et al., 2008a; Aghazadeh et al., 2015; Pandey et al., 2018).

3. Diamondiferous lamprophyres

In the following sections, all known occurrences of diamond-bearing lamprophyres are reported and described, together with the available petrographic, mineralogical, geochemical and isotopic data. Where possible, diamonds from each locality are also described in terms of their

Table 2
Selected data from major diamondiferous lamprophyre occurrences.

Locality	Age	Classification	Mineral phases		
			Phenocrysts	Groundmass	Diamonds
CAL					
Canada (Northwest Territories - Parker Lake area)	1.8 Ga[1]	Minettes[1]		K-feldspar, Calcite, epidote, brown mica, apatite, carbonate, titanite, zircon, rutile and pyrite[1,2]	Abundant microdiamonds (≥ 2930 diamonds)[1,2]
Canada (Ontario - Wawa region)	2.6–2.7 Ga[3,4]	Spessartite (volcaniclastic breccia)[3]	Juvenile clasts of actinolite, titanite, chlorite and albite.		Abundant microdiamonds and few macrodiamonds (0.2 to 1 ct/t)[22,26]
		Spessartite (dyke)[3]	Hornblende, biotite[3,4]	Porphyritic dykes: actinolite, biotite and chlorite[3,4]	
Canada (Ontario - Abitibi Greenstone Belt)	2.7 Ga[5]	Minette and kersantite[5]	Brown mica ± hornblende and clinopyroxene[5]	Sanidine, plagioclase, carbonate, chromite, apatite, titanite, quartz and rutile[15]	
Canada (Manitoba - Knee Lake Area)	2.73 Ga[6]	Volcanic conglomerates and sandstones[6]	Blasts of igneous ultramafic, mafic or intermediate rocks in a chlorite sandstone matrix[6]		Abundant microdiamonds and few macrodiamonds (≥ 3412)[23]
		Lapilli tuffs and stones[6]	Brown mica and pyroxene[6]	Lapilli tuffs and stones: glass[6]	
South America (French Guiana - Dachine outcrop)	2.2 Ga[7]		Olivine and diopside[8]	Talc, chlorite, carbonate, actinolite, albite, phlogopite, ilmenite and chromite[8]	Mostly microdiamonds[7]
AL					
Australia (Western Australia - Wandagee area, Carnavor basin)		Monchiquite[9]	Olivine, diopside and spinel[10]	Serpentine, alkali feldspars, apatite, calcite, analcime, brown mica, kearsutite, magnetite[10]	4 microdiamonds[9]
Japan (Shikoku Island)	17.7 Ma	Camptonite[11]	Plagioclase, augite, kaersutite, olivine[11,12]	Plagioclase, Ti-augite, k-feldspar, olivine, Ti-biotite, Ti-magnetite, ilmenite, apatite, magnesite, dolomite, chlorite, epidote, zoisite[11,12]	3 microdiamonds[24]
UML					
Australia (Western Australia - Bulljah, Earaheedy Basin)	280 Ma	Aillikite, damjernite, alnöite, melnoite and CROL[13,14,15]	Phlogopite and olivine[13,14,15]	Spinel, perovskite, apatite, diopside, baryte, titanite, zircon, carbonate, clay minerals, chlorite, serpentine and carbonate[13,14,15]	1 microdiamond[13]
Australia (Southern Australia - Eurelia dikes - Adelaide Fold Belt)	Jurassic[28]	Aillikite[28]	Phlogopite and olivine[28]	Phlogopite, clinopyroxene, spinel, perovskite, carbonates and serpentine[28]	Micro and macrodiamonds[29]
Greenland (Disko Bay - Qeqertaa dike)	1.8 Ga[17]	Aillikites[16]	Phlogopite[16]	Carbonate, amphibole, oxides, apatite, titanite, serpentine and chlorite[16]	Mostly microdiamonds[17]
Greenland (Diamond Province - Sisimiut, Sarfartoq and Maniitsoq)	550–610 Ma[18]	Aillikites[18]	Olivine[18]	Phlogopite, ilmenite, Ti-magnetite, spinel, diopside, perovskite, apatite, dolomite, calcite, serpentine, chlorite[19]	Micro and macrodiamonds[25]
India (Cuddapah Basin - Wajrakarur kimberlite field)	1.1 Ga[19]	Aillikites[19]	Olivine altered to serpentine[19]	Diopside, phlogopite, K-richterite, ilmenite, Ti-magnetite, rutile, Ti-schorlomite, perovskite and carbonate[19]	
Canada (Labrador and Quebec - Torngat Mountains)	550–610 Ma[20]	Aillikites[20]	Olivine, phlogopite, Cr-diopside, Cr spinel, perovskite[20]	Olivine, phlogopite, Ti-richterite, carbonate, garnet, ilmenite, rutile, apatite, perovskite and sulphides[20]	Micro and macrodiamonds (≥ 3478)[21,27]

Microdiamonds refer to diamonds smaller than 0.5 mm. [1]Kaminsky et al. (1998), [2]Macrae et al. (1995), [3]O'Neill and Wyman (2006), [4]Lefebvre et al. (2005), [5]Wyman and Kerrich (1993), [6]Anderson (2016), [7]Smith et al. (2016), [8]Bailey (1999), [9]Jaques (1994), [10]Kerr et al. (1986), [11]Yagi et al. (1975), [12]Uto et al. (1987), [13]Hamilton and Rock (1990), [14]Graham et al. (1999), [15]Choi et al. (2021), [16]Larsen and Rex (1992), [17]Hutchison et al. (2024), [18]Nielsen et al. (2009), [19]Dongre et al. (2020), [20]Tappe et al. (2008a, 2008b), [21]Moorhead et al. (2000), [22]De Stefano et al. (2006), [23]Pezzera et al. (2025), [24]Mizukami et al. (2008), [25]Hutchison and Frei (2009), [26]Buckle (2002), [27]Coates et al. (2006), [28]Dalton et al. (2025), [29]Tappert et al. (2009a).

physical features, mineral inclusions and impurities (e.g., nitrogen content and aggregation state). A summary of this information is also reported in Table 2.

It is important to highlight that sampling bias may have affected the known distribution of diamonds in lamprophyres (and to a lower extent in lamproites). Lamprophyres typically host small and thus not economical diamonds, which are less likely to be found, studied and mined. This may have led to a systematic under-sampling of lamprophyres for diamonds and so the proportion of lamprophyres that are diamond-bearing is likely a minimum.

In some studies, classification of volcanic rocks purported to be lamprophyres is contentious and unclear, leaving many open questions regarding their actual paragenesis. Moreover, lamprophyric samples are often strongly weathered (common secondary phases are serpentine, chlorite, zeolite, clay minerals and carbonates), further complicating the analytical and subsequent interpretive work. Despite these uncertainties, all the petrographic and geochemical data collected for the different lamprophyre occurrences play a key role in elucidating lamprophyre petrogenesis and the possible genetic link with other peculiar rock types (e.g., kimberlites) and diamonds.

3.1. Australia

Lamprophyres are widespread in Australia and are often spatially associated with diamond-bearing kimberlites and lamproites, such as in the Kimberley craton (Western Australia; Sutherland, 1996; Jaques

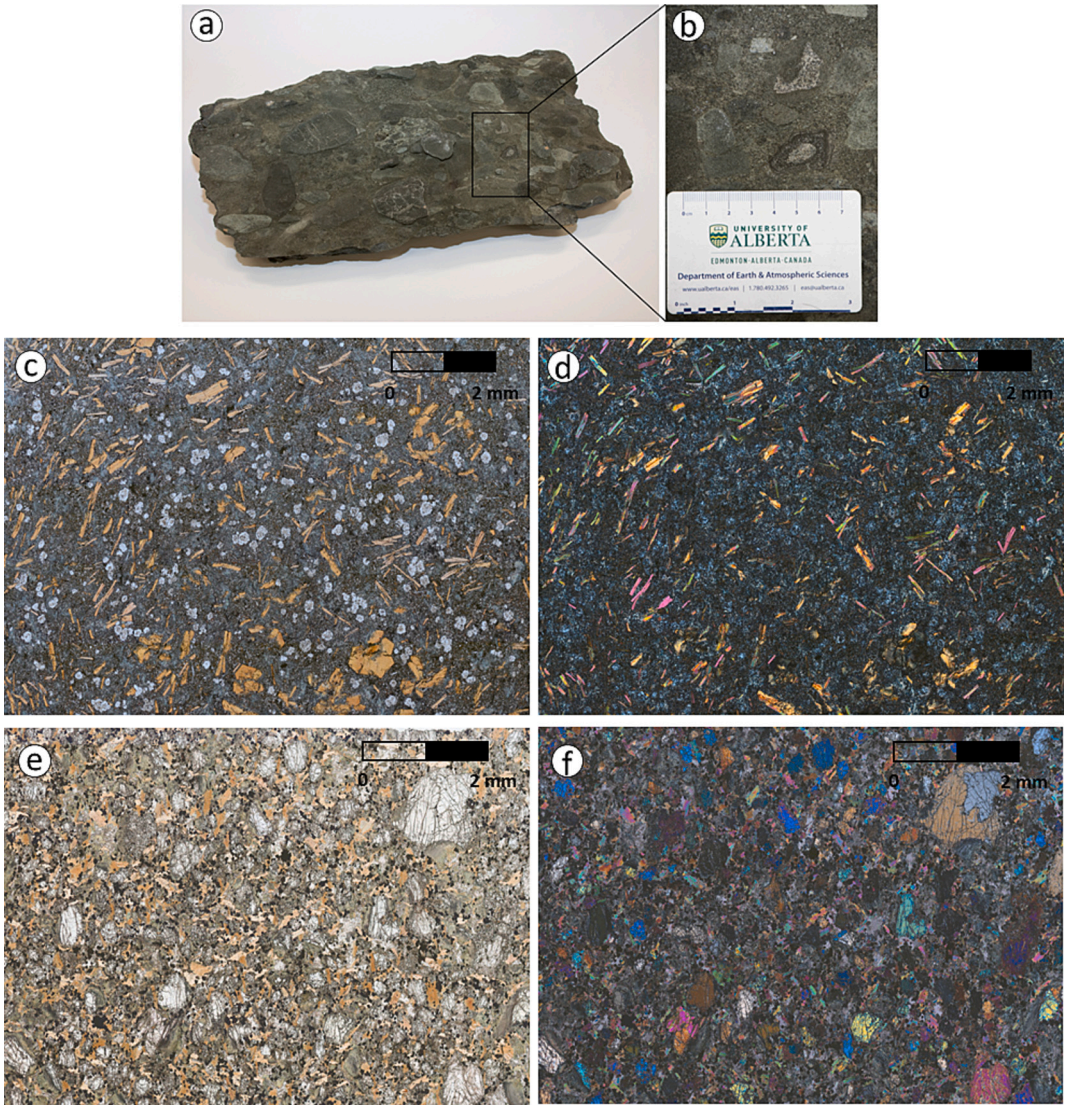


Fig. 5. Location of diamond-bearing lamprophyres discussed in this study. (a) Geological map of Australia, legend: the Geoscience Australia Portal (https://portal.ga.gov.au/). (b) Geological map of Western Greenland, legend: The Greenland Mineral Resources Portal (https://www.greenmin.gl/). (c) Geological map of Japan, legend: Geological Survey of Japan, AIST (GSJ/AIST) Portal (https://www.gsj.jp/en/database/db-portal/). (d) Geological map of India, legend: Geological Survey of India (Maps and Cartography Division, Southern Region, Hyderbad). (e) Geological map of Canada, legend: Canada-3D (https://canada3d.geosciences.ca/mapActions). (f) Geological map of French Guyana, legend: the portal of the Bureau de Recherches Géologiques et Minières: Service géologique national (https://www.brgm.fr/fr). Green stars represent the diamondiferous CALs, red stars the diamondiferous ALs and blue stars the diamondiferous UMLs. (For interpretation of the references to colour in this figure legend, the reader is referred to the web version of this article.)

et al., 1986a, 1986b; Jaques, 2002). >450 occurrences of kimberlites, lamproites and lamprophyres have been reported in Australia (Jaques and Milligan, 2004).

Diamond-bearing UMLs are reported in the Earaheedy Basin (Western Australia; Fig. 5a), a sedimentary basin between the Paleoproterozoic Capricorn Orogen and the Archean Yilgarn craton (Graham et al., 1999). Here, small UML pipes and sills (Bulljah UML) are spatially associated with the Nabberu and Jewill kimberlites (Jaques, 1994; Sutherland, 1996; Hamilton and Rock, 1990; Graham et al., 1999).

U—Pb dating of zircons from Earaheedy Basin UMLs indicate an emplacement age of ~305 Ma (Hamilton and Rock, 1990), whereas *Re*—Os and Rb—Sr systematics indicate an age of ~1280 Ma (Graham et al., 1999), and 1406 Ma, respectively (Choi et al., 2021). Only one microdiamond (<0.5 mm) has been found in these deposits.

The second occurrence of diamond-bearing UMLs is located in Southern Australia, in the Adelaide Fold Belt (found between the Gawler Craton and the Curnamona Province). Here, Dalton et al. (2025) reclassified three Jurassic kimberlites (i.e., Eurelia, Angaston and Terowie) as UMLs. Only the Eurelia kimberlites are reported to be diamondiferous (Tappert et al., 2009a).

Four microdiamonds have been found in the AL variants in the Wandagee area (Carnavor basin, WA; Jaques, 1994). Twenty-two bodies (mostly diatremes but also dykes and sills) intruded during the Upper Jurassic along the eastern edge of the Wandagee Ridge (Fig. 5a). These AL bodies have been classified as olivine monchiquite (Jaques et al., 1986a, 1989).

3.1.1. *Petrographic and geochemical data*

Hamilton and Rock (1990) describe the Bulljah UML as strongly altered rocks, where clay minerals, chlorite, serpentine and carbonates partially, or totally, replace the original liquidus phases. Euhedral phenocrysts of phlogopite and olivine are set in a groundmass of spinel, perovskite, apatite, clinopyroxene, baryte, titanite, zircon and other accessory phases. The occurrence of primary carbonate (i.e., sourced from the melt) in the groundmass of some Bulljah samples allowed classification as aillikites, whereas the identification of alkali feldspars

(enriched in Ba and Sr) and pseudomorphed minerals (probably nepheline) as a minor groundmass phase in some other UML Bulljah samples, led the authors to classify these rocks as damtjernites (Archer, 1987; Hamilton and Rock, 1990). Later, the Bulljah UML were re-classified as phlogopite- and diopside-bearing melnoites, due to the absence of feldspathoids (Graham et al., 1999), and as CROLs, due to the presence of phlogopite phenocrysts and a groundmass containing phlogopite, titanite, spinel and primary calcite (Choi et al., 2021).

Micas from the Bulljah UML are tetraferriphlogopites, with high BaO (up to 2.3 wt%) and TiO_2 (up to 7 wt%). Clinopyroxenes are classified as diopside, with low TiO_2 and Al_2O_3 contents. Carbonate is poor in MgO, FeO and MnO, but SrO reaches 1 wt% (Hamilton and Rock, 1990).

Fresh Bulljah UML are ultrabasic to basic (silica = 36.9–46.1 wt%) with a high MgO (up to 20.2 wt%), CaO (up to 7.8 wt%), alkali (K_2O up to 3.7 wt% and Na_2O up to 0.7 wt%) and LILE content (Hamilton and Rock, 1990; Choi et al., 2021).

The Eurelia, Angaston and Terowie UMLs are porphyritic and often aphanitic. These UMLs are strongly altered with macro- and microcrysts of olivine altered to serpentine or carbonates. Micro-, macrocrysts and phenocrysts of olivine and/or phlogopite are set in a groundmass of phlogopite, clinopyroxene, spinel, perovskite, carbonates and serpentine. Carbonate patches are also observed. Phlogopite crystals may show rims of tetraferriphlogopite (Dalton et al., 2025). Based on this mineral paragenesis, Eurelia, Angaston and Terowie UMLs should be classified as aillikites.

Eurelia, Angaston and Terowie UMLs are enriched in TiO_2, CaO, K_2O and CO_2. Moreover, Al_2O_3 and Fe_2O_3 contents are higher than in the neighbouring kimberlites, while the MgO content is lower (Dalton et al., 2025). All samples are strongly enriched in incompatible trace elements (such as LILE and REE, and HFSE - High Field Strength Elements - in Angaston; Dalton et al., 2025). The Nd isotopic composition shows a broad range, with εNd_i varying from +3.9 (in Terowie samples) to +0.3 (in Eurelia and Angaston rocks; Dalton et al., 2025).

AL sills and dykes from the Wandagee area were first described as picrites with a porphyritic texture and a high porphyritic index. Olivine is the main phenocryst phase whereas diopsidic clinopyroxene and spinel occur predominately as microphenocrysts. The groundmass is composed of serpentine, alkali feldspars and apatite. Calcite, analcime, brown mica, amphibole (kaersutite), magnetite and clinopyroxene also occur as segregated pockets and/or veins (Kerr et al., 1986; Jaques et al., 1986a, 1989). Tuffs are mainly composed of lapilli, coarse ash and crustal (Jaques et al., 1986a, 1989). These rocks were later classified as olivine monchiquite (Jaques et al., 1986a, 1989).

Wandagee ALs are MgO-rich (up to 28 wt%) and alkali poor (~ 1 wt %) with variable silica content. The samples are weakly enriched in LILE and HREE, with high LREE contents (Kerr et al., 1986; Jaques et al., 1989). Wandagee ALs display both radiogenic Sr and Nd isotopic ratios, which may have been affected by post-emplacement alteration processes (Jaques et al., 1989).

3.1.2. Diamonds

Diamond samples from three different dykes belonging to the Eurelia UMLs were studied by Tappert et al. (2009a). Eurelia diamonds are 0.5–5 mm in size, colourless to brown and grey in colour, and have octahedral and dodecahedral to pseudomorphic and irregular habits, respectively (Tappert et al., 2009a). The majority of these diamonds show peculiar surface features, such as roots and etch pits, which are related to an oxidized hosting melt. Deformation lamellae are also observed (Tappert et al., 2009a).

Eurelia diamonds show extremely variable N content, between 5.5 and 2568 at.ppm. Samples also record different N aggregation states, classified as Type IaA, IaAB and IaB, with $\%N_B$ (Day et al., 2026) between 0 and 100 (Tappert et al., 2009a). The most abundant inclusion in Eurelia diamonds is graphite, which is commonly found as flakes and is often associated with fractures (Tappert et al., 2009a). The $\delta^{13}C$ values roughly fit the mantle range with a mode at −6‰ but range between −15.8 and − 2.5‰ (Tappert et al., 2009a, 2009b).

Tappert et al. (2009b) reported the presence of six ferropericlase inclusions coexisting with a likely former perovskite-structured magnesium silicate (i.e., $MgSiO_3$), and therefore were related to a deep mantle origin (> 670 km). For these diamonds, $\delta^{13}C$ ranges between −9.5 and − 1.9‰, with a few values displaced towards −15.7‰ (Tappert et al., 2009b).

3.2. Greenland

West Greenland hosts a wide variety of exotic igneous rocks including kimberlites, lamproites, carbonatites and UMLs, which have emplacement ages from >2.5 Ga to 30 Ma,h (e.g., Larsen and Rex, 1992; Nielsen et al., 2009; Tappe et al., 2009). The Disko Bay UML dykes (e.g., the Qeqertaa dike; Fig. 5b) and lamproite pipes were emplaced at the end of Paleoproterozoic, while in the southern area of West Greenland, Neoproterozoic intrusives comprise a Diamond Province (Larsen and Rex, 1992; Nielsen et al., 2009; Hutchison, 2005).

The Qeqertaa UML is considered the most diamond-rich deposit in the Greenland portion of the Rae Craton. These dikes intrude Archean orthogneiss and underwent metamorphism (up to amphibolite facies) and deformation after emplacement (Bernstein et al., 2013).

The West Greenland Diamond Province includes three regions: Sisimiut, Sarfartoq and Maniitsoq (Fig. 5b). Sarfartoq and Maniitsoq host carbonatite, UML and kimberlite dikes and sills, which intruded the Archean and Paleoproterozoic basement between 550 and 610 Ma (Scott, 1982; Nielsen et al., 2009; Tappe et al., 2009; Steenfelt et al., 2009). At first, many of these hypabyssal rocks were erroneously classified as kimberlites (e.g., Escher and Watterson, 1973), but Mitchell et al. (1999), after a detailed petrographic and mineral chemical characterization, re-classified these rocks as aillikite (or alnöite if melilite is present). Nevertheless, many of the Maniitsoq dykes are still referred to as kimberlites (e.g., Tappe et al., 2011).

The Diamond Province straddles different geodynamic settings: the Maniitsoq region intrudes the Archean North Atlantic craton nucleus, while the Sisimiut region intrudes the Nagssugtoqidian Paleoproterozoic mobile belt. The Sarfartoq region is located in the foreland region of the Nagssugtoqidian orogen (Nielsen et al., 2009; Steenfelt et al., 2009). Intrusive bodies show almost no evidence of interaction with the wallrocks and minimal contamination, despite the presence of lithic clasts and mantle xenoliths (Hutchison and Frei, 2009; Nielsen et al., 2009). Diamonds have only been found in the Maniitsoq and Sarfartoq dikes. The Garnet Lake (Sarfartoq) intrusion is one of the most studied localities in West Greenland and hosted the largest diamond recovered from this area ($1.9 \times 1.7 \times 1.4$ mm^3; Hutchison, 2005; Hutchison and Frei, 2009).

3.2.1. Petrographic and geochemical data

UML dykes (probably aillikites) from the Disko Bay area are mainly fine-grained and heterogeneous, hosting phlogopite phenocrysts in a groundmass of carbonate (up to 50–70%), amphibole, oxides, apatite and titanite. Alteration phases, probably serpentine and chlorite, are also observed (Marker and Knudsen, 1988; Larsen and Rex, 1992). UML dykes are enriched in protogranular mantle xenoliths, mainly dunites, with extremely rare spinel, garnet, brown mica and orthopyroxene (Bernstein et al., 2013). UML dykes from the Disko Bay are ultrabasic, ultramafic and potassic rocks, enriched in TiO_2, CaO, volatiles and alkalis, especially K_2O (higher Na_2O; Larsen and Rex, 1992). The dykes show high Nb and REE contents and negative K and Sr anomalies on chondrite-normalized diagrams (Larsen and Rex, 1992).

Sarfartoq, Sisimiut and Maniitsoq aillikites and mela-aillikites contain euhedral to subhedral phenocrysts of olivine in a groundmass of euhedral to anhedral phlogopite, ilmenite, titanomagnetite, spinel, diopside, perovskite, apatite, baddeleyite and carbonate, and alteration phases such as serpentine and chlorite (Fig. 6c-f). Macrocrysts of olivine and phlogopite, as well as lherzolite and dunite xenoliths, are also

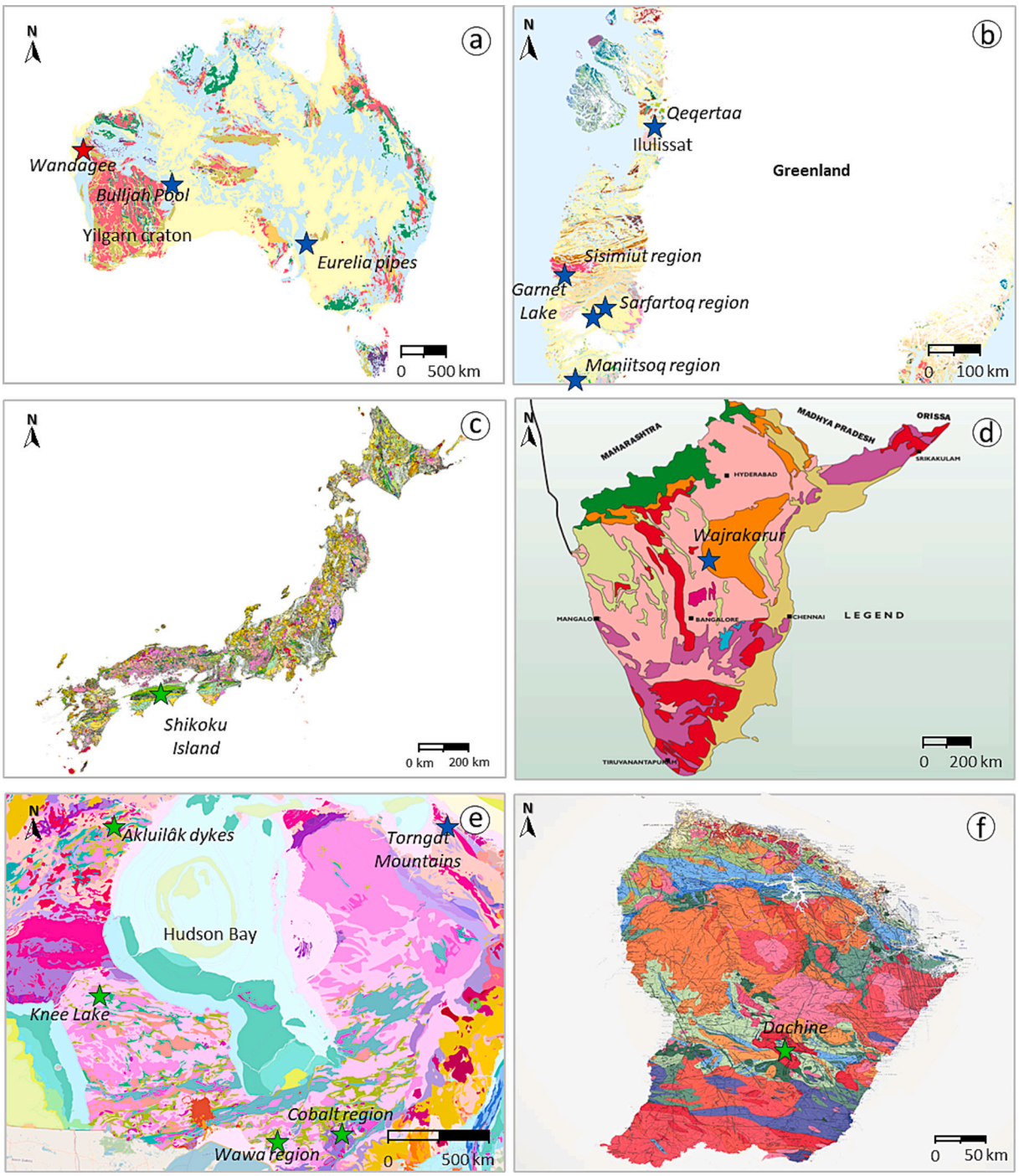


Fig. 6. (a) Volcaniclastic rock sample belonging to the Ultramafic Facies Association of the Oxford Lake Group - Knee Lake, Canada (Pezzera et al., 2025). (b) Mantled clasts (i.e., pelletal lapilli) from the volcaniclastic sample. (c) Thin section microphotograph under plane polarized light of the Kangerlussuaq aillikites (Diamond Province, Greenland). (d) Thin section microphotograph under crossed polarized light of the Kangerlussuaq aillikites (Diamond Province, Greenland). (e) Thin section microphotograph under plane polarized light of the Sisimiut mela-ailikites (Diamond Province, Greenland). (f) Thin section microphotograph under crossed polarized light of the Sisimiut mela-ailikites (Diamond Province, Greenland). Images c, d, e and f from Troels Nielsen.

observed (Mitchell et al., 1999; Hutchison and Frei, 2009; Nielsen et al., 2009; Pilbeam et al., 2024). Sarfartoq dikes are enriched in peridotite xenoliths, ranging from dunite to lherzolite and harzburgite ± garnet ± spinel ± ilmenite (Bizzarro and Stevenson, 2003).

Olivines are commonly zoned, with a Mg# [i.e., Mg/(Mg + Fe)] that, on average, ranges between 84 and 90 at low NiO content. Phlogopites are enriched in TiO_2 and FeO but show low BaO contents. They are characterized by a strong core to rim zonation, and all rims show a tetraferriphlogopite composition. Clinopyroxenes are Cr-poor diopsides, with a strong enrichment in TiO_2 only in the groundmass. Spinels from the groundmass have high Ti/(Ti + Al + Cr) ratios and low Fe^{3+} content, while spinel xenocrysts are classified as chromites, with low Ti/(Ti + Al + Cr) ratios. Carbonate phases include predominant dolomite and subordinate calcite (Mitchell et al., 1999; Hutchison and Frei, 2009; Nielsen et al., 2009; Pilbeam et al., 2024).

Sarfartoq, Sisimiut and Maniitsoq aillikites are strongly ultrabasic and are characterized by increasing TiO_2, Al_2O_3, Na_2O and K_2O and decreasing MgO contents compared to rocks from Maniitsoq and

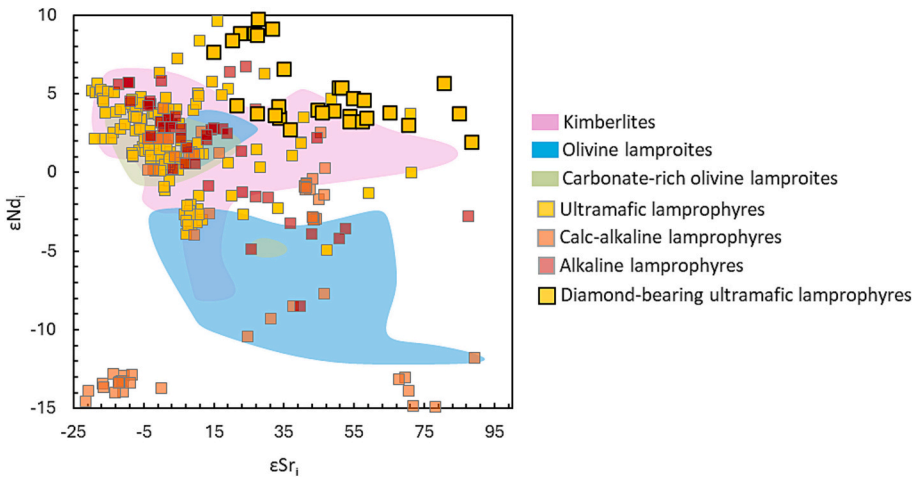


Fig. 7. εNd_i vs. εSr_i diagram for the barren and diamond-bearing rock-types discussed in the paper (references are reported in Supplementary Material 1).

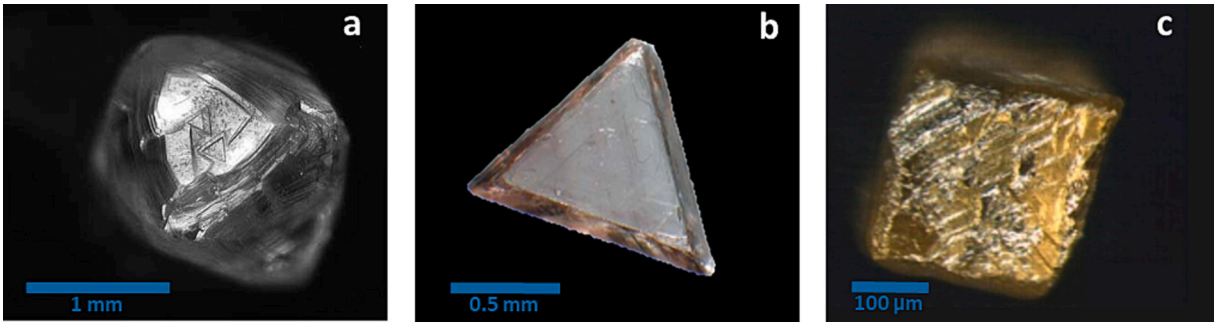


Fig. 8. Microphotographs of different diamond samples from lamprophyre deposits. (a) Octahedral/dodecahedral diamond, with an etched surface, from Sarfartoq (Greenland). From Hutchison and Heaman (2008). (b) Diamond sample from Wawa (Canada), showing macles and deformation. From Stachel et al. (2006). (c) Yellow diamond with a cuboid morphology from Knee Lake (Canada). From Pezzera et al. (2025). (For interpretation of the references to colour in this figure legend, the reader is referred to the web version of this article.)

Sisimiut (Nielsen et al., 2009). In general, these aillikites are ultramafic, depleted in alkalis and have high TiO_2, CaO and L.O.I. (Loss On Ignition) and thus a high volatile content (Nielsen et al., 2009; Tappe et al., 2011). Sarfartoq and Maniitsoq rocks are extremely enriched in trace elements, such as LILE, HFSE and LREE. These samples also show low P, Pb, Zr, Hf and HREE contents (Tappe et al., 2011).

Sarfartoq and Maniitsoq rocks have slightly radiogenic Nd isotopic ratios ($\varepsilon Nd_i = +2.2$ to $+3.3$ for Sarfartoq aillikites and $\varepsilon Nd_i = +1.9$ to $+3.6$ for Maniitsoq kimberlites) and mostly unradiogenic initial Sr isotope ratios (0.70238–0.70299 for Sarfartoq aillikites and 0.70260–0.70603 for Maniitsoq kimberlites, Fig. 7; Tappe et al., 2011).

3.2.2. Diamonds

The diamond-bearing Garnet Lake sheet (Sarfartoq region) hosts many diamonds (> 10 macrodiamonds and hundreds of micro-diamonds) that are colourless (with rarer pink, yellow and amber samples) and with irregular to octahedral habits (Fig. 8a; Table 3). These diamonds often exhibit surficial resorption features. The diamonds have high N contents (up to 2021 ppm) but relatively low aggregation states (average value = 26% N_B, where % N_B refers to the proportion of B-centers compared to A-centers; Hutchison and Heaman, 2008; Hutchison and Frei, 2009). About 9% of the studied diamonds contain mineral inclusions, hypothesized to be mostly graphite and sulphides (Hutchison and Heaman, 2008) though no systematic inclusion study has yet been carried out.

3.3. Japan

The island archipelago of Japan is the result of a prolonged and complex geodynamic evolution being located at intersection of four different tectonic plates. In particular, the southwestern arc overlies the subducting slab of the Philippine Sea (Gao et al., 2024). Here, Shikoku Island hosts three lamprophyre dikes (17.7 Ma) associated with an intense Cenozoic magmatic phase producing basalts, alkali basalts and more evolved, silica-rich plutons (Uto et al., 1987; Mizukami et al., 2008; Kiminami et al., 2017; Gao et al., 2024). The Shikoku Island lamprophyres are emplaced in the Sanbagawa metamorphic lithologies and contain abundant mantle xenoliths that are variably metasomatized (such as dunite, lherzolite, wehrlite, websterite and clinopyroxenite; Goto and Arai, 1987). In these xenoliths, three xenocrysts of micro-diamonds have been found (Fig. 5c) as inclusions in clinopyroxene, together with CO_2 inclusions (Mizukami et al., 2008).

3.3.1. Petrographic and geochemical data

Lamprophyre samples are mostly holocrystalline, but along the contacts with the host rocks, a hypohyaline groundmass can be observed (Uto et al., 1987). The main phenocryst phases are plagioclase, clinopyroxene (augite), amphibole (kaersutite) and olivine set in a groundmass of plagioclase, clinopyroxene (Ti-augite), olivine, Ti-rich biotite, Ti-magnetite, ilmenite, apatite and carbonate (both magnesite and dolomite; Yagi et al., 1975; Uto et al., 1987; Kiminami et al., 2017). Groundmass carbonate is considered primary, despite it also being present as an alteration phase, along with chlorite, epidote and zoisite (Uto et al., 1987). It is important to highlight that the presence of

Table 3
Literature data for the diamonds recovered from major diamondiferous lamprophyre occurrences.

Locality	Colour	Habit	Resorption	Inclusions	N content	N-aggregation state
Sarfartoq region – Greenland[a,b]	Mostly colourless, rare pink, yellow and amber	Irregular to octahedral	Yes	Probably graphite and sulphides	High - up to 2021 at.ppm	26%N_B
Eurelia dikes – Southern Australia[l,m]	Mostly colourless, brown and grey	Dodecahedral, octahedral and irregular	Yes	Graphite, periclase, $MgSiO_3$	From low to high −5.5 and 2568 at.ppm	*Type IaA, Type IaAB and Type IaB*
Wajrakarur field – India[c]	Mostly colourless, rare brown, pink, yellow and green colour	Dodecahedral, octahedral and irregular	Yes		High	Low
Torngat Mountains – Canada[d,k]	Colourless and greyish to brown	Mostly irregular	Yes			
Wawa – Canada[e,f]	Colourless, rare brown, yellow, black and grey	Cubic, octahedra, cubo-octahedral, dodecahedral, irregular and macles	Yes	Olivine, clino and orthopyroxene, Fe—Ni sulphide and plagioclase	From low to medium - 740 at.ppm	*Type II, Type IaA, Type IaAB and Type IaB*
Knee Lake – Canada[g]	Colourless, rare yellow and brown	Irregular, polycrystalline, aggregates, twins, re-entrant cubes, cuboid, octahedra, rounded dodecahedra and tetrahexahedra cubo-octahedra	Yes	Olivine, pyrrhotite, Mg-chromite, garnet and omphacite	Low (*Type IIa*) to high - up to 3110 at.ppm	*Type Ib, Type IaA and Type IaAB*
Akluilâk – Canada[h,i,j]	Green, yellow, burgundy and brown	Cubo-octahedral, octahedra, cubic and dodecahedral, macles, aggregates	Yes		High - up to 9300 at.ppm	*Type Ib* and *Type IaA*

[a] Hutchison and Heaman (2008)
[b] Hutchison and Frei (2009).
[c] Ravi et al. (2012).
[d] Moorhead et al. (2000).
[e] De Stefano et al. (2006).
[f] Stachel et al. (2006).
[g] Pezzera et al., 2025
[h] Chinn et al. (2000).
[i] Macrae et al. (1995).
[j] Cartigny et al. (2004).
[k] Coates et al. (2006).
[l] Tappert et al. (2009a).
[m] Tappert et al. (2009b).

plagioclase phenocrysts, following the IUGS rules (Le Maitre, 2002), should rule out the classification of such rocks as lamprophyres. Plagioclase has a composition ranging from oligoclase to albite. Anorthoclase ($Or_{60-76}Ab_{25-40}$) is often found as a rim around plagioclase. Kaersutites show a well-defined trend of decreasing Mg and Ti with increasing Fe^{2+}, K, Na and Al^{IV} towards the rims (Yagi et al., 1975).

These lamprophyres have been classified as camptonite (AL), due to the abundance of plagioclase and the prevalence of amphibole compared to biotite (Yagi et al., 1975; Kiminami et al., 2017). However, Uto et al. (1987) do not report amphibole, and according to the classification of Rock (1987) and Le Maitre (2002), camptonites should contain feldspathoids which are not reported in the Shikoku Island rocks. Therefore, these samples can be more aptly classified as kersantite (CAL).

The diamondiferous Shikoku Island lamprophyres are ultrabasic to basic rocks (SiO_2 = 39.7–56.9 wt%) with low MgO and CaO and high alkali contents (Na_2O up to 5.4 wt% and K_2O up to 4.6 wt%; Yagi et al., 1975; Kiminami et al., 2017; Gao et al., 2024). These diamondiferous lamprophyres are strongly enriched in REE and LILE, are depleted in HFSE and have high Th, U and Pb contents. In some samples, Eu positive peaks are observed in chondrite-normalized plots (Yagi et al., 1975; Kiminami et al., 2017; Gao et al., 2024).

3.4. India

The Wajrakarur kimberlite field of the Archean Eastern Dharwar Craton is located along the western edge of the Cuddapah sedimentary basin and contains 48 intrusive bodies including kimberlites, olivine-bearing lamproites, CROL, lamprophyres and carbonatites (e.g., Smith et al., 2013; Shaikh et al., 2017; Dongre et al., 2020). Intrusive bodies were emplaced during the Mesoproterozoic, with only one set of perovskite macrocrysts recording an Upper Cretaceous age, linked to the Madagascar Large Igneous Province (Chalapathi Rao et al., 2016).

Lamprophyres reported in the Wajrakarur kimberlite field have been classified as K_2O-rich lamprophyres (Khan et al., 2019; Pandey et al., 2017; Chalapathi Rao et al., 2020) and as UMLs (Dongre et al., 2020; Phani and Kamvisis, 2026). The presence of primary melilite (and therefore alnöite) is still controversial (Chalapathi Rao et al., 2020). Here, many kimberlites are reported to be diamondiferous, but only one aillikite pipe (1.1 Ga; Dongre et al., 2020) contains diamonds (Fig. 5d).

3.4.1. Petrographic and geochemical data

UMLs from Pipe-8 in the Wajrakarur kimberlite field are porphyritic rocks, where olivine, usually altered to serpentine, is the only phenocryst phase. The groundmass contains abundant euhedral to subhedral diopside, phlogopite and amphibole (classified as K-richterite and Ti-rich K-richterite). Accessory phases include ilmenite, spinel, rutile, garnet, perovskite and carbonate (Dongre et al., 2020). Samples are classified as aillikite, due to the presence of primary carbonate in the groundmass and the lack of feldspathoids and alkali feldspars, as well as melilite (Tappe et al., 2005).

Phlogopites from Pipe-8 show high TiO_2 (up to 6.4 wt%) and BaO contents (up to 4.4 wt%), coupled with low Al_2O_3 (lower than 12 wt%). Clinopyroxenes are classified as diopside, with low FeO, TiO_2 and Cr_2O_3. Spinels belong to the titanomagnetite series, whereas garnets are Ti-schorlomite ($Schorlomite_{68.6-87}Pyrope_{1-19.5}Almandine_{8-10}Grossular_{1.7-3.8}$; Dongre et al., 2020).

Pipe-8 UML are ultrabasic (SiO_2 < 42 wt%) and ultramafic rocks, with high CaO and CO_2 contents. The low K_2O + Na_2O (< 1 wt%)

content may be the result of weathering and post-emplacement alteration. These samples are enriched in incompatible elements and LREE, but show low HREE and Hf (Dongre et al., 2020).

Isotopic data indicates strongly radiogenic $^{87}Sr/^{86}Sr$ (0.70786) and unradiogenic $^{143}Nd/^{144}Nd$ ($\varepsilon Nd = +1.2$; Fig. 7; Dongre et al., 2020).

3.4.2. Diamonds

Diamonds from Pipe-8 UML are macrodiamonds, similar to diamonds from the other kimberlite pipes from the Wajrakarur field. In general, they are mostly colourless (with rarer brown, pink, yellow and green samples), with dodecahedral, octahedral or irregular morphologies, often characterized by surficial resorption features (Ravi et al., 2012). Diamonds from the Wajrakarur field show variable N content and aggregation state, with those from the Pipe-8 having relatively high N content and low aggregation state (Table 3; Ravi et al., 2012).

3.5. North America

The Archean North Atlantic craton hosts numerous UML dykes, especially in the regions of Labrador and Quebec. In particular, the Paleoproterozoic Torngat Mountains comprise extremely large swarms of aillikite and mela-aillikite (i.e., aillikites with low modal carbonate content), emplaced between 550 and 610 Ma, covering almost 1500 km^2 (Wardle et al., 1994; Digonnet et al., 2000; Tappe et al., 2008a). Here, UML dykes are intruded into the Tasiuyak gneisses, together with carbonatites (Tappe et al., 2008a). Some of the aillikites (Fig. 5e) host rare diamonds, often gem-quality (Fig. 1; Tappe et al., 2008a, 2008b). Hundreds of small diamonds and rarer macrodiamonds have been recovered from the different dykes (Coates et al., 2006).

In the Rae craton, NW of Rankin Inlet, around the Parker Lake area (Northwest Territories; Fig. 5e), diamond-bearing CAL (i.e., minette) dykes have been identified in the Paleoproterozoic crust of the Western Churchill Province (Kaminsky et al., 1998; Peterson et al., 2002). Three locations, the Thirsty Lake dyke, the South dyke and the North dyke, belong to the Akluilâk dyke group (Macrae et al., 1995; Kaminsky et al., 1998; Chinn et al., 2000). These Paleoproterozoic minettes (1832 Ma; Macrae et al., 1995) are metamorphosed and contain abundant microdiamonds. The origin of these microdiamonds is still debated but it has been suggested that they are xenocrysts from UHP metamorphic rocks (Kaminsky et al., 1998; Chinn et al., 2000; Cartigny et al., 2004), included later by the lamprophyre. Although several thousand microdiamonds were recovered, only one was just greater than the cut-off size of 0.5 mm for microdiamond classification.

In the Michipicoten greenstone belt (Wawa region, Southern Superior Craton – Ontario; Fig. 5e), occurrences of diamondiferous CAL have been reported and described as either polymictic volcaniclastic breccias or dykes. The breccia is dated at 2.68–2.4 Ga and represents one of the oldest diamond-bearing deposits worldwide. The dykes are slightly younger (~2.67–2.72 Ga) and, like the breccias, underwent metamorphism (greenschist facies) and deformation (e.g., Lefebvre et al., 2005; De Stefano et al., 2006). Diamonds from the Wawa subprovince are also found in Neoarchean metaconglomerate (Stachel et al., 2006; Miller et al., 2012). Similar CAL occurrences are also reported in the Abitibi Greenstone Belt (Cobalt area, Southern Superior Craton, Ontario; Ayer et al., 2003; Lefebvre et al., 2005; Kopylova et al., 2011) and in the Jackfish lamprophyre, Slave craton (Yellowknife, Northwest Territories; Armstrong and Barnett, 2003). In the latter case, two yellow microdiamonds have been recovered from minette (Armstrong and Barnett, 2003). More recently, Pezzera et al. (2025) reported 11,587 microdiamonds and 29 macrodiamonds hosted in Neoarchean ultramafic volcano-sedimentary deposits from the Knee Lake area (NW Superior Craton - Manitoba, Fig. 5e; Anderson, 2016). This outcrop area is associated with other alkaline (such as syenites, shoshonite lavas and alkaline to calc-alkaline lamprophyre dykes) and carbonatite lithologies, to the Oxford Lake-Knee Lake greenstone belt, a Neoarchean oceanic block, accreted to the Superior province (e.g., Anderson, 2016).

Other minor and less studied occurrences of diamond-bearing lamprophyres in Canada are from: i) the Mountain Lake area (Alberta), which hosts weakly diamondiferous lamprophyres and kimberlites (Kjarsgaard and Levinson, 2002); ii) the Kechika River diatreme (Cassiar Mountains; British Columbia), classified as AL (Ijewliw and Pell, 1996); iii) the Ospika pipe (Rocky Mountains; British Columbia), classified as UML (aillikite; Ijewliw and Pell, 1996); iv) the Golden cluster in British Columbia, which includes diatremes and dykes classified either as CAL (kersantite) in the Bush area, or as AL (camptonite) in the Mons Creek and Valenciannes River regions (Ijewliw, 1991; Ijewliw and Pell, 1996; Hausel, 2006); and v) Mesoproterozoic UML (aillikite) in the Kapuskasing structural zone (Ontario) (Clark et al., 2024). The only known diamond-bearing lamprophyres from the USA are located in NW Wisconsin, associated with the Six-Pak diatreme (i.e., a hypabyssal alnöite), in the Superior Craton (Carlson and Adams, 1997; Hausel, 2006).

3.5.1. Petrographic and geochemical data

UML from the Torngat Mountains comprises both aillikites and mela-allikites which host variable amounts of primary carbonate. Aillikites are porphyritic with a modal content of groundmass carbonate >10% (Fig. 5b). The main phenocrysts are olivine (also observed as macrocrysts) and phlogopite, whereas clinopyroxene (Cr-diopside) is rare. Microphenocrysts of Cr-spinel and perovskite are also present (Digonnet et al., 2000; Tappe et al., 2004; 2008). Mela-aillikites contain <4% intergranular carbonate (Fig. 5c). The main mineral phases are olivine, phlogopite, diopsidic clinopyroxene and amphibole. The groundmass of both rock-types contains olivine, phlogopite, garnet, spinel (Ti-magnetite and Cr-spinel), ilmenite, rutile, apatite (hydroxy-fluorapatite in aillikite), sulphides (pyrite and chalcopyrite) and perovskite. Compared to aillikites, mela-aillikites contain a lower concentration of oxides and olivine in the groundmass (Tappe et al., 2004, 2008a) and contain magnetite and titanite (Digonnet et al., 2000; Tappe et al., 2004, 2008a).

UMLs from the Torngat Mountains host olivine with a Fo content varying from 81 to 93, with rarer occurrences of Fa-rich crystals (Fa of 76). Here, MnO and CaO contents are low (below 0.4 wt%) and show normal zoning towards the rims. Aillikite micas fall in between phlogopite, tetraferriphlogopite, annite and eastonite compositions. Crystals are zoned, with rims enriched in FeO and depleted in Al_2O_3. Such micas also show moderately low TiO_2 ($\leq$ 4 wt%) and BaO ($\leq$ 1 wt%; Tappe et al., 2004) contents. Phlogopites in mela-aillikites have higher TiO_2, up to 8 wt%. Amphibole has a composition between richterite and magnesiokatophorite, with high TiO_2, and with Na_2O always higher than K_2O. Garnets are classified as Ti-andradite, schorlomite, zirconian schorlomite (ZrO_2 up to 10.5 wt%) and kimzeyite. Carbonates are mostly calcite, with less abundant dolomite. Calcite has low MgO, MnO and FeO, with SrO up to 3 wt% and BaO up to 0.3 wt% (Tappe et al., 2004).

UMLs from the Torngat Mountains are strongly ultrabasic (SiO_2 = 23.40–32.64 wt% in aillikites and = 29.86–37.40 wt% in mela-aillikites) and enriched in MgO (8.00–26.30 wt% in aillikites and 14.80–28.70 wt % in mela-aillikites), CaO (6.15–20.00 wt% in aillikites and 5.82–13.90 wt% in mela-aillikites) and K_2O (1.05–3.14 wt% in aillikites and 1.74–3.49 wt% in mela-aillikites; Digonnet et al., 2000; Tappe et al., 2004, 2008a). Torngat Mountain UMLs are enriched in incompatible elements (high LILE, HFSE, TE - Transition Element - and LREE), with negative anomalies for K, Sr, P, Zr and Hf on the Primitive Mantle-normalized diagram. They also show low HREE contents (Tappe et al., 2004, 2008a).

Isotopically, these aillikites and mela-aillikites fall between different end-members for Sr and Nd (both enriched and depleted compositions). The Nd (εNd_i = −4.9 to +1.6) and the Sr isotope ratios (0.70323–0.70713) are variable. Pb isotopic ratios ($^{206}Pb/^{204}Pb$ = 17.76–18.48, $^{207}Pb/^{204}Pb$ = 15.43–15.65 and $^{208}Pb/^{204}Pb$ = 28.07–46.25; Tappe et al., 2008a) are weakly radiogenic.

Rae craton Parker Lake lamprophyres are holocrystalline with a fine

to medium grain size. The main minerals are K-feldspar (microcline and orthoclase), apatite, carbonate (calcite) and epidote. Microcline is poikilitic, containing brown mica, apatite and carbonate. Brown micas exhibit high Al_2O_3 and FeO contents and are also moderately enriched in TiO_2, BaO and F (Macrae et al., 1995). Accessory phases are titanite, zircon, rutile and pyrite (Macrae et al., 1995; Kaminsky et al., 1998). Abundant crustal fragments (gneiss and gabbro) have also been observed (Macrae et al., 1995; Kaminsky et al., 1998). Parker Lake CAL are ultrabasic to intermediate (SiO_2 up to 57.90 wt%) and are variably enriched in MgO (up to 14.9 wt%), CaO (up to 10.7 wt%) and alkalis (K_2O = 1.71–10.9 wt% and Na_2O = 0.51–3.12 wt%; Macrae et al., 1995). Parker Lake CAL are ultrapotassic with low TiO_2 (0.47–1.07 wt %) and show high LILE and LREE contents and low Cr and Ni contents (Macrae et al., 1995).

Wawa lamprophyres are divided into: i) volcaniclastic breccias - mafic rocks metamorphosed to greenschist facies. These breccias are described as polymictic deposits, from matrix to grain supported, with heterogeneous lithic fragments (smaller than 9 mm) of metavolcanic (from mafic to felsic composition) and plutonic lithologies (from mafic to intermediate composition). These breccias also contain juvenile clasts consisting of actinolite, titanite, chlorite and albite set in an inequigranular matrix of actinolite, chlorite, albite, titanite, epidote and biotite. ii) CAL dikes - inequigranular and porphyritic (the porphyritic index is 5–10%) rocks characterized by hornblende, actinolite, epidote and biotite and by a groundmass of actinolite, biotite and chlorite. Psuedomorphism is common, as hornblende is often replaced by biotite, actinolite and chlorite (Kaminsky et al., 2003; Lefebvre et al., 2005). Despite the metamorphism to greenschist facies, the original igneous rocks (1 and 2) have been reconstructed as CAL (probably spessartite), with phenocrysts of hornblende, biotite and clinopyroxene (Lefebvre et al., 2005; O'Neill and Wyman, 2006). Primary Ca-amphiboles have been classified as edenite, Mg-hornblende and pargasite with low Cr_2O_3 (Lefebvre et al., 2005).

Wawa CALs, both dykes and volcaniclastic breccias, are basic to intermediate (SiO_2 <58.96 wt%) with a high MgO content (up to 24.32 wt %) and variable alkali content ($K_2O + Na_2O$ up to 10 wt%). The low total alkali content recorded in some of these CALs is probably related to metamorphism and alteration (Macrae et al., 1995; Lefebvre et al., 2005; Wyman et al., 2006).

Abitibi CALs are strongly weathered and metamorphosed with phenocrysts of brown mica (phlogopite with biotite rims) ± amphibole (hornblende) and clinopyroxene set in a medium-grained groundmass of sanidine, plagioclase, carbonate, chromite, (fluor)apatite, titanite, quartz and rutile (Wyman and Kerrich, 1993; Wyman et al., 2006). Clinopyroxene has two distinct populations; the first represented by Fe-rich diopside and the second by diopside, both with low Cr_2O_3. Phlogopites are typically zoned, with MgO- and Cr_2O_3-richer cores, that also have lower FeO, TiO_2 and BaO. Carbonates are both primary (i.e., calcite with moderate SrO contents) and secondary (i.e., calcite with low SrO and Fe-dolomite; Wyman and Kerrich, 1993). These samples are classified as minette where hornblende is absent, or as kersantite where hornblende is present (Wyman and Kerrich, 1993). Abitibi CALs are ultrabasic to intermediate (SiO_2 lower than 59 wt%), enriched in CaO (5.73–15.0 wt%), with variable MgO contents (4 to 15 wt%) and low TiO_2 contents (0.43–1.44 wt%). The most primitive samples are potassic to ultrapotassic (K_2O/Na_2O ranges between 1 and 4; Wyman and Kerrich, 1993).

Wawa and Abitibi CALs show similar trace element contents, with moderately high LILE, LREE, Th and U, coupled with negative anomalies for Nb, Ta and Ti on the MORB - Mid-ocean Ridge Basalts - normalized diagram (Wyman and Kerrich, 1993; Wyman et al., 2006). Interestingly, Wawa CALs also have high contents of Ni, Cr and Co (Lefebvre et al., 2005).

Anderson et al. (2015) reported the Knee Lake *Ultramafic facies association* (UFA; Fig. 6a-b) to be composed of: i) very altered rocks, such as ultramafic volcanic conglomerates, sandstones and ii) ultramafic volcaniclastic rocks. The first is a polymictic deposit, from poorly to unsorted and from clast to matrix supported (Anderson, 2016). The clasts are volcanic and intrusive rocks with an ultramafic, mafic or intermediate composition, the matrix is a chlorite sandstone (Anderson, 2016). The volcaniclastic rocks comprise lapilli tuffs and lapilli stones, where lapilli are aphyric to weakly porphyritic, with phenocrysts of brown mica and pyroxene set in an aphanitic or fine-grained groundmass (Anderson, 2016). Knee Lake UFAs are ultrabasic to basic (SiO_2 up to 45.9 wt%) and MgO-rich. The ultramafic volcanic conglomerate and sandstones are enriched in LILE and LREE, but have low HREE, Nb, Zr and Ti contents. Clasts have an ultramafic to mafic and an ultrapotassic affinity (Anderson, 2016).

3.5.2. Diamonds

Several hundred diamonds were recovered from the Torngat Mountains UML, mostly colourless to greyish-brown microdiamonds (Moorhead et al., 2000). Most of these diamonds are characterized by an irregular shape and resorption features (Coates et al., 2006). No inclusion study has been carried out.

Most diamonds recovered from Canadian CALs share similar features (Table 3). Interestingly, almost all the studied diamonds are microdiamonds (Macrae et al., 1995; Chinn et al., 2000; Cartigny et al., 2004; Stachel et al., 2006; Pezzera et al., 2025), e.g., the average size of the 3412 diamonds from the Knee Lake deposit is <150 μm. These samples are colourless, brown and yellow and are variably abundant depending on locality (Fig. 8b-c). In Wawa, rarer black and grey diamonds are reported (De Stefano et al., 2006), whereas green and burgundy samples are observed in the Akluilâk CAL (Chinn et al., 2000; Cartigny et al., 2004). Another common characteristic of these diamonds is the presence of resorption features, and many samples have morphologies indicative of resorption (i.e., dodecahedroids and tetrahexahedroids; Chinn et al., 2000; Cartigny et al., 2004; De Stefano et al., 2006; Stachel et al., 2006; Pezzera et al., 2025).

Based on the N content and N-aggregation state (Table 3), these CAL diamonds have been classified as *Type IIa* (Wawa and Knee Lake diamonds), *Type Ib* (mostly yellow in colour, in Knee Lake and Akluilâk diamonds), *Type IaA* (Wawa, Knee Lake and Akluilâk diamonds), and *Type IaB* (Wawa diamonds; Chinn et al., 2000; Cartigny et al., 2004; Stachel et al., 2006; De Stefano et al., 2006; Pezzera et al., 2025). Only a small subset of Wawa diamonds has higher N aggregation states with % N_B >60% (De Stefano et al., 2006; Stachel et al., 2006). H-related peaks are reported in all the three localities, but further studies are required to better constrain these features (Cartigny et al., 2004; De Stefano et al., 2006; Pezzera et al., 2025). The relatively low N-aggregation states of the diamonds in Archean lamprophyres are consistent with their short mantle residence times associated with a cool lithosphere setting formed by stacked slabs (Pezzera et al., 2025).

Knee Lake diamonds have a range of $\delta^{13}C$ from −16.4 to +1.3‰ (Pezzera et al., 2025), which is similar to that of the Akluilâk diamonds (−16.4 to −2.2‰; Kaminsky et al., 1998; Chinn et al., 2000) but wider than the range of C isotope compositions for most of the Wawa diamonds ($\delta^{13}C$ = −5.5 to −0.74‰; Stachel et al., 2006; De Stefano et al., 2008; Howell et al., 2020). Interestingly, a single diamond from Wawa gave a $\delta^{13}C$ value of −26.2‰, clearly outside the mantle range (De Stefano et al., 2008). The $\delta^{15}N$ values for Wawa diamonds ranges from −17.6 to +14.7‰ (De Stefano et al., 2008) and from 2.7 to 12.9‰ for Akluilâk diamonds (Cartigny et al., 2004).

Mineral inclusions of both peridotitic (e.g., olivine, pyrrhotite, magnesiochromite and garnet for Knee Lake and olivine and orthopyroxene for Wawa) and eclogitic (omphacite) parageneses are observed (De Stefano et al., 2006; Pezzera et al., 2025). This association, along with Mg# of the olivines at scatter around a mean value of 93, together indicate clearly a lithospheric mantle origin to the diamonds. Other mineral and fluid inclusions in Wawa diamonds include Fe- and Ni-rich sulphide (De Stefano et al., 2006), carbonate and water (Stachel et al., 2006).

3.6. South America

In French Guiana, the diamondiferous Dachine deposit (Fig. 5d) comprises metamorphosed talc schists and was emplaced in the Paleoproterozoic during the Transamazonian orogen (2.2 Ga; Smith et al., 2016). Despite deformation, and subsequent weathering and alteration, the original texture of the pyroclastic deposit (probably a lapilli and ash tuff) is still visible (Bailey, 1999; Smith et al., 2016). The body was initially classified as a komatiite based on whole-rock geochemical data (Bailey, 1999), but later works (e.g., Wyman et al., 2008; Smith et al., 2016), highlighting strong similarities with the Wawa diamond host-rocks (see 3.5 North America paragraph for more information), reclassified this deposit as a CAL.

3.6.1. Petrographic and geochemical data

The Dachine CAL is a foliated rock, characterized by porphyroblasts set in a fine-grained groundmass. The main phases (in order of abundance) are talc, chlorite, carbonate, actinolite, albite, phlogopite, oxides (such as ilmenite and chromite). Relicts of liquidus olivine and diopside are present (Bailey, 1999).

Dachine CALs are ultrabasic to basic rocks (SiO_2 = 40.3–50.7 wt%) with high MgO (17.1–24.1 wt%) and low CaO (0.12–5.59 wt%), TiO_2 (0.47–1.11 wt%) and P_2O_5 (0.08–0.36 wt%) contents. Total alkali (K_2O = 0.05–3.28 wt% and Na_2O = 0.05–0.43 wt%) and trace element concentrations are low, probably due to metamorphism and weathering (Bailey, 1999). Only one sample, more enriched in phlogopite laths, shows high LILE and REE contents (Bailey, 1999).

3.6.2. Diamonds

Most diamonds from the Dachine CALs are smaller than 1 mm, with variable morphologies, ranging from octahedral and cubo-octahedral to cuboid and irregular. Strongly resorbed shapes (such as tetrahexahedroids) are reported by Letendre et al. (1998) and Bailey (1999) but were not found in the diamonds studied by Smith et al. (2016). Diamonds are colourless, yellow, brown, pink, green and grey (Letendre et al., 1998; Bailey, 1999; Smith et al., 2016).

Dachine diamonds have relatively low N-aggregation states and are *Type IIa* (i.e., no N), *Type Ib* and *Type IaA* (Cartigny, 2010; Smith et al., 2016). Many H-related peaks have also been observed (Smith et al., 2016). The $\delta^{13}C$ ranges from −36 to +0.15‰ and $\delta^{15}N$ ranges from −5 to +21‰ (Letendre et al., 1998; Bailey, 1999; Cartigny et al., 2001; Cartigny, 2010; Smith et al., 2016). Mineral inclusions include sulphide, clinopyroxene, garnet and coesite, consistent with an eclogitic paragenesis (Bailey, 1999; Smith et al., 2016), typical of eclogitic diamonds of lithospheric origin.

4. Discussion

In the following sections, we focus on diamond-bearing CALs and UMLs rather than ALs, as only two diamondiferous ALs are known and the diamonds from such localities have not been described in detail. To date, and to the best of the authors knowledge, no clear evidence exists for a genetic link between diamonds and their host lamprophyres, nor it has been published. While this does not preclude a genetic relationship between diamonds and lamprophyres, it is likely that for many deposits (localities) two different (and probably unrelated) metasomatic melt/fluids attributed to the formation of diamond and lamprophyric melts are required. As such, our current view, along with others, is that diamonds in lamprophyres are xenocrysts.

4.1. Constraints on CAL petrogenesis

Despite the different petrographic and geochemical features of different types of CAL, similar mantle sources, geodynamic settings and aspects of their petrological evolution can be invoked to explain the majority of CAL occurrences.

CAL melts are interpreted to be crystal- and volatile-rich liquids, formed at shallow depth, within the spinel- (Hari et al., 2000) or the garnet-stability field (Ehrenberg, 1979; Pandey et al., 2018; Sargazi et al., 2022; Li et al., 2024). The strong enrichment in K_2O and/or Na_2O and trace elements, as well as radiogenic isotopic compositions, are related to subduction (Abdelfadil et al., 2013; Aghazadeh et al., 2015; Pandey et al., 2018; Sargazi et al., 2022; Li et al., 2024). In particular, the high Sr and Pb isotopic compositions, the low $^{143}Nd/^{144}Nd$ and specific trace elements ratios (e.g., Ba/Nb), suggest the recycling of sediments (mostly siliciclastic) in the respective mantle sources (Abdelfadil et al., 2013; Ma et al., 2014; Aghazadeh et al., 2015; Pandey et al., 2018).

Low degree melting of slab sediments may stabilize hydrous phases such as phlogopite and amphibole (potassium richterite; Aghazadeh et al., 2015; Pandey et al., 2018; Belyaev et al., 2021; Kumar Giri et al., 2021; Li et al., 2024). Indeed, most of the CAL occurrences are associated with post-collisional or subduction-related settings (e.g., Abdelfadil et al., 2013; Aghazadeh et al., 2015; Belyaev et al., 2021). Moreover, in some cases, fractionation, crustal assimilation and magma mixing are suggested and supported by the genetic link found between CALs and evolved rocks (such as granitoids), which is also evidenced by the presence of crustal xenoliths (e.g., Rock, 1984; Xu et al., 2007; Prelević, 2004).

Despite the importance of metasomatic lithologies in the mantle, their exact mineral paragenesis has yet to be constrained because of the few available high pressure experiments. A near-liquidus experimental study (Esperança and Holloway, 1987) demonstrated that minettes can be produced from a hydrous peridotite (+ garnet) at pressures >2 GPa or from a phlogopite-rich wehrlite at pressure of 1.7–2 GPa. The lack of orthopyroxene can be explained by the reaction phlogopite + enstatite = forsterite + melt (Esperança and Holloway, 1987; Foley, 1990). Later experiments showed similar results, suggesting that the primitive minette from Milk River (Canada) may have formed by partial melting (i.e., 37%) of clinopyroxene and phlogopite (at 1.8–2.2 GPa), and that during ascent, the melt would have interacted with (and modified) harzburgitic mantle (Funk and Luth, 2012, 2013).

Diamond-bearing CALs described in this work fit the general framework reconstructed for the other CAL lithologies except that they require deeper, higher pressure origins. For example, Wawa lamprophyres and volcaniclastic breccias (interpreted as a lahar) have been related to the same parental CAL melt, emplaced around 2.7 Ga (Lefebvre et al., 2005), and are associated with a similar setting compared to the Abitibi sub-province (Wyman and Kerrich, 1993; Lefebvre et al., 2005). In particular, Lefebvre et al. (2005) suggested that Wawa CALs were emplaced along local graben, related to the subduction that affected the Superior Craton during the Archean. Wawa and Abitibi CALs have been interpreted as the result of partial melting of variably refertilized and subduction-related (hydrous phase-bearing) sources, probably a spinel lherzolite at a depth <80 km in the shallow arc mantle (Wyman and Kerrich, 1993; Ayer and Wyman, 2003; Wyman et al., 2015). Here, metasomatism is probably related to slab dehydration (Fig. 2) as magmatic activity associated with these CALs occurs during an extensional phase, following the collision and formation of the Michipicoten and Abitibi Greenstone belts (Wyman and Kerrich, 1993; Lefebvre et al., 2005). A complex petrological evolution has been proposed for these rocks. Abitibi CAL probably underwent fractional crystallization of olivine, clinopyroxene, titanite and apatite and interacted, to variable degrees, with crustal wall-rocks (Wyman and Kerrich, 1993), while Wawa melts may have mixed with a komatiitic melt (Ayer and Wyman, 2003). The relatively low-pressure origins of the lamprophyres proposed in these studies are not easily reconciled with the deep mantle sampling required by the diamonds and their inclusions. Stachel et al. (2006) reported the presence of harzburgitic garnet, Cr-diopside and enstatite (both pyroxenes belonging to a peridotitic paragenesis), olivine (from an harzburgitic or dunitic paragenesis) and Mg-chromites. In particular, the majoritic garnets from Wawa seem to

suggest a depth of about 250–300 km. An additional problem is the rather cool conditions of the host lithosphere required by the diamonds they contain (see below and Stachel et al., 2006).

An alternative model, which would be able to explain the development of a veined lithosphere, as well as the formation of Archean CALs and their diamond-bearing nature, may be related to subduction and collisional settings, with slab stacking (e.g., Pearson et al., 2024; Pearson et al., 2026). A later gradual temperature increase, up to the melting point of such metasomes, would also guarantee the CALs melt generation [see section 4.2.1 Insights from Fourier-Transform Infrared spectroscopy].

Unfortunately, all the other diamond-bearing CALs reported in this study have not been analysed in detail, and thus petrogenetic models that satisfy the conditions required by the diamond xenocrysts have not been constructed.

4.1.1. Constraints from mantle xenoliths in CALs

Occurrences of mantle xenoliths in CALs are much rarer than for other types of lamprophyres. A study of mantle xenoliths (mafic rocks metamorphosed to greenschist facies) from the Wawa CALs provided evidence of two different metasomatic events, one related to an H_2O-rich fluid and the other related to a more generic shoshonitic melt or to an ancient sub-arc mantle domain (Wyman et al., 2015). In particular, different geochemical and isotopic affinities of the mantle xenoliths have been used by these authors to propose a complex multistage model: at 2.72 Ga, subduction took place beneath Wawa subprovince, in combination with a mantle plume that affected the flux from the subducting slab. Later, at about 2.68 Ga, slab roll-back and tearing started, triggering melting in the mantle wedge and probably lamprophyre magmatism (Wyman et al., 2015). Such hypothesis supports the involvement of a shallow mantle source, in the arc tectonic setting, which would be in agreement with the subduction model, as Wyman et al. (2015) also proposed the occurrence of a flat subducting plate, allowing the presence of the diamond stability field at lower pressure (e.g., Wyman et al., 2006, 2008; O'Neill and Wyman, 2006). Alternatively, Wyman et al. (2015) suggest that the mantle plume may be responsible for the entrainment of diamonds in the deeper mantle. However, no additional evidence has been subsequently published supporting this very complex model invoking a deep mantle plume or flat subduction.

Ultramafic xenoliths from Eocene lamprophyres in NE India (Deccan Large Igneous Province) are phlogopite-, spinel- and apatite-bearing wehrlite (Pandey et al., 2018b), interpreted as the result of carbonatitic fluid, enriched in K, metasomatism (Pandey et al., 2018b). Geothermobarometry on clinopyroxene points to a formation temperature of 1188–1232 °C and a pressure of 0.9–1.1 GPa (Pandey et al., 2018b).

A deeper source has been proposed for the Thumb Minette (New Mexico), where abundant garnet-bearing lherzolite xenoliths have been studied. Such xenoliths have been related to a depleted mantle, which has been refertilized by deep melts enriched in FeO and TiO_2, at a temperature of 930–1230 °C and a depth of about 130 km (Ehrenberg, 1979).

4.2. Implications for diamond genesis and CAL formation

One of the main problems with diamondiferous CALs is reconciling the shallow (usually below 100 km) depth of implied CAL formation (see 4.1 Constraints on CAL petrogenesis) with the mantle sampling carried out by these rocks in the diamond stability field (depth ranging from 120 to 200 km). To address this issue, a model of diamond formation based on a subduction-related setting has been proposed to explain the origin of diamonds in Eastern Australia (Barron et al., 1996; Griffin et al., 1998). In this model, oceanic crust is extremely enriched in carbon, containing variable amounts of organic matter, C-rich inorganic sediments and graphite (common in altered igneous rocks). A thick and old oceanic lithospheric subducting slab can stabilize diamond (over graphite) at much lower pressures than normal due to its relatively lower temperature compared to the 'normal' peridotitic mantle (Barron et al., 1996). According to this model, diamond would crystallize at 80–100 km depth (~ 2–3 GPa) and 200–600 °C (Barron et al., 1996; Griffin et al., 1998). These subduction-related diamonds can move to the surface by obduction of the slab or if they are entrained by ascending magmas, such as lamprophyres, melilites or leucitites.

However, this model has several problems (e.g., Stachel et al., 2006). The form of C necessary to crystallize diamonds is the first problem: carbonate or graphite. Stachel et al. (2006) point out that in a $CaCO_3 + FeO + H_2O$ system, at conditions (temperatures of 500 °C and pressures <8 GPa) expected along the slab, reduction of the carbonate phase will produce methane and not diamond (Scott et al., 2004). On the other hand, diamonds can form from graphite from a thermodynamic point of view, but from a kinetic point of view this process is inhibited (i.e., the graphite-diamond activation energy is not met at these slab-related P/T conditions; Stachel et al., 2006). Moreover, to avoid graphitization, the diamond entrainment and lamprophyre eruption must occur immediately after diamond formation (Barron et al., 1996; Griffin et al., 1998). Thus, very short (< 10 Myr), and relatively low temperature, mantle residence histories for these diamonds are expected. However, this appears to be at odds with the high N-aggregation states of some of these subduction-related diamonds. Intense deformation of diamonds, that can be observed via cathodoluminescence, is often invoked to justify this contradiction (Griffin et al., 1998) but a mechanistic physical explanation to how deformation-related features in diamond could enhance N aggregation has yet to be published and has not been experimentally demonstrated.

A similar subduction-related model for diamond formation was also applied to the Southern Superior province (O'Neill and Wyman, 2006), where a shallow-angle Archean slab could have resulted in diamond crystallization in the mantle wedge, at low pressure and variable temperature conditions (Wyman et al., 2015). A short-lived partial melting event in the mantle wedge may produce CAL melts that could transport these diamonds to the surface (O'Neill and Wyman, 2006). This model would also explain the presence of plagioclase (interpreted as a relict of the subducted assemblage trapped during diamond growth) as mineral inclusions in Wawa diamonds (De Stefano et al., 2006). Again, the main problem with this model is related to the high N-aggregation state ($\%N_B$ >60%) which indicates relatively long residence times (up to several hundreds of Myr) and/or high residence temperatures (up to 1390 °C), and that cannot be explained by invoking deformation-related enhancement of N-aggregation (De Stefano et al., 2006; Stachel et al., 2006). The other problem is that the inclusions in Wawa diamonds are archetypal cratonic in composition and do not resemble the mineral compositions of peridotites thought to be derived from the hydrated mantle wedge (Stachel et al., 2006). A final issue with a mantle wedge model is that the low temperature thermal histories of the diamonds and their inclusions are not consistent with this regime (Pearson et al., 2026).

To avoid the above issues, Stachel et al. (2004, 2006) proposed that Wawa diamonds formed in a harzburgite cratonic mantle, at a depth > 250 km and at temperatures of 1250 °C. Further support for these conditions comes from the majoritic garnet inclusions hosted by the Wawa diamonds, which indicate depths of entrapment of 250 to 300 km (Stachel et al., 2006). The presence of these ultra-deep inclusions poses significant problems in terms of sampling by CALs. Interestingly, Kopylova et al. (2011) related some mineral phases from the Wawa and Abitibi metaconglomerates (i.e., diamond, picroilmenite, pyrope and corundum) to a kimberlitic magma, that comes from the deep cratonic roots that were present beneath the Superior Craton before the Neoarchean and that were later destroyed through continuous subduction and tectonic erosion. No Archean kimberlites have yet been reported.

Knee Lake diamonds have been interpreted to form in a heterogeneous mantle, where oceanic crust (and associated carbonate-rich sediments) has been largely recycled probably resulting in a cooling

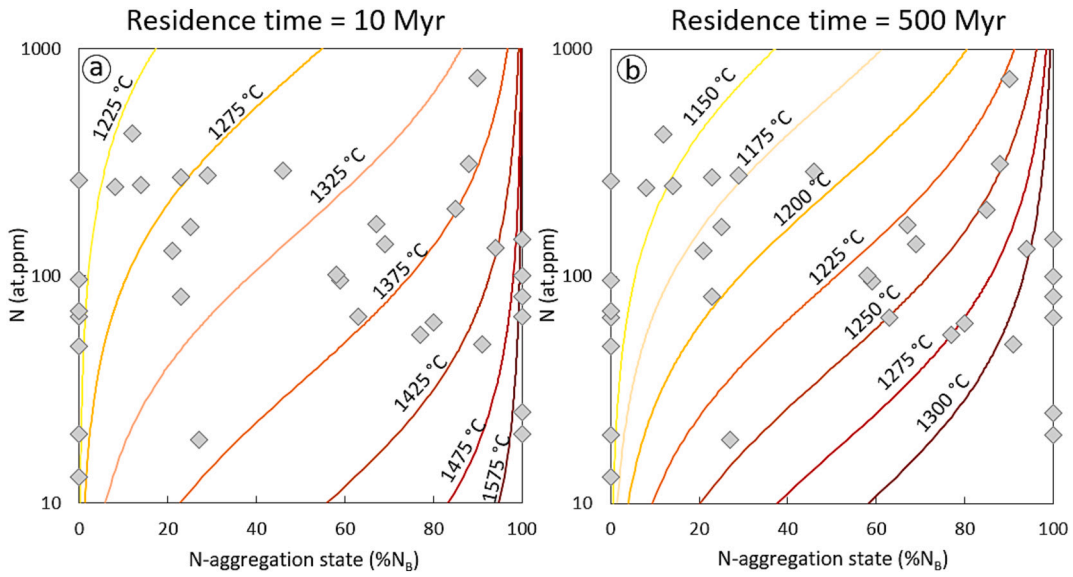


Fig. 9. N content (at.ppm) for Wawa diamonds (from De Stefano et al., 2006) plotted as a function of N-aggregation state (%N_B). (a) Isochrons are plotted for a residence time of 10 Myr. (b) Isochrons are plotted for a residence time of 500 Myr.

carbonatitic high density fluid percolating through the mantle peridotites (Pezzera et al., 2025). A subduction or collisional setting with slab stacking likely resulted in a cool lithospheric mantle beneath the NW Superior Craton during the Neoarchean (Pezzera et al., 2025). This proposed setting is supported by the common occurrence of cubic growth morphologies in the Knee Lake diamonds (the low-T growth form of diamond) and the very low N content and N-aggregation state of the Knee Lake diamonds indicating low mantle residence temperatures (< 1170 °C) and short mantle residence times (0.01 Ma; Pezzera et al., 2025).

The diamonds recovered from Akluilâk minettes are considered metamorphic phases that formed in a cold subduction setting associated with Paleoproterozoic continental collision (Fig. 2) between the Slave, Superior and Churchill cratons (Thelon or Trans-Hudson orogenic cycles; Chinn et al., 2000; Cartigny et al., 2004). Recycling of the oceanic lithosphere and subsequent slab dehydration and metamorphism produced C-O-H diamond-forming fluids (Chinn et al., 2000; Cartigny et al., 2004). The high N content, the low N-aggregation state and the C (slightly more negative $\delta^{13}C$ than the typical mantle values) and N (slightly more positive $\delta^{15}N$ than the typical mantle values) isotope compositions suggest a subduction setting, supporting this scenario (Chinn et al., 2000; Cartigny et al., 2004), though we note that no inclusion study has yet been published to support the model.

Regarding other diamondiferous CALs, Dachine diamonds have been associated with a more complicated history compared to 'normal' lithospheric diamonds. Here, diamond precipitation may have occurred along a subducting slab as evidenced by the extremely peculiar $\delta^{13}C$ and $\delta^{15}N$ values suggesting involvement of recycled crustal material (eclogite, carbonaceous lithologies and metalliferous deposits; Smith et al., 2016). According to Smith et al. (2016), Dachine diamonds would have precipitated along the boundary between the slab and the lithospheric mantle, at a depth of 200–250 km (calculated by garnet-pyroxene barometry) and at temperatures of 800–1000 °C (based on the thermal model proposed by Syracuse et al., 2010). The diamond-forming media must have formed from dehydration of H-bearing minerals (such as serpentine and chlorite) in the slab and mobilization of C from organic sediments. Later input of H_2O from the subducted material would have caused mantle partial melting forming volatile-rich ultramafic melts that sampled the diamonds from the surrounding wall-rock (Smith et al., 2016). The low N-aggregation state supports this scenario and argues against previous work (i.e., Cartigny, 2010) that invoked komatiite magmatism, which occurs at extremely high temperatures (~1700 °C; Smith et al., 2016).

An alternative model (Cartigny, 2010) links Dachine diamonds to carbonado diamonds, mainly due to their similar and uncommon C and N isotopic signatures. Both are interpreted to be intimately associated with upwelling komatiites: the ascent of a proto-komatiite from the transition zone would cause fractures in the surrounding reduced lithospheric mantle, where volatile and mobile elements (CO_2, H_2O, N) concentrate and crystallize diamonds, later entrained by a separate pulse of komatiitic magma (Cartigny, 2010).

4.2.1. *Insights from Fourier-Transform infrared (FTIR) spectroscopy*

The time-temperature dependance of aggregation of nitrogen defects in diamond offers a way to evaluate the thermal evolution of the mantle that diamonds resided in prior to their sampling by the host magma. This then provides constraints on the potential tectonic setting just prior to lamprophyre eruption and diamond sampling. Fig. 9a shows the N content plotted as a function of N-aggregation state (%N_B) for the Wawa diamonds from De Stefano et al. (2006), showing that it is impossible to

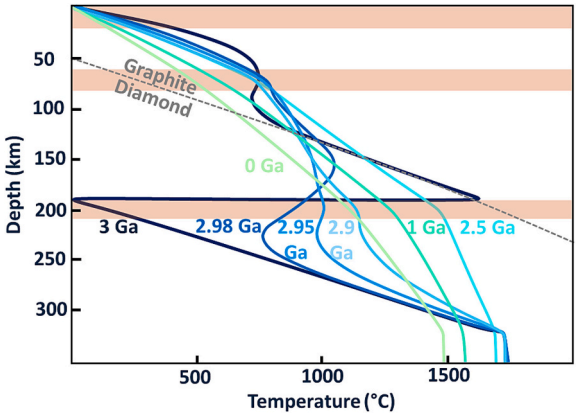


Fig. 10. Geotherm evolution through time for the slab-stacking model, considering three slabs, calculated in Pearson et al. (2024). The first slab has a thickness of 60 km, while the second and third slabs have a thickness of 130 km. In all cases, there are 20 km of basaltic crust. Light orange areas represent the subducted oceanic crust. Modified after Timmerman et al. (2022) and Pearson et al. (2024; 2026).

reach the high N-aggregation states observed for the Wawa diamonds at the temperatures suggested for the very cold subduction model of Griffin et al. (1998: 200 to 600 °C), which would require unrealistically long mantle residence times. For example, a N-aggregation state of 50%N_B and a total N content of 150 at.ppm (the average %N_B and N content reported by De Stefano et al., 2006), correspond to a mantle residence time of ~806 Myr at 1200 °C. This time is considerably longer than the maximum 10 Myr residence time proposed for the subduction model suggested by some authors, and requires much higher temperatures than previously suggested (Barron et al., 1996; Griffin et al., 1998). Even if a short-lived 1 Myr heating event, related to the magma ascent, is considered, temperatures of 1400 °C would be required to reach 50%N_B. Considering an average temperature for alkaline melts of 1100–1200 °C, such high N-aggregation states cannot be reliably explained using the subduction model (Tappe et al., 2025).

In Fig. 9b, 1150–1300 °C model isotherms, representative of the normal cratonic mantle in the diamond stability field, are plotted for an assumed residence time of 500 Myr. The Wawa diamonds plot well within the normal temperature range for a residence time 500 Myr.

Given the above considerations, other models to explain the occurrence of diamond in CALs have to be explored. Such models involve a complex multistage exhumation history, invoking a deeper diamondiferous melt that crystallized at depth, without reaching the surface (Cartigny, 2010). Alternatively, lithospheric exhumation-related models have been proposed (e.g., Stachel et al., 2006), where tectonic uplift and collision resulted in lithospheric exhumation, as suggested for diamonds from West Africa (Smit et al., 2016).

An alternative model, which is able to explain diamond formation in the lithospheric mantle (as indicated by the inclusions) sometime during the Archean and eruption by the CALs by the Neoarchean, is represented by the lithospheric stacking, which can take place during the very initial phases of a craton formation. The stacking of two or three lithospheric slabs, with a thickness between 60 and 130 km, with oceanic crust (with at least 20 km of MgO-rich compositions) and lithospheric mantle, as consequence of subduction and collision events, is considered a valid explanation for craton formation e.g., Mareschal and Jaupart (2006), Michaut and Jaupart (2007), Timmerman et al. (2022), and Pearson et al., 2026). These authors point out that the geotherm resulting from slab-stacking is not in a steady state but instead is highly transient, with rapid thermal changes occurring, especially in the first 500 Ma (Fig. 10). These conditions would provide a diamond stability field at much shallower conditions than a similarly thick lithosphere in “steady-state” conditions, as it would start from 100/110 km depth (Pearson et al., 2024; 2026). Moreover, the slab-stacking model would guarantee a melt-formation depth, from metasomes within the lithosphere, more compatible with the mantle sources hypothesized for CALs melts, while also providing extremely variable thermal conditions through time (Fig. 10), potentially explaining the highly varied N aggregation conditions of diamonds erupted in Archean times such as Wawa (Pearson et al., 2026). A variation in lithospheric temperature of hundreds of °C, at depths pertaining to the diamond stability field, in a very limited time (<500 Ma; Fig. 10) can readily explain the extremely variable N aggregation state of the Archean diamonds in CALs, especially in Wawa and Knee Lake, where they range from *Type Ib* to *Type IaA* and/or *Type IaB* (Table 3). Following this hypothesis, different diamond-forming episodes must be invoked, probably related to an extremely heterogeneous subducted slab (e.g., Plank and Langmuir, 1998), where neighbouring carbonate lithologies may have different melting temperature, depending on their compositions (e.g., the alkali contents). For example, the presence of Na in magnesite or calcium-carbonate drastically reduces the solidus temperatures of such phases (e.g., Edwards, 2019; Podborodnikov et al., 2019). Despite most of the carbonate sediments in the oceanic crust being represented by $CaCO_3$, minimal amount of K_2O and Na_2O can still be found (mostly lower than 1 wt%) and they are also stored, in much larger amount, in other marine sediments, such as clays and chert (e.g., Plank and Langmuir, 1998; Edwards, 2019) and this would lower the solidus of the carbonate mix, producing carbonate melts over a range of temperatures.

To test this model, we recalculated the minimum and the maximum residence temperatures in the mantle, for a residence time ranging between 100 and 800 Myr. FTIR data collected for Wawa diamonds (Stachel et al., 2006; De Stefano et al., 2006) were processed using the Caxbd_Inherit_2024-Ib Excel spread sheet (Day et al., 2025). The required average residence temperatures for *Type IaA′* diamonds (Day et al., 2026) are approximately 880–1180 °C (for 100 Myr) and 840–1120 °C (for 800 Myr). Apart from *Type IaA′* diamonds (i.e., 100% N_A), the remaining diamonds have highly variable aggregation state (% N_B) and thus residence temperatures range approximately from 1100 to 1400 °C (for residence times of 100 to 800 Myr). This is in line with numerous diamonds forming events producing diamonds that then experienced highly variable time-integrated mantle residence temperatures, as discussed above and as indicated in the model presented in Fig. 10.

4.3. The diamond-CALs connection

CALs are much more common than kimberlites and lamproites (Rock, 1984). However, diamondiferous CAL are extremely rare, leading to an open question about the reason for this discrepancy. The very shallow depths (usually lower than 100 km km) hypothesized for sources of CALs, compared to depths associated with the diamond stability field (120 to 200 km), is probably one of the main reasons for the scarcity of diamond-bearing CALs.

Thus far, studies carried out on both diamonds and CAL host rocks have found no genetic relationship, but their occurrence is related to similar geodynamic environments (i.e., active convergent margins) and to peculiar mantle conditions (e.g., Ayer and Wyman, 2003; De Stefano et al., 2006), resulting in diamonds from different CALs with very similar characteristics. The absence of a genetic link between diamonds and CALs is also supported by the high N-aggregation state of some CAL diamonds, which would require long and/or high temperature residence time, which is at odds with shallow subduction-related environments associated with formation of CALs (Fig. 9).

The extremely large number of microdiamonds found in some CALs has been attributed to an extremely fast nucleation rate, a consequence of formation within a relatively cold lithospheric mantle such as that produced by slab stacking (e.g., Pezzera et al., 2025). A subduction-related setting and recycled crustal material, presumably oceanic sediments, are needed not only to explain the features of the CAL melts, but to explain all the characteristics of the diamonds that are hosted in the CALs. Such characteristics include the C and N isotope composition of diamonds and the presence of mineral inclusions of eclogite paragenesis (e.g., Cartigny et al., 2004; De Stefano et al., 2008; Pezzera et al., 2025).

Despite the relatively fast ascent rates of CAL melts, as suggested by their high volatile contents, CALs are mostly found as dykes, sills, plugs and stocks, and rarely as lava flows (Rock, 1984). Moreover, a complex petrological evolution of CAL magmas, including stagnation, fractionation and magma mixing at shallow depth must be accounted for when considering the stability and transport of the diamonds in such magmas (e.g., Rock, 1984; Wyman and Kerrich, 1993). Due to these processes, diamonds may be hosted in the CAL melts for a relatively longer time compared to kimberlitic melts. Thus, the CAL composition itself appears to be extremely hostile for diamonds, consistent with the variety of resorption features on CAL diamonds which are observed in all the considered localities (see Section 4.5 The diamond-UMLs connection). All these factors contribute to the smaller average size of diamonds in CALs, compared to other diamondiferous igneous bodies.

4.4. Constraints on aillikites petrogenesis

All the diamond-bearing UMLs mentioned above have been classified as aillikites (and mela-aillikites), except for the Western Australian

occurrence of the Bulljah bodies - Earaheedy Basin, whose classification remains controversial as they have been previously classified as aillikite, damtjernite, alnöite and CROL (Archer, 1987; Hamilton and Rock, 1990; Graham et al., 1999; Choi et al., 2021; see section 3.1.1 Petrographic and geochemical data). For this reason, the following sections will be solely focused on aillikite petrogenesis and on the aillikite-diamond association, rather than including the whole UML rock group.

Following the assumption that UMLs represent mantle melts that underwent minimal crustal contamination (e.g., Foley et al., 2002; Tappe et al., 2008a; Nielsen et al., 2009; Downes et al., 2023; Pilbeam et al., 2024), the respective mantle sources can be reconstructed. Petrographic evidences, such as the presence of primary carbonate in aillikites, coupled with geochemical data, such as low silica content and moderately high alkali content, point to a UML source that is different from the classical peridotitic mantle (olivine + orthopyroxene + clinopyroxene + spinel/garnet).

Due to the lack of a general consensus on UML petrogenesis, there are several hypotheses concerning the potential mantle sources for UMLs. These include: i) a carbonated and variably metasomatized peridotite; ii) a veined lithospheric mantle where the peridotite wall-rocks host carbonate-rich metasomes (e.g., Foley and Andronikov, 2003); or iii) a deep asthenospheric source (similar to PREMA - PREvalent MAntle, after Zindler and Hart, 1986; Choi et al., 2021; Dalton et al., 2022).

For both lithospheric mantle hypothesis, infiltration of mobile carbonatite liquids in the mantle wall-rocks would guarantee the absence of orthopyroxene (and the resultant low silica content of the melts), the CO_2-rich conditions of the system and the stabilization of high modal contents of clinopyroxene (e.g., Yaxley et al., 1991). In particular, a sodic diopside can be produced by a metasomatic agent with a Na-rich dolomite composition, ensuring a sufficiently high Na_2O budget in the resulting melts. Beside the presence of carbonate phases, aillikite mantle sources are likely enriched in a hydrous phase. The presence of both CO_2- and H_2O-rich phases would ensure a lower melting temperature in the metasomatic veins, when compared to the surrounding peridotitic mantle. Usually, the phases invoked to host hydrogen in the upper mantle in concentrations on the order of a few thousand ppm are amphibole and phlogopite. Pargasite amphibole is the shallowest phase, as it is stable up to ~3 GPa at depths of ~90–100 km (e.g., Sudo and Tatsumi, 1990; Trønnes, 2002; Foley and Pintér, 2018), or to ~4 GPa at depths of ~120 km in the fertile mantle (Mandler and Grove, 2016). In general, amphibole stability in the mantle strongly depends on the composition of the system, i.e., fluorine, H_2O, Na_2O, K_2O and Cl contents, as well as the Na/Ca ratio and fO_2 (Sudo and Tatsumi, 1990; Konzett and Ulmer, 1999; Foley and Pintér, 2018). Phlogopite, depending on the mantle mineral assemblage, may be stable up to ~6–12 GPa (e.g., Trønnes, 2002; Foley and Pintér, 2018). At pressures higher than 9 GPa phlogopite can react with clinopyroxene to produce K-richterite + garnet. Indeed, K-richterite may be stable to higher pressures, up to 10 GPa at about 1450 °C and up to 14 GPa at about 1000 °C (e.g., Sudo and Tatsumi, 1990; Konzett and Ulmer, 1999; Trønnes, 2002; Foley and Pinter, 2018).

In many cases (e.g., E Antarctica, Canada, Australia, Greenland and Oman), and especially for the depth of aillikite formation (considering the lithospheric mantle source hypothesis), phlogopite is likely the best hydrous source candidate for the UML (e.g., Foley et al., 2002; Tappe et al., 2008a; Nasir et al., 2011; Downes et al., 2023; Pilbeam et al., 2024), as it would also explain the high alkali content (especially K_2O) and the low silica of aillikitic melts. However, pargasite has been reported as a major mantle constituent in some UML source rocks e.g., in the sub-continental lithospheric mantle underlying the Mount Webb (Gibson Desert, central Australia) aillikites (Sudholz et al., 2023).

The model of a veined lithospheric mantle proposed by Foley (1992) can explain UMLs petrogenesis from a phase equilibria view-point. A mantle source consisting of a garnet peridotite matrix, pervaded by a hydrous phase- (phlogopite and/or amphibole), clinopyroxene- and carbonate-rich veins, can explain all the main elemental geochemical features of UML lamprophyres. In some cases, the presence of apatite is also inferred in the UML source (e.g., for the Batain Nappes aillikites in Oman; Nasir et al., 2011; Nasir, 2016). Mantle refertilization could also explain the moderate enrichment in LILE of the studied samples.

Interestingly, though the radiogenic isotope compositions of UMLs are broadly similar to kimberlites (e.g., Giuliani et al., 2024), the Sr—Nd isotopic ratio of diamondiferous UMLs shows slightly different compositions when compared to the other UMLs and to kimberlites, only partially overlapping because diamondiferous UMLs have more radiogenic $^{87}Sr/^{86}Sr$ and more unradiogenic $^{143}Nd/^{144}Nd$ ratios. This isotopic composition lies between different end-members (such as HIMU - High μ -, EMI - Enriched mantle I - and EMII - Enriched mantle II), clearly reflecting the need for a mixed mantle source (e.g., Giuliani et al., 2024 and references therein). For example, Tappe et al. (2008a) explain the unradiogenic to weakly radiogenic Sr, Nd and Pb isotopic ratios of aillikites and mela-aillikites from the Torngat Mountains by invoking the occurrence of a veined cratonic lithospheric mantle. A 5–12% contribution of the metasomatic veins to the partial melting of a depleted mantle would produce the trace elements and the isotopic compositions of the studied UMLs (Tappe et al., 2008a).

Alternative models to explain the exotic composition of UMLs invoke a similar petrogenesis between these melts and kimberlites, inferring a deep mantle source, located at asthenospheric depths, and a later interaction between the ascending melts and metasomatised lithospheric mantle domains. For example, Dalton et al. (2019) report the presence of a Mesoproterozoic aillikitic dyke (Dyke 15) in the Kuusamo area (Karelian craton – Finland). These authors suggest that the aillikitic melt formed from an asthenospheric source and acquired its geochemical features via interaction with a metasomatized lithosphere, enriched in hydrous phases, such as phlogopite and K-richterite (i.e., an assemblage similar to MARID, Dalton et al., 2019). A PREMA-like melt and a contribution of about 10/20% from this subcontinental lithospheric mantle would ensure the low Nd and Hf isotopic compositions recorded by this UML (Dalton et al., 2022).

In both cases, the origin of the metasomatic assemblages in UML sources is not fully understood. Their formation has been related to metasomatic fluids produced by recycled crust (e.g., Nielsen et al., 2009) or to fluids coming from a deeper source (input from a mantle plume and/or asthenospheric source, see e.g., Foley et al., 2006; Tappe et al., 2008a; Pandey et al., 2019; Dongre et al., 2020; Pilbeam et al., 2024; Wang et al., 2023).

Diamondiferous and barren UMLs are typically found in extensional rift settings (e.g., Foley et al., 2006; Tappe et al., 2008a; Pandey et al., 2019; Carniel et al., 2020; Sudholz et al., 2023). For example, emplacement of the diamondiferous UMLs from Disko Bay is associated with a magmatic phase triggered by rifting events related to the break-up of Paleo-Pangea which developed after continental collision between the Rea and North Atlantic Cratons (Larsen and Rex, 1992; Hutchison et al., 2024). The emplacement of the non-diamondiferous aillikites in the Yilgarn Craton – Australia is linked to the break-up of Rodinia (Choi et al., 2021) and the emplacement of the Kuusamo aillikites is linked to an extensional tectonic phase and to the break-up of Laurentia and Baltica terranes during the Mesoproterozoic (Dalton et al., 2022). Both examples represent UMLs related to phases of extensional rifting and supercontinent break-up.

Those conditions seem to be necessary for i) the early production of exotic mantle metasomes (i.e., uprise of hot asthenospheric mantle); and ii) melting events, which (would start from the metasomatic veins, characterized by a lower liquidus temperature, and eventually affect the surrounding peridotite mantle (e.g., Foley, 1992; Foley et al., 2006; Tappe et al., 2008a).

The presence of diamonds within UMLs accords with the different petrogenetic models described above because these magma source regions are significantly deeper than those invoked for CALs. For the Sarfartoq, Sisimiut and Maniitsoq aillikites, Mitchell et al. (1999) suggested a variably metasomatized, phlogopite-bearing carbonated

lherzolite source. In this scenario, aillikite would be genetically related to carbonatites, representing a lower degree of partial melting of the same mantle source (Mitchell et al., 1999). Tappe et al. (2008a) invoke a veined lithospheric mantle to explain the formation of the Torngat Mountains UML and the Greenland equivalent (i.e., Sarfartoq) UML with two different types of metasomes: one older, similar to a MARID assemblage, and one composed of phlogopite and carbonate. The latter are related to deeper asthenospheric contributions (Tappe et al., 2008a).

On the other hand, the origin of Eurelia aillikites has been explained invoking a deep asthenospheric mantle source and a later interaction between the ascending melt and the metasomatised lithospheric wall-rocks (e.g., Dalton et al., 2025). In particular, for the Eurelia UMLs, metasomatic agents enriched in carbonate may have strongly affected the subcontinental lithospheric mantle beneath the Adelaide Fold Belt, where phlogopite-bearing veins must be present to explain the extreme enrichment in K_2O and mica in the UML samples (Dalton et al., 2025). Based on Nd isotopic data, Dalton et al. (2025) also suggested that small amounts of crustal material, recycled along the southern edge of Pangea, led to metasomatism of the UML convecting mantle sources. The lower Nd isotopic values of these UMLs compared to others (e.g. Safatoq) are explained via mixing of a PREMA mantle with a subducted slab composed of 90% MORB and of 10% GloSS. This model is further supported by the identification of *superdeep* diamonds in the Eurelia UMLs, which have been associated with the lower section of the asthenosphere or with the lower mantle (e.g., Tappert et al., 2009b).

4.4.1. Constraints from mantle xenoliths in aillikites

Thermobarometric estimates for mantle xenoliths from Garnet Lake UMLs indicate a pressure of ~6 GPa and a temperature of 1252–1327 °C (Hutchison, 2005). Similarly, other mantle samples from Sarfartoq equilibrated at 2–5 GPa and 650–1300 °C (Bizzarro and Stevenson, 2003; Sand et al., 2009), defining a cool cratonic geotherm that is close to "steady-state" at the time of eruption (Sand et al., 2009).

For some of the non-diamondiferous UML occurrences, similar mantle conditions are reported. For the Mount Webb aillikites, garnet and Cr-diopside xenocrysts indicate a pressure of 1.7–4 GPa and a temperature of 750–1320 °C (Sudholz et al., 2023).

Metasomatic events are also recorded from mantle xenoliths in the UMLs, providing further evidence of the importance of a veined and variably refertilized lithospheric mantle source. Peridotite xenoliths from the Safartoq UMLs show both depleted (due to 30-45% of melt extraction) and deeper fertile (garnet- and clinopyroxene-bearing) compositions (Bizzarro and Stevenson, 2003; Wittig et al., 2008).

4.4.2. Petrogenetic constraints from similar UMLs (alnöite)

Unfortunately, to the best of the authors' knowledge, no HP-HT experiments have been carried out on aillikites, and only one abstract has been published on alnöites. Foley and Andronikov (2003) performed near-liquidus experiments on alnöite (from eastern Antarctica, Beaver Lake outcrop) to constrain the mantle source. Olivine and clinopyroxene were the main liquidus phases (at pressures lower than 2.5 GPa), with hydrous minerals and carbonates appearing in the lower temperature experiments. Orthopyroxene never crystallized in this system (Foley and Andronikov, 2003). These results seem to exclude carbonated peridotites as a mantle source for UMLs, in agreement with other petrological experiments conducted on similar K_2O-rich compositions, thus highlighting the need for clinopyroxene, phlogopite and/or amphibole and olivine, plus different accessory phases (such as apatite and Ti—Mg oxides) to produce potassic or ultrapotassic, ultrabasic and CaO-rich melts (e.g., Novella and Frost, 2014; Foley et al., 2022; Shu et al., 2024; Innocenzi et al., 2024a, 2025; Prelević et al., 2024).

The need for a strongly metasomatised lithospheric mantle with such a composition (i.e., orthopyroxene-free and enriched in clinopyroxene, phlogopite ± amphibole ± accessory minerals), either as a source or as a mantle domain that interacted with the ascending melt, is also highlighted by natural samples. Non-diamondiferous alnöites from New Zealand host an abundant cargo of peridotite xenoliths pervaded by hydrous metasomes (phlogopite + pargasite + clinopyroxene + carbonate + rutile + ilmenite + apatite), interpreted to be a mineral assemblage similar to the mantle source of the UMLs (Cooper et al., 2024). Overall, future research directions should include more experiments designed to address UML genesis.

4.4.3. Implications for diamond genesis and aillikite formation

Unfortunately, only a limited number of studies have been completed on diamonds from UMLs. For the Garnet Lake diamonds (Greenland), Hutchison and Heaman (2008) suggested that diamonds were fully formed before being entrained in the UML melt. Surprisingly, these authors also suggested that the small yellow diamonds (and their consequently short mantle residence time) may have formed in the melts, rather than prior to UML magmatism, to explain the very low N-aggregation state. However, many different surface features (such as ribs and serrate laminations) point to variable degrees of diamonds resorption prior to eruption, suggesting a lack of equilibrium between the diamonds and the hosting melt.

At 6 GPa and 1252–1327 °C (conditions reconstructed from the xenoliths, see 4.4.1 Constraints from mantle samples), a relatively short mantle residence time of <42 Myr would be required to ensure the low N-aggregation state (26%N_A, Hutchison and Heaman, 2008). This is in agreement with the work of Hutchison and Frei (2009) who proposed an extremely short mantle residence time, of about 5 Ma, for almost half of the studied diamonds from the Garnet Lake UML. However, without an inclusion study it is impossible to know the residence temperature for these diamonds, which could be significantly longer if they resided close to the graphite stability field.

Constraints on the pressures and depth of Eurelia diamonds are based on their superdeep mineral inclusion assemblages, which indicate a formation depth >670 km (Tappert et al., 2009b). For these diamonds, a short residence time (about 100 Myr) at high temperature (about 1300 °C) is inferred based on the low N contents and high N-aggregation states (Tappert et al., 2009b). Moreover, the C isotopic composition of the Eurelia *superdeep* diamonds is unlike typical mantle compositions of kimberlites/alnoites and suggests that recycling of oceanic carbonate sediments must have taken place beneath Southern Australia, probably as a consequence of the subduction processes occurring along the southern edge of Gondwana, which started between the Early to Middle Cambrian (Tappert et al., 2009b).

In Eurelia UMLs, *superdeep* diamonds coexist with lithospheric diamonds, which may have been entrained during ascent of UML melts to the surface.

4.5. The kimberlite-aillikite connection

Kimberlites are often spatially and temporally related with other related rock-types, such as carbonatites (e.g., Alto Paranaíba Igneous Province in Brazil; Guarino et al., 2013) and ultramafic lamprophyres (e.g., the Karelian craton in Finland, the Batain Nappes in Oman or the Torngat Mountains in Canada; Tappe et al., 2008a; Nasir et al., 2011; Dalton et al., 2019). The genetic link between kimberlite, lamproites, lamprophyres and carbonatites is highly debated (e.g., Tappe et al., 2008b; Mitchell and Tappe, 2010; Dalton et al., 2019). Some authors support the idea of a common source (a carbonate-bearing lherzolitic mantle) for kimberlites and UMLs, particularly aillikites (e.g., Dalton and Presnall, 1998; Francis and Patterson, 2009; Smith et al., 2013; Kargin et al., 2021). Parental melts (enriched in carbonate) would produce aillikites at slightly higher degrees of partial melting while producing kimberlite as a consequence of interaction with the surrounding harzburgitic mantle (Francis and Patterson, 2009). This hypothesis is supported by petrological experiments, which demonstrated that kimberlites may be produced by an aillikite residual magma that variably interacted (and assimilated) with the surrounding peridotitic mantle rocks (Kargin et al., 2021). Nevertheless, many authors (e.g.,

Tappe et al., 2008b; Mitchell and Tappe, 2010; Dalton et al., 2019; Giuliani et al., 2024) tend to refute this hypothesis based on evidence from the many natural examples. For example, in one of the UML type localities (i.e., Aillik Bay, Canada), kimberlites are not observed, despite the UML melts having ascended through a depleted and harzburgitic mantle. Alternatively, a genetic relationship may exist between aillikites and carbonatites, since aillikites probably represent primitive melts, which may later differentiate to form carbonatites (e.g., by Tappe et al., 2008b; Nasir et al., 2011).

Despite the possible absence of a genetic relationship between kimberlites and aillikites, recent reviews of this topic (e.g., Pearson et al., 2019; Giuliani et al., 2024) report an overall similar radiogenic isotope composition.

From a petrographic and mineralogical point of view, despite the similar paragenesis, kimberlites are characterized by a general absence of feldspar and feldspathoid, and amphibole (e.g., Giuliani et al., 2024 and reference therein). Moreover, clinopyroxene is not a constituent of fresh and unaltered kimberlites. Kimberlites also show strongly zoned phlogopite (the amount of Al and Ba increases with decreasing Fe and Ti contents) and spinel (with a chromite core transitioning to a rim of titanomagnetite; Giuliani et al., 2024). In contrast, in aillikites, clinopyroxene and amphibole represent principal minerals (phenocrysts or groundmass phases) and the mineral chemical composition of the common phases is slightly different. For example, when compared to kimberlites, aillikite phlogopites (but also UMLs and CALs in general) have higher values of TiO_2, FeO, with similar Al_2O_3 contents (e.g., Giuliani et al., 2024 and reference therein).

A strong overlap (for both major oxides and isotopic data) is observed between kimberlite and aillikites (see Supplementary Material 1), although this is in part due to the large variability in kimberlite compositions. Considering only the values included between the first and the third interquartile, kimberlite and aillikites have a similar SiO_2 content (27.1–34.8 wt% for kimberlites and 26.8–34.3 wt% for aillikites). Aillikites show higher TiO_2 (2.2–4.2 wt% vs. 0.8–2.3 wt% in kimberlite), Fe_2O_3 (11.3–15.4 wt% vs. 7.5–10.8 wt% in kimberlite) and K_2O (0.9–2.3 wt% vs. 0.3–1.5 wt% in kimberlite) but also slightly lower MgO (15.9–25.2 wt% vs. 22.7–31.4 wt% in kimberlite; see Supplementary Material 1). In most cases, trace element compositions overlap for kimberlites and aillikites (e.g., Pearson et al., 2019; Giuliani et al., 2024). From an isotopic point of view, a rough match can be observed between diamond-bearing aillikites and kimberlites. Nevertheless, Fig. 7 shows that, on average, diamond-bearing aillikites have slightly higher εNd_i and εSr_i (Fig. 7).

This broad similarity between kimberlites and aillikites probably suggests a similar metasomatized lithospheric mantle component involved in the formation of these rare melts (e.g., Dalton et al., 2019, 2022) that diversifies the signature of a parental melt coming from the sub-lithospheric convecting mantle. The differences may be related to slightly different metasomatic agents or fertilization events, depending on the time-integrated history of the lithospheric mantle as well as different metasome compositions and/or different degree of interaction. The mantle sources of kimberlites have yet to be constrained in terms of depth, paragenesis and composition, in spite of the large number of studies. A strongly metasomatized source, probably a H_2O- and CO_2-rich peridotite, may be needed to explain all the geochemical and isotopic features of kimberlites. Giuliani et al. (2024) identify three different source components for kimberlitic magmas: i) a mildly depleted convecting mantle, ii) a recycled crustal component (probably with a high sediment content); and iii) a metasomatized mantle associated with melt upwelling. For the Kuusamo Area (Karelian craton – Finland), Dalton et al. (2019) reported the presence of a UML dike (aillikite), together with kimberlites and lamproites, also suggesting a possible genetic link between UML and lamproites, but not with kimberlites, due to a significant difference in the emplacement age of the two lithologies. To explain the similarities (particularly observed in the ratios of incompatible trace elements) recorded between the kimberlitic pipes and the UML dike, they propose similar asthenospheric sources and melts that passed through similar metasomatised lithospheric mantle domains, during ascent to the Earth's surface (Dalton et al., 2019).

4.6. The diamond-aillikites association

As is the case for CALs, kimberlites and lamproites, no rigorous evidence indicating a genetic link between aillikites and the diamonds they contain has been proposed. However, it is likely that a temporal and spatial link exists between diamonds and their host aillikites. The formation of diamondiferous aillikites appears to depend on many factors, such as the presence of metasomatized mantle characterized by C- and H-bearing phases. In particular cratonic mantle regions, several (re-) enrichment processes stabilized C- and H-bearing phases, making them good candidates also to generate aillikitic melts and also to host diamond-forming events (see below). Moreover, in order for the melt to entrain diamonds from the mantle wall-rock, it must form at specific depth ranges (in the diamond stability field) and have particular ascent rates. These variables can strongly affect the stability of the diamonds in aillikitic melts, resulting in much rarer diamondiferous aillikites occurrences when compared to kimberlites.

The depth of melting is fundamental, as the typical depth for diamond formation in the cratonic lithospheric mantle ranges from 120 to 250 km (e.g., Day et al., 2023). It is generally accepted that kimberlite represents magma derived from the deepest mantle source as evidenced by the presence of *superdeep* (300–800 km) diamonds in kimberlites (e.g., Day et al., 2023; Giuliani et al., 2024). Interestingly, many studies report kimberlites that form below the lithosphere-asthenosphere boundary, down to the transition zone and/or the uppermost lower mantle (e.g., Pearson et al., 2019; Giuliani et al., 2024 and reference therein). On the other hand, even if aillikite magmas form within the diamond-stability field, they are probably characterized by a relatively shallower source compared to kimberlites, reducing the probability that aillikites entrain diamonds. This depends on the different geodynamic settings in which the various magma types are emplaced. Indeed, detailed studies on >1000 kimberlite, lamproite and lamprophyre rock-types (Skinner et al., 1992; Jaques and Milligan, 2004), both in Australia and southern Africa, highlighted a concentration of kimberlites on stable cratonic nuclei (also along their borders), of lamproites along the edges of cratonic nuclei and in the orogenic belts that comprise the broader cratonic framework (using the definition of Pearson et al., 2021), and of lamprophyres along cratonic edges (Chalapathi Rao, 2006). UMLs are mostly emplaced in extensional settings, along rift systems within or at the edges of cratons (e.g., the aillikite occurrences in western Greenland and in Labrador, which are often related to the Mesoproterozoic extension and the later formation of the Labrador Sea; Tappe et al., 2007, 2009).

Another crucial factor in controlling the occurrence of diamonds is the ascent velocity of magmas. Due to their enrichment in volatile elements (CO_2 up to 10–20 wt% and H_2O up to 15 wt%; Pearson et al., 2019; Giuliani et al., 2024) and low viscosity, kimberlites are considered among the fastest ascending melts on Earth – an observation also supported by Ar isotopic zoning studies on phlogopites in kimberlites (Kelley and Wartho, 2000). Volcanological models suggests that kimberlite melt ascends through very narrow fissures (<1 m thickness), with a maximum velocity between 16 and 90 m/s, until it reaches and breaks the surface, causing a drastic increase in speed (e.g., Sparks et al., 2006; Wilson and Head, 2007; Russell et al., 2019). As UMLs have received much less attention than kimberlites, detailed volcanological reconstructions have yet to be made. The presence of mantle xenoliths is very common in UMLs (e.g., Foley et al., 2006; Bernstein et al., 2013; Cooper et al., 2024), whether they contain diamonds or not, testifying to a relatively rapid ascent rate. This is also documented by the volatile-rich composition of UML magmas (e.g., median CO_2 and H_2O contents of ~5.3 wt% and ~ 4.7 wt%, respectively; Giuliani et al., 2024).

If the presence of extensively metasomatized mantle regions, the

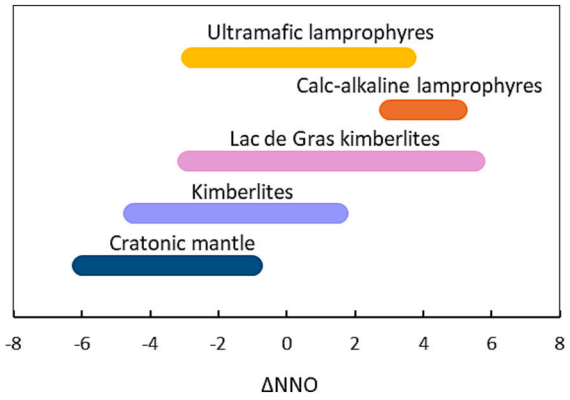


Fig. 11. Oxygen fugacity (ΔNNO) for the diamond-bearing rocks discussed in this study. References for kimberlites are from Canil and Bellis (2007); Dongre and Tappe (2019); Ogilvie-Harris et al. (2009) and Chalapathi Rao et al. (2011), for ultramafic lamprophyres (to have more constraints not only aillikites are reported, but the data for the whole UML rock group) are form Tappe et al. (2006); Nosova et al. (2018); Prokopyev et al. (2020); Carniel et al. (2020); Nugumanova et al. (2021); Starikova et al. (2021); and Doroshkevich et al. (2022), for calc-alkaline lamprophyres are from Carmichael (1991); and for the cratonic mantle are from McCammon and Kopylova (2004) and Woodland and Koch (2003). Modified after Canil and Bellis (2007).

depth of aillikitic melt formation and their ascent rate all conspire to ensure the presence of diamond in aillikites, there are many other factors that influence the diamond stability in such melts. The large abundance of microdiamonds (and the scarcity of macrodiamonds), coupled with common resorption features for aillikitic diamonds suggest a general lack of equilibrium between the diamond and the hosting magma, which in-turn, also supports the absence of any genetic connection.

Aillikites are commonly observed as hypabyssal bodies (dykes and sills, e.g., Foley et al., 2002; Tappe et al., 2008a, 2009) and are therefore considered to have slower final magma ascent rates and much lower magma volumes and hence melt-transfer rates, in the upper crust, compared to the explosive eruptions that characterize kimberlites (Kamvisis and Phani, 2024).

It follows that the low volumes, and hence low magma fluxes of aillikitic melt during ascent should also be added. Russell and Jones (2023) suggested that duration and volume of magma emplacement (magma flux) may significatively affect the presence and the abundance of xenoliths (including diamonds) in the final deposit (Russell and Jones, 2023). Indeed, the strong density contrast between the xenoliths and the alkaline melts, which are characterized by low viscosity, result in a quick settling of the xenoliths in the host magma and in a significant lag time for the xenoliths (i.e., a xenolith reaches the surface later compared to the melt that first carried it, Russell and Jones, 2023). If the eruption is short-lived, the magma volume is not sufficient and/or the melt stagnate at depth, the xenoliths may not be able to reach the surface (Russell and Jones, 2023). Moreover, for diamonds in aillikites, a prolonged lag time may result in a total dissolution.

Lower ascent rates, xenocrysts settling and a longer lag time for lamproites and lamprophyres could explain the morphology of the diamonds they contain, which commonly have irregular morphologies, which may indicate partial dissolution (e.g., Hall and Smith, 1984; Iakoubovskii and Adriaenssens, 2002; Hausel, 2006). Moreover, most of the diamondiferous aillikites contain mostly micro or small (< 0.5–1 mm) diamonds (e.g., Sutherland, 1996; Jaques, 1994; Hutchison and Frei, 2009). For example, Hutchison and Heaman (2008) suggested that the diamonds recovered from the Garnet Lake body have undergone resorption due to the composition of the aillikitic magma, a factor that may be crucial for diamond preservation.

Diamond dissolution and resorption are very common processes that may occur in all diamond-bearing rocks including kimberlites and lamproites. The oxygen fugacity of the hosting melts is a key factor controlling diamond stability. When compared to the average kimberlite fO_2, UMLs show more oxidizing redox conditions, and even higher values are recorded for CALs (Fig. 11). Literature studies report that oxygen fugacity ranges between −3 to almost +4 ΔNNO units for UMLs (Tappe et al., 2006; Nosova et al., 2018; Prokopyev et al., 2020; Carniel et al., 2020; Nugumanova et al., 2021; Starikova et al., 2021 and Doroshkevich et al., 2022) and between +2.5 and + 5 ΔNNO units for CALs (Carmichael, 1991). Such values may indicate that lamprophyric melts are oxidized during crystallization and during their ascent to the surface, providing a hostile environment for the diamonds they may entrain. It is also important to keep in mind that the metasomatised lithospheric mantle plays an important role in the aillikites formation (whether it represents the source or simply a minor mantle component) and it may represent an oxidized domain, at least in part (e.g., Foley, 2008), strongly affecting the conditions of the melts and the stability of diamonds.

Moreover, redox conditions strongly control the speciation of carbon. In the most reducing areas of the depleted peridotitic mantle beneath cratons, C is stabilized (due to redox freezing) as diamonds. In more oxidized conditions, such as in some metasomatised portion of the lithospheric mantle, that undergoes several refertilization events, carbonates may be present (e.g., Foley and Fischer, 2017; Yaxley et al., 2019). At fO_2 higher than −1.2 to −0.5 units FMQ, CO_2, dolomite or magnesite are stable, depending on the depth and the local cratonic geotherm (Yaxley et al., 2019). As for the formation of UMLs, carbonate is invoked as a mantle source phase (e.g., Foley et al., 2002; Tappe et al., 2008a) under oxidized conditions, the presence of CO_2 may play a fundamental in the formation of aillikitic melts, by lowering melting temperature of the mantle rocks (e.g., Foley and Fischer, 2017).

However, Fig. 11 highlights the extremely large range of ΔNNO for the Lac de Gras kimberlites, which approach +6. Despite these oxidized conditions (even higher than in lamprophyres) Lac de Gras kimberlites represent an extremely important source for natural diamonds (e.g., Curtolo et al., 2023). Moreover, Dalton et al. (2022) report a larger interaction between lamproites and the metasomatised lithospheric mantle when compared to the aillikites, resulting in oxidizing conditions also in lamproitic magmas. As a lamproite hosts the largest magmatic deposit for diamonds on Earth, diamond dissolution is not solely controlled by oxygen fugacity, additional factors (e.g., the volume of magma emplaced, the velocity of ascent and the prolonged lag time) play a crucial role.

Experimental studies, carried out at different pressure conditions, show that the melt composition (especially the volatile content), the oxygen fugacity and the temperature of the system strongly affect the stability and the preservation of diamonds (e.g., Fedortchouk et al., 2007; Khokhryakov et al., 2021). Most importantly, the presence of a fluid (either H_2O or CO_2), rather than the melt itself, seems to drastically increase the degree of diamond resorption (Fedortchouk et al., 2007).

Magmas with higher H_2O content (up to 10 wt% in the experiments compared to ~15 wt% in kimberlites and ~ 2–6 wt% in UMLs) are the most reactive with diamonds (e.g., Khokhryakov et al., 2021). The highest degree of diamond resorption is recorded for H_2O-rich melts (intermediate composition between carbonatites and kimberlites), at 1200 °C and specific redox conditions, and in carbonatite melts (containing H_2O), in a more oxidizing system (Khokhryakov et al., 2021). At higher temperatures (up to 1400 °C), carbonatites are the most conducive to diamond resorption (Khokhryakov et al., 2021). Unfortunately, most of these experiments focus solely on kimberlite melts and thus the effect of lamprophyre melt composition on diamond resorption rates is still largely unknown. However, it is likely that the oxygen fugacity and H_2O + CO_2 contents of UML and CAL melts, along with slower ascent velocities, are responsible for the small size and common resorption features of diamonds recovered from lamprophyres. As kimberlite magma temperatures are believed to be higher than for lamprophyres (e.

g., Tappe et al., 2025), it follows that temperature may affect diamond resorption rates less than magma composition.

5. Conclusions

The term lamprophyre refers to a wide range of geochemical (from ultrabasic to intermediate, variably enriched in alkalis, CaO and MgO) and mineralogical (different contents of phlogopite, amphibole, feldspathoids and feldspars) compositions. They can be divided into CAL - calc-alkaline (feldspar-bearing rocks with amphibole ± biotite ± clinopyroxene ± olivine), AL - alkaline (feldspathoid and feldspars-bearing rocks with brown amphibole + augite + olivine + brown mica) and UML - ultramafic (ultramafic, potassic or ultrapotassic and silica-undersaturated compositions, rich in olivine and phlogopite) lamprophyres.

Despite their scarcity, diamonds have been reported for all three lamprophyre rock-types:

1) Diamondiferous CALs are found in Canada (Parker Lake area - Akluilâk dykes, Wawa and Abitibi sub-province and Knee Lake area) and South America (Dachine ultramafic outcrop - French Guiana). CAL magmas form from low degree partial melting of shallow metasomatized (amphibole- and/or phlogopite-bearing) mantle resulting from crustal recycling and slab dehydration. To reconcile the shallow (relatively low P/T) formation depth of CAL magmas with the presence of diamonds, a subduction-related model has been proposed, ensuring the formation of diamond-stable conditions at relatively low pressures (80–100 km and 2–3 GPa), in a cold and thick shallow-angle slab. To address several implausibilities with this hypothesis, a multi-stage transport model was proposed where diamonds would first be transported from the deeper mantle to a shallower environment in which CAL magmas can form and thus entrain such diamonds. We proposed an alternative hypothesis to explain the Archean diamond-bearing CALs, in which lithospheric stacking occurs during the initial phases of cratons formation. The geotherm resulting from the stacking of two or three slabs is highly transient for the first 500 Ma and experiences rapid thermal fluctuations, especially in the first 5–100 Ma. It follows that the diamond stability field can be much shallower than in "steady-state" conditions would suggest, starting around 100/110 km depth, and time-integrated mantle residence temperatures, even for long mantle residence times, are significantly lower (Pearson et al., 2026).
2) Diamondiferous ALs are found in Australia (Wandagee area) and Japan (Shikoku Island). Unfortunately, no studies have been conducted on these diamonds and thus genetic links between AL magmatism and diamond formation have not been constrained.
3) Diamondiferous UMLs are found in Australia (Bulljah pipes - Earaheedy Basin and Eurelia - Adelaide Fold Belt), Canada (Torngat Mountains; Ontario), Greenland (the Diamond Province and the Qeqertaa dike - Disko Bay) and India (Wajrakarur kimberlite field). Petrological, geochemical and experimental studies highlight the need for a veined mantle, with metasomes of carbonate, phlogopite and variable accessory phases (such as oxides and apatite), to produce ultrabasic and potassic to ultrapotassic aillikites. As a direct genetic link between diamonds and aillikitic magmas can be excluded, the occurrence of diamondiferous aillikites is best interpreted as the result of a spatial and temporal association. This may depend on the presence of lithospheric to asthenospheric mantle assemblages, enriched in C—H fluids, coupled with the high ascent rate of aillikitic melts, that can explain the occurrence and the entrainment of diamond by aillikitic melts. Nevertheless, aillikites are an extremely hostile magma for diamonds, mostly due to their high oxygen fugacity and their high $H_2O + CO_2$ contents, along with slower ascent velocities and longer lag times, suggesting that only those melts with the highest magma flux manage to transport their diamond cargo into the crust.

Despite recent progress in understanding the petrogenesis of lamprophyres, several fundamental questions regarding their occurrence, magmatic evolution and, in particular, their genetic relationship with diamond, remain largely unanswered. This is likely related to the comparatively small amount of available data (compared to kimberlites) on lamprophyres, particularly diamondiferous lamprophyres. Consequently, petrogenetic models for lamprophyres, and/or the diamonds they contain, are likely overly simplistic and few studies have been conducted on the lamprophyre-diamond association. To close this gap, detailed mineralogical, petrological and geochemical studies must be conducted on the lamprophyres and the diamonds they host. Characterization of the mineral inclusions in lamprophyric diamonds is still very limited and will be fundamental to reconstruct the mantle paragenesis and to highlight differences with kimberlitic and lamproitic diamonds. Dating such inclusions will allow temporal reconstruction of the lamprophyre-diamond associations. On the other hand, a systematic study of global occurrences, combining mineral chemical, geochemical and isotopic data is required to reconstruct the petrogenesis and evolution of the different lamprophyres. Unconventional isotope analyses may provide further constraints on the nature of the metasomatic agents and the involvement of recycled crustal materials. In situ isotopes may help to mitigate the effect of the quite common alteration effect in many lamprophyres, but also to distinguish the origin of different mineral phases.

Moreover, HP-HT experiments aimed at reconstructing the exact paragenesis of the respective mantle sources (e.g., peridotitic, hydrous pyroxenitic or eclogitic paragenesis) and associated $P/T/fO_2$ conditions of lamprophyre formation, as well as the related metasomatic processes, are needed to further advance our understanding of lamprophyres. Experimental petrology may be fundamental in reconstructing the exact depth of formation of lamprophyres, possibly providing other solutions for the presence of diamonds in CALs. Finally, HP-HT experiments may also shed light on the stability of diamonds in lamprophyric melts, specifically clarifying how parameters such as volatile content and speciation, fO_2 and P/T may affect diamond resorption rates. Volcanological models may also play a crucial role in constraining the ascent rate of lamprophyric and lamproitic magmas. Understanding these geochemical, geodynamic and volcanological processes is a fundamental first-step in constructing a comprehensive framework to explain the genetic relationship between lamprophyres and diamonds.

Declaration of competing interest

The authors have no financial or non-financial conflicts of interest to disclose. The authors confirm that this work is original and has not been published elsewhere, nor is it currently under consideration for publication elsewhere. No artificial intelligence tools or services were used to write, construct or organize any part of this manuscript.

Acknowledgements

The authors thank Andrea Pezzera and Troels Nielsen for sharing the photograph of their lamprophyre samples. The authors thank A. Lynton Jaques, Hilary Downes, Dejan Prelević and Anna Nosova reviewer for their constructive reviews which improved the manuscript considerably.

This work was funded by the European Union (ERC, INHERIT, starting Grant No. 101041620). Views and opinions expressed are, however, those of the author(s) only and do not necessarily reflect those of the European Union or the European Research Council Executive Agency. Neither the European Union nor the granting authority can be held responsible for them.

Appendix A. Supplementary data

Supplementary data to this article can be found online at https://doi.org/10.1016/j.earscirev.2026.105603.

Data availability

The online version contains Supplementary Material 1 available at https://doi.org/10.1016/j.earscirev.2026.105603. Supplementary Material can also be accessed from the University of Padova repository at https://researchdata.cab.unipd.it/id/eprint/1860.

References

Abdelfadil, K.M., Romer, R.L., Seifert, T., Lobst, R., 2013. Calc-alkaline lamprophyres from Lusatia (Germany)-evidence for a repeatedly enriched mantle source. Chem. Geol. 353, 230–245. https://doi.org/10.1016/j.chemgeo.2012.10.023.

Aghazadeh, M., Prelević, D., Badrzadeh, Z., Braschi, E., van den Bogaard, P., Conticelli, S., 2015. Geochemistry, Sr–Nd–Pb isotopes and geochronology of amphibole- and mica-bearing lamprophyres in northwestern Iran: Implications for mantle wedge heterogeneity in a palaeo-subduction zone. Lithos 216–217, 352–369. https://doi.org/10.1016/j.lithos.2015.01.001.

Anderson, S.D., 2016. Alkaline Rocks at Oxford Lake and Knee Lake, Northwestern Superior Province, 653 Manitoba (NTS 53L13, 14, 15): Preliminary Results of New Bedrock Mapping and Lithogeochemistry.

Anderson, S.D., Syme, E.C., Corkery, M.T., Bailes, A.H., Lin, S., 2015. Preliminary results of bedrock mapping at 792 southern knee Lake, northwestern Superior province. Manitoba (Parts of NTS 53L14, 15) 9–23 (Report of 793 Activities 2015).

Archer, N.R., 1987. Ultramaflc Lamprophyres of the Yilgarn Craton Western Australia (Master Thesis). University of Western Australia, Perth.

Armstrong, J.P., Barnett, R.L., 2003. The association of Zn-chromite with diamondiferous lamprophyres and diamonds: unique compositions as a guide to the diamond potential of non-traditional diamond host rocks. In: International Kimberlite Conference: Extended Abstracts, Vol. 8.

Atkinson, W.J., Hughes, F.E., Smith, C.B., 1984. A review of the kimberlitic rocks of Western Australia. In: Kornprobst, J. (Ed.), Kimberlites 1: Kimberlites and Related Rocks. Elsevier, Amsterdam, pp. 195–224.

Atkinson, W.J., Smith, C.B., Danchin, R.V., Janse, A.J.A., 1990. Diamond deposits of Australia. In: Hughes, F.E. (Ed.), Geology of the Mineral Deposits of Australia and Papua New Guinea. Melbourne, pp. 69–76.

Ayer, J.A., Wyman, D.A., 2003. Origin of Diamondiferous Archean Lamprophyres in the Evolution of the Michipicoten and Abitibi Greenstone Belts, in: 8th International Kimberlite Conference Long Abstract.

Ayer, J.A., Conceicao, R.V., Ketchum, J.W.F., Sage, R.P., Semenyna, L., Wyman, D.A., 2003. The Timing and Petrogenesis of Diamondiferous Lamprophyres in the Michipicoten and Abitibi Greenstone Belts. Summary of Field Work and Other Activities 2003.

Bailey, D.K., 1970. Volatile flux, heat focusing and generation of magma. Geol. J. Spec. Iss. 2, 177–186.

Bailey, D.K., 1972. Uplift, rifting and magmatism in continental plates. J. Earth Sci. 8, 225–239.

Bailey, L.M., 1999. An Unusual Diamond-Bearing Talc Schist from the Dachine Area of French Guiana. Queen's University Kingston, Ontario, Canada.

Barron, L.M., Lishmund, S.R., Oakes, G.M., Barron, B.J., Sutherland, F.L., 1996. Subduction model for the origin of some diamonds in the Phanerozoic of eastern New South Wales. Austral. J. Earth Sci. 43, 257–267. https://doi.org/10.1080/08120099608728253.

Belyaev, V.A., Gornova, M.A., Gordienko, I.V., Karimov, A.A., Medvedev, A.Ya., Ivanov, A.V., Dril, S.I., Grigoriev, D.A., Belozerova, O.Yu., 2021. Late Cambrian calc-alkaline magmatism during transition from subduction to accretion: Insights from geochemistry of lamprophyre, dolerite and gabbro dikes in the Dzhida terrain, Central Asian orogenic belt. Lithos 386–387, 106044. https://doi.org/10.1016/j.lithos.2021.106044.

Bernstein, S., Szilas, K., Kelemen, P.B., 2013. Highly depleted cratonic mantle in West Greenland extending into diamond stability field in the Proterozoic. Lithos 168–169, 160–172. https://doi.org/10.1016/j.lithos.2013.02.011.

Bizzarro, M., Stevenson, R.K., 2003. Major element composition of the lithospheric mantle under the North Atlantic craton: evidence from peridotite xenoliths of the Sarfartoq area, southwestern Greenland. Contrib. Mineral. Petrol. 146, 223–240. https://doi.org/10.1007/s00410-003-0499-1.

Bodinier, J.-L., Godard, M., 2014. Orogenic, Ophiolitic, and Abyssal Peridotites. In: Treatise on Geochemistry. Elsevier, pp. 103–167. https://doi.org/10.1016/B978-0-08-095975-7.00204-7.

Brett, R.C., Russell, J.K., Andrews, G.D.M., Jones, T.J., 2015. The ascent of kimberlite: Insights from olivine. Earth Planet. Sci. Lett. 424, 119–131. https://doi.org/10.1016/j.epsl.2015.05.024.

Brown, R.J., Manya, S., Buisman, I., Fontana, G., Field, M., Niocaill, C. Mac, Sparks, R.S. J., Stuart, F.M., 2012. Eruption of kimberlite magmas: physical volcanology, geomorphology and age of the youngest kimberlitic volcanoes known on earth (the Upper Pleistocene/Holocene Igwisi Hills volcanoes, Tanzania). Bull. Volcanol. 74, 1621–1643. https://doi.org/10.1007/s00445-012-0619-8.

Buckle, J., 2002. The Wawa diamond enigma. CIM Bull. 95, 85–87.

Canil, D., Bellis, A.J., 2007. Ferric iron in CaTiO3 perovskite as an oxygen barometer for kimberlite magmas II: applications. J. Petrol. 48, 231–252.

Carlson, J.A., Adams, G.W., 1997. The diamondiferous six-pack ultramafic lamprophyre diatreme, Kenosha, Wisconsin, USA. Institute on Lake Superior Geology. In: Proceedings of the 43rd Annual Meeting. Sudbury, Ontario, pp. 11–12.

Carmichael, I.S.E., 1991. The redox states of basic and silicic magmas: a reflection of their source regions? Contrib. Mineral. Petrol. 106, 129–141.

Carniel, L.C., Conceição, R.V., Klemme, S., Berndt, J., Jalowitzki, T., 2020. Origin and redox conditions of the Rosário-6 alnöite of southern Brazil: Implications for the state of the mantle during Gondwana breakup. Lithos 376–377, 105751. https://doi.org/10.1016/j.lithos.2020.105751.

Cartigny, P., 2010. Mantle-related carbonados? Geochemical insights from diamonds from the Dachine komatiite (French Guiana). Earth Planet. Sci. Lett. 296, 329–339. https://doi.org/10.1016/j.epsl.2010.05.015.

Cartigny, P., Harris, J.W., Javoy, M., 2001. Diamond genesis, mantle fractionations and mantle nitrogen content: a study of δ13C–N concentrations in diamonds. Earth Planet. Sci. Lett. 185, 85–98. https://doi.org/10.1016/S0012-821X(00)00357-5.

Cartigny, P., Chinn, I., Viljoen, K.S., Robinson, D., 2004. Early proterozoic ultrahigh pressure metamorphism: evidence from microdiamonds. Science 1979, 853–855.

Chalapathi Rao, N.V., 2006. Mesoproterozoic diamondiferous ultramafic pipes at Majhgawan and Hinota, Panna area, Central India: Key to the nature of sub-continental lithospheric mantle beneath the Vindhyan basin. J. Earth Syst. Sci. 115, 161–183. https://doi.org/10.1007/BF02703032.

Chalapathi Rao, N.V., Paton, C., Lehmann, B., 2011. Origin and diamond prospectivity of mesoproterozoic kimberlites from the Narayanpet field, Eastern Dharwar Craton, southern India: insights from groundmass mineralogy, bulk-chemistry and perovskite oxybarometry. Geol. J. 47, 2–3.

Chalapathi Rao, N.V., Dongre, A., Wu, F.-Y., Lehmann, B., 2016. A late cretaceous (ca. 90 Ma) kimberlite event in southern India: Implication for sub-continental lithospheric mantle evolution and diamond exploration. Gondwana Res. 35, 378–389. https://doi.org/10.1016/j.gr.2015.06.006.

Chalapathi Rao, N.V., Giri, R.K., Sharma, A., Pandey, A., 2020. Lamprophyres from the Indian shield: a review of their occurrence, petrology, tectonomagmatic significance and relationship with the Kimberlites and related rocks. Episodes 43, 231–248. https://doi.org/10.18814/EPIIUGS/2020/020014.

Chinn, I., Kyser, K., Viljoen, F., 2000. Microdiamonds from the Thirsty Lake (Akluilâk) Dyke, Northwest Territories, Canada. J. Confer. Abstr. 5, 307–308.

Choi, E., Fiorentini, M.L., Giuliani, A., Foley, S.F., Maas, R., Graham, S., 2021. Petrogenesis of Proterozoic alkaline ultramafic rocks in the Yilgarn Craton, Western Australia. Gondwana Res. 93, 197–217. https://doi.org/10.1016/j.gr.2021.01.011.

Clark, F., Sarkar, C., Stahcel, T., Grütter, H.S., Pearson, D.G., 2024. Magmatic expressions of the Mesoproterozoic Midcontinent Rift and consequences for sampling diamonds – Ultramafic lamprophyres from the Superior craton. In: In: 12th International Kimberlite Conference Extended Abstract. Yellowknife. https://doi.org/10.1016/j.lithos.2022.106966.

Coates, H.J., Sobie, P.A., Brett, S., 2006. Technical Report on the Torngat Diamond Property, Nunavik Region. Quebec For Twin mining corporation, Toronto, Ontario, Canada.

Cooper, N.P., Scott, J.M., Brenna, M., Palmer, M.C., le Roux, P.J., Cooper, A.F., Reid, M. R., Stirling, C.H., 2024. Hydrous veined mantle lithosphere and implications for the source of Zealandia intraplate magmas. Lithos 478–479. https://doi.org/10.1016/j.lithos.2024.107608.

Curtolo, A., Novella, D., Logvinova, A., Sobolev, N.V., Davies, R.M., Day, M.C., Pamato, M.G., Nestola, F., 2023. Petrology and geochemistry of Canadian diamonds: an up-to-date review. Earth Sci. Rev. 246, 104588. https://doi.org/10.1016/j.earscirev.2023.104588.

Curtolo, A., Day, M.C., Innocenzi, F., Bolfan-Casanova, N., Pamato, M.G., Falvard, S., Nestola, F., Harris, J.W., Novella, D., 2025. H2O in nominally anhydrous mineral inclusions in diamonds and the volatile composition of diamond forming media. Earth Planet. Sci. Lett. 658, 119311. https://doi.org/10.1016/j.epsl.2025.119311.

Dalton, H., Giuliani, A., O'Brien, H., Phillips, D., Hergt, J., Maas, R., 2019. Petrogenesis of a hybrid cluster of evolved kimberlites and ultramafic lamprophyres in the Kuusamo area, Finland. J. Petrol. 60, 2025–2050.

Dalton, H., Giuliani, A., Hergt, J., Phillips, D., O'Brien, H., Ballmer, M.D., Maas, R., Woodhead, J., 2022. Geodynamic and isotopic constraints on the genesis of kimberlites, lamproites and related magmas from the Finnish segment of the Karelian craton. Geochem. Geophys. Geosyst. 23, e2021GC010324. https://doi.org/10.1029/2021GC010324.

Dalton, H., Giuliani, A., Fitzpayne, A., Peters, B.J., 2025. New geochemical and Sr-Nd-Hf isotopic constraints on the genesis of kimberlites and ultramafic lamprophyres from the Adelaide Fold Belt and Gawler Craton, South Australia. Mineral. Petrol. 119, 1043–1068. https://doi.org/10.1007/s00710-025-00938-w.

Dalton, J.A., Presnall, D.C., 1998. The Continuum of primary Carbonatitic-Kimberlitic Melt Compositions in Equilibrium with Lherzolite: Data from the System CaO-MgO-Al2O3-SiO2-CO2 at 6 GPa. J. Petrol. 39, 1953–1964. https://doi.org/10.1093/petroj/39.11-12.1953.

Davis, F.A., Hirschmann, M.M., Humayun, M., 2011. The composition of the incipient partial melt of garnet peridotite at 3 GPa and the origin of OIB. Earth Planet. Sci. Lett. 308, 380–390. https://doi.org/10.1016/j.epsl.2011.06.008.

Dawson, J.B., 1984. In: Kornprobst, J. (Ed.), Contrasting Types of Upper-Mantle Metasomatism?. The Mantle and Crust-Mantle Relationships, Kimberlites II, pp. 289–294. https://doi.org/10.1016/B978-0-444-42274-3.50030-5.

Day, M.C., Pamato, M.G., Novella, D., Nestola, F., 2023. Imperfections in natural diamond: the key to understanding diamond genesis and the mantle. Riv. Nuovo Cimento 46, 381–471. https://doi.org/10.1007/s40766-023-00045-6.

Day, M.C., Jollands, M.C., Novella, D., Nestola, F., Dovesi, R., Pamato, M.G., 2024. Hydrogen-related defects in diamond: a comparison between observed and calculated FTIR spectra. Diam. Relat. Mater. 143, 110866. https://doi.org/10.1016/j.diamond.2024.110866.

Day, M.C., Innocenzi, F., Pearson, D.G., Stachel, T., Kohn, S.C., Jollands, M.C., Chinn, I., Jalowitzki, T.L.R., La Fortezza, M., Nestola, F., Newton, M.E., Novella, D., Shirey, S.

B., Smit, K.V., Speich, L., Timmerman, S., Pamato, M.G., 2026. An Updated and Expanded Type Classification Scheme for Diamonds Based on FTIR Spectroscopic Data. Am. Min. https://doi.org/10.2138/am-2026-10296.
Day, Maxwell C., Jollands, M.C., Innocenzi, F., Novella, D., Nestola, F., Pamato, M.G., 2025. Infrared spectroscopy of natural Type Ib diamond: insights into the formation of Y -centers and the early aggregation of nitrogen. Am. Mineral. https://doi.org/10.2138/am-2024-9722.
De Stefano, A., Lefebvre, N., Kopylova, M., 2006. Enigmatic diamonds in Archean calc-alkaline lamprophyres of Wawa, southern Ontario, Canada. Contrib. Mineral. Petrol. 151, 158–173. https://doi.org/10.1007/s00410-005.
De Stefano, A., Kopylova, M.G., Cartigny, P., Lefebvre, N.S., 2008. C and N isotope compositions of diamonds from the calc-alkaline lamprophyres of Wawa (Superior craton). In: In International Kimberlite Conference: Extended Abstracts, Vol. 9.
Digonnet, S., Goulet, N., Bourne, J., Stevenson, R., Archibald, D., 2000. Petrology of the Abloviak aillikite dykes, New Québec: evidence for a Cambrian diamondiferous alkaline province in northeastern North America. Can. J. Earth Sci. 37, 517–533.
Dilek, Y., 2003. Ophiolite concept and its evolution. In: Dilek, Y., Newcomb, S. (Eds.), Ophiolite Concept and the Evolution of Geological Thought. Geological Society of America, Boulder, Colorado, p. 1. https://doi.org/10.1130/0-8137-2373-6.1.
Dilek, Y., Furnes, H., 2014. Ophiolite genesis and global tectonics: Geochemical and tectonic fingerprinting of ancient oceanic lithosphere. Geol. Soc. Am. Bull. 123, 387–411.
Dongre, A., Tappe, S., 2019. Kimberlite and carbonatite dykes within the Premier diatreme root (Cullinan Diamond Mine, South Africa): New insights to mineralogical-genetic classifications and magma CO_2 degassing. Lithos 338-339, 155–173.
Dongre, A., Viljoen, K.S., Belyanin, G., Le Roux, P., Malandkar, M., 2020. Petrogenesis of the diamondiferous Pipe-8 ultramafic intrusion from the Wajrakarur kimberlite field of Southern India and its relation to the worldwide Mesoproterozoic (~1.1 Ga) magmatism of kimberlite and related rocks. Geosci. Front. 11, 793–805. https://doi.org/10.1016/j.gsf.2019.07.010.
Doroshkevich, A., Prokopyev, I., Kruk, M., Sharygin, V., Izbrodin, I., Starikova, A., Ponomarchuk, A., Izokh, A., Nugumanova, Y., 2022. Age and petrogenesis of ultramafic lamprophyres of the Arbarastakh alkaline-carbonatite complex, Aldan-Stanovoy shield, South of Siberian Craton (Russia): evidence for ultramafic lamprophyre-carbonatite link. J. Petrol. 63, egac073.
Downes, H., 2001. Formation and modification of the shallow sub-continental lithospheric mantle: a review of geochemical evidence from ultramafic xenolith suites and tectonically emplaced ultramafic Massifs of Western and Central Europe. J. Petrol. 42, 233–250. https://doi.org/10.1093/petrology/42.1.233.
Downes, P.J., Jaques, A.L., Talavera, C., Griffin, W.L., Gain, S.E.M., Evans, N.J., Taylor, W.R., Verrall, M., 2023. Perovskite geochronology and petrogenesis of the Neoproterozoic Mad Gap Yards ultramafic lamprophyre dykes, East Kimberley region, Western Australia. Contrib. Mineral. Petrol. 178, 21. https://doi.org/10.1007/s00410-023-02002-2.
Edwards, D.M., 2019. Investigating the Deep Carbon Cycle through the Experimental Study of Simple Carbonate Systems. University of Bristol.
Ehrenberg, S.N., 1979. Garnetiferous ultramafic inclusions in minette from the Navajo volcanic field. In: The Mantle Sample: Inclusion in Kimberlites and Other Volcanics. American Geophysical Union, Washington, D. C., pp. 330–344. https://doi.org/10.1029/SP016p0330
Escher, A., Watterson, J., 1973. Kimberlites and assocaited rocks in the Holsteinborg - Sondre Stromfjord region, central West Greenland. Rapp. Grønl. Geol. Unders. 55, 26–27.
Esperança, S., Holloway, J.R., 1987. On the origin of some mica-lamprophyres: experimental evidence from a mafic minette. Contrib. Mineral. Petrol. 95, 207–216. https://doi.org/10.1007/BF00381270.
Faure, S. World Kimberlites CONSOREM Database (Version 3). Consortium de Recherche en Exploration Minérale CONSOREM, Université du Québec à Montréal.
Fedortchouk, Y., Canil, D., Semenets, E., 2007. Mechanisms of diamond oxidation and their bearing on the fluid composition in kimberlite magmas. Am. Mineral. 92, 1200–1212. https://doi.org/10.2138/am.2007.2416.
Fitzpayne, A., Giuliani, A., Hergt, J., Phillips, D., Janney, P., 2018. New geochemical constraints on the origins of MARID and PIC rocks: Implications for mantle metasomatism and mantle-derived potassic magmatism. Lithos 318–319, 478–493. https://doi.org/10.1016/j.lithos.2018.08.036.
Foley, S., 1992. Vein-plus-wall-rock melting mechanisms in the lithosphere and the origin of potassic alkaline magmas. Lithos 28, 435–453.
Foley, S.F., 1990. A review and assessment of experiments on Kimberlites, Lamproites and Lamprophyres as a guide to their Origin. Proc. Indian Natl. Sci. Acad. 99, 57–80.
Foley, S.F., 2008. Rejuvenation and erosion of the cratonic lithosphere. Nature geoscience 1 (8), 503–510.
Foley, S.F., Andronikov, A.V., 2003. The Genesis of Ultramafic Lamprophyres, in: 8th International Kimberlite Conference Long Abstract (Victoria).
Foley, S.F., Fischer, T.P., 2017. An essential role for continental rifts and lithosphere in the deep carbon cycle. Nature Geoscience 10 (12), 897–902.
Foley, S.F., Pintér, Z., 2018. Primary melt compositions in the earth's mantle. In: Magmas Under Pressure: Advances in High-Pressure Experiments on Structure and Properties of Melts. Elsevier, pp. 3–42. https://doi.org/10.1016/B978-0-12-811301-1.00001-0.
Foley, S.F., Andronikov, A.V., Melzer, S., 2002. Petrology of ultramafic lamprophyres from the Beaver Lake area of Eastern Antarctica and their relation to the breakup of Gondwanaland. Mineral. Petrol. 74, 361–384. https://doi.org/10.1007/s007100200011.
Foley, S.F., Andronikov, A.V., Jacob, D.E., Melzer, S., 2006. Evidence from Antarctic mantle peridotite xenoliths for changes in mineralogy, geochemistry and geothermal gradients beneath a developing rift. Geochim. Cosmochim. Acta 70, 3096–3120. https://doi.org/10.1016/j.gca.2006.03.010.
Foley, S.F., Ezad, I.S., van der Laan, S.R., Pertermann, M., 2022. Melting of hydrous pyroxenites with alkali amphiboles in the continental mantle: 1. Melting relations and major element compositions of melts. Geosci. Front. 13, 101380. https://doi.org/10.1016/j.gsf.2022.101380.
Foley, S.F., Ezad, I.S., Shu, C., Förster, M.W., 2025. Melting of amphibole-apatite-rich metasomes in the continental mantle and comparison of melt compositions with natural igneous rocks. Lithos 500–501, 107976. https://doi.org/10.1016/j.lithos.2025.107976.
Foley, S.F., Venturelli, G., Green, D.H., Toscani, L., 1987. The ultrapotassic rocks: characteristics, classification, and constraints for petrogenetic models. Earth-Science Reviews 24, 81–134.
Francis, D., Patterson, M., 2009. Kimberlites and aillikites as probes of the continental lithospheric mantle. Lithos 109, 72–80. https://doi.org/10.1016/j.lithos.2008.05.007.
Frey, F.A., Green, D.H., Roy, S.D., 1978. Integrated models of basalt petrogenesis: a study of quartz tholeiites to olivine melilitites from South Eastern Australia utilizing geochemical and experimental petrological data. J. Petrol. 19, 463–513.
Funk, S.P., Luth, R.W., 2012. An experimental study of a minette from the Milk River area, southern Alberta. Canada Contrib. Mineral. Petrol. 164, 999–1009. https://doi.org/10.1007/s00410-012-0785-x.
Funk, S.P., Luth, R.W., 2013. Melting phase relations of a mica-clinopyroxenite from the Milk River area, southern Alberta, Canada. Contrib. Mineral. Petrol. 166, 393–409. https://doi.org/10.1007/s00410-013-0881-6.
Gao, P., Santosh, M., Tsunogae, T., Yang, C.X., Nakagawa, M., Kim, S.W., Dong, Y., Liu, H.D., 2024. Miocene lamprophyre and felsic volcanics in the outer zone of SW Japan: arc building through multiple sources in an active convergent margin. Int. Geol. Rev. 66, 1335–1351. https://doi.org/10.1080/00206814.2023.2235691.
Giuliani, A., Pearson, D.G., 2019. Kimberlites: from deep earth to diamond mines. Elements 15, 377–380. https://doi.org/10.2138/GSELEMENTS.15.6.377.
Giuliani, A., Schmidt, M.W., Torsvik, T.H., Fedortchouk, Y., 2023. Genesis and evolution of kimberlites. Nat. Rev. Earth Environ. 4, 738–753. https://doi.org/10.1038/s43017-023-00481-2.
Giuliani, A., Dalton, H., Pearson, D.G., 2024. Kimberlites: the deepest geochemical probes of Earth. In: Reference Module in Earth Systems and Environmental Sciences. Elsevier. https://doi.org/10.1016/b978-0-323-99762-1.00064-4.
Goldschmidt, V.M., 1922. On the metasomatic processes in silicate rocks. Econ. Geol. 17, 105–123.
Goto, K., Arai, S., 1987. Petrology of peridotite xenoliths in lamprophyre from Shingu, southwestern Japan: implications for origin of Fe-rich mantle peridotites. Mineralogy and Petrology 37 (2), 137–155.
Graham, S., Shee, S., Smith, C.B., Hamilton, R., 1999. Re-Os and Sm-Nd Isotopic Constraints on the sources of Kimberlites and Melnoites, Earaheedy Basin. In: Western Australia-re-Os and Sm-Nd Isotopic Constraints on the Sources of Kimberlites and Melnoites, Earaheedy Basin, Western Australia.
Green, D.H., 1971. Composition of basaltic magmas as indicators of conditions of origin: application to oceanic volcanism. Philos. Trans. R. Soc. Lond. Ser. A 268, 707e725.
Griffin, W.L., O'Reilly, S.Y., Davies, R.M., Vokes, F.M., 1998. In: Marshall, B., Spry, P.G. (Eds.), Subduction-Related Diamond Deposits? Constraints, Possibilities, and New Data from Eastern Australia. Metamorphic and Metamorphogenic Ore Deposits. Society of Economic Geologists, pp. 1–20. https://doi.org/10.5382/Rev.11.13.
Griffin, W.L., Shee, S.R., Ryan, C.G., Win, T.T., Wyatt, B.A., 1999. Harzburgite to lherzolite and back again: metasomatic processes in ultramafic xenoliths from the Wesselton kimberlite, Kimberley, South Africa. Contrib. Mineral. Petrol. 134, 232–250.
Guarino, V., Wu, F.-Y., Lustrino, M., Melluso, L., Brotzu, P., Gomes, C. de B., Ruberti, E., Tassinari, C.C.G., Svisero, D.P., 2013. U–Pb ages, Sr–Nd- isotope geochemistry, and petrogenesis of kimberlites, kamafugites and phlogopite-picrites of the Alto Paranaíba Igneous Province, Brazil. Chem. Geol. 353, 65–82. https://doi.org/10.1016/j.chemgeo.2012.06.016.
Gumbel, C.W., 1874. Das japanische gesteine. Das Ausland.
Gurney, A., Helmstaedt, H.H., Le Roex, A.P., Nowicki, T.E., Richardson, S.H., Westerlund, K.J., 2005. Diamonds: crustal distribution and formation processes in time and space and an integrated deposit model. Soc Econ Geol 142–177.
Hall, A.E., Smith, C.B., 1984. Lamproite diamonds - are they different?. In: Kimberlite Occurrence and Origin: A Basis for Conceptual Models in Exploration. University of Western Australia - Special Publication, pp. 167–212.
Hamilton, R., Rock, N.M.S., 1990. Geochemistry, mineralogy and petrology of a new find of ultramafic lamprophyres from Bulljah Pool, Nabberu Basin, Yilgarn Craton, Western Australia Introduction and setting. Lithos 275–290.
Hari, K.R., Kumar, M.S., Santosh, M., Rai, S.K., 2000. Melt inclusions in olivine and pyroxene phenocrysts from lamprophyres of Chhaktalao Area, Madhya Pradesh, India. J. Asian Earth Sci. 18, 155–161. https://doi.org/10.1016/S1367-9120(99)00042-5.
Harris, J.W., Smit, K.V., Fedortchouk, Y., Moore, M., 2022. Morphology of Monocrystalline Diamond and its Inclusions. Rev. Mineral. Geochem. 88, 119–165. https://doi.org/10.2138/rmg.2022.88.02.
Hausel, W.D., 2006. Diamond Deposits of the North American Craton and Adjacent Accreted Terrains.
Heaman, L.M., Creaser, R.A., Cookenboo, H.O., Chacko, T., 2006. Multi-stage modification of the northern Slave mantle lithosphere: evidence from zircon- and diamond-bearing eclogite xenoliths entrained in Jericho kimberlite, Canada. J. Petrol. 47, 821–858.
Heaman, L.M., Phillips, D., Pearson, G., 2019. Dating kimberlites: methods and emplacement patterns through time. Elements 15, 399–404.

Hidas, K., Borghini, G., Tommasi, A., Zanetti, A., Rampone, E., 2021. Interplay between melt infiltration and deformation in the deep lithospheric mantle (External Liguride ophiolite, North Italy). Lithos 380–381, 105855. https://doi.org/10.1016/j.lithos.2020.105855.

Howell, D., Stachel, T., Stern, R.A., Pearson, D.G., Nestola, F., Hardman, M.F., Harris, J. W., Jaques, A.L., Shirey, S.B., Cartigny, P., Smit, K.V., Aulbach, S., Brenker, F.E., Jacob, D.E., Thomassot, E., Walter, M.J., Navon, O., 2020. Deep carbon through time: Earth's diamond record and its implications for carbon cycling and fluid speciation in the mantle. Geochim. Cosmochim. Acta 275, 99–122. https://doi.org/10.1016/j.gca.2020.02.011.

Huang, J.X., Griffin, W.L., Gréau, Y., Pearson, N.J., O'Reilly, S.Y., Cliff, J., Martin, L., 2014. Unmasking xenolithic eclogites: progressive metasomatism of a key Roberts Victor sample. Chem. Geol. 364, 56–65.

Hutchison, M.T., 2005. Diamondiferous kimberlites from the Garnet Lake area, West Greenland: exploration methodologies and petrochemistry. Danmark. Grønland. Unders. Rapport 68, 33–42.

Hutchison, M.T., Frei, D., 2009. Kimberlite and related rocks from Garnet Lake, West Greenland, including their mantle constituents, diamond occurrence, age and provenance. Lithos 112, 318–333. https://doi.org/10.1016/j.lithos.2009.05.034.

Hutchison, M.T., Heaman, L.M., 2008. Chemical and physical characteristics of diamond crystals from Garnet Lake, Sarfartoq, West Greenland: an association with carbonatitic magmatism. Can. Mineral. 46, 1063–1078. https://doi.org/10.3749/canmin.46.4.1063.

Hutchison, M.T., Kirkland, C.L., Ribeiro, B.V., Bernstein, S., 2024. Geochronology of the Qeqertaa Diamondiferous Ultramafic Lamprophyre, West Greenland. In: 12th International Kimberlite Conference Extended Abstract. Yellowknife. https://doi.org/10.22008/FK2/VYJX5D.

Iakoubovskii, K., Adriaenssens, G.J., 2002. Optical characterization of natural Argyle diamonds. Diam. Relat. Mater. 11, 125–131.

Ijewliw, O.J., 1991. Petrology of the Golden Cluster Lamprophyres, Southeastern British Columbia, Canada (M.Sc thesis).. Queens University, Kingston, ON, Canada.

Ijewliw, O.J., Pell, J., 1996. Diatreme Breccias in the Cordillera: Searching for Diamonds in Canada.

Innocenzi, F., Ezad, I.S., Ronca, S., Agostini, S., Lustrino, M., Foley, S.F., 2024a. Experimental petrology constraints on kamafugitic magmas. Eur. J. Mineral. 36, 899–916. https://doi.org/10.5194/ejm-36-899-2024.

Innocenzi, F., Ronca, S., Foley, S., Agostini, S., Lustrino, M., 2024b. Carbonatite and ultrabasic magmatism at Toro Ankole and Virunga, western branch of the East African Rift system. Gondwana Res. 125, 317–342. https://doi.org/10.1016/j.gr.2023.09.005.

Innocenzi, F., Ezad, I.S., Ronca, S., Agostini, S., Lustrino, M., Shcheka, S., Foley, S.F., 2025. Mantle sources of kamafugitic magmas: insights from partial melting experiments on phlogopite clinopyroxenite and clinopyroxene glimmerite. Mineral. Mag. 1–36. https://doi.org/10.1180/mgm.2025.10160.

Ionov, D.A., Dupuy, C., O'Reilly, S.Y., Kopylova, M.G., Genshaft, Y.S., 1993. Carbonated peridotite xenoliths from Spitsbergen: implications for trace element signature of mantle carbonate metasomatism. Earth Planet. Sci. Lett. 119, 283e297.

Irving, A.J., 1980. Petrology and geochemistry of composite ultramafic xenoliths in alkalic basalts and implications for magmatic processes within the mantle. Am. J. Sci. 280, 389e426.

Jacob, D.E., 2004. Nature and origin of eclogite xenoliths from kimberlites. Lithos 77 (1–4), 295–316.

Jaques, A.L., 1994. Diamonds in Australia. In: Solomon, M., Groves, D.I. (Eds.), The Geology and Origin of Australian Mineral Deposits. Clarendon Press, Oxford, pp. 782–820.

Jaques, A.L., Milligan, P.R., 2004. Patterns and controls on the distribution of diamondiferous intrusions in Australia. Lithos 77, 783–802. https://doi.org/10.1016/j.lithos.2004.03.042.

Jaques, A.L., 2002. Australian diamond deposits, kimberlites, and related rocks. 1:5 million map. Geoscience Australia.

Jaques, A.L., Kerr, I.D., Lucas, H., Sun, S.-S., Chappell, B.W., 1986a. Mineralogy and Petrology of Picritic Monchiquites from Wandagee, Carnarvon Basin, Western Australia, in: Fourth International Kimberlite Conference, 1986 - Perth, Australia. Geological Society of Australia by Blackwell Scientific Publications, Melbourne.

Jaques, A.L., Lewis, J.D., Smith, C.B., 1986b. The Kimberlites and Lamproites of Western Australia. Government Printing Office, Perth.

Jaques, A.L., Kerr, I.D., Lucas, H., Sun, S.-S., Chappell, B.W., 1989. Mineralogy and petrology of picritic monchiquites from Wandagee, Carnarvon Basin, Western Australia. In: Ross, J. (Ed.), Kimberlites and Related Rocks: Their Composition, Occurrence, Origin and Emplacement. Geological Society of Australia Special Publication, pp. 120–140.

Kaminsky, F.V., Sablukov, S.M., Sablukova, L.I., Shpanov, V.E., Zhuravlev, D.Z., 1998. Diamondiferous Minette Dykes from the Parker Lake Area. In: International Kimberlite Conference: Extended Abstracts, 7, pp. 392–394.

Kaminsky, F.V., 2007. Non-kimberlitic diamondiferous igneous rocks: 25 years on. Journal of the Geological Society of India 69 (3), 557–575.

Kaminsky, F.V., Sablukov, S.M., Sablukova, L.I., 2003. Diamondiferous Archaean lamprophyres with komatiitic affinities from the Wawa area, Ontario, Canada. In: International Kimberlite Conference: Extended Abstracts, vol. 8.

Kamvisis, I., Phani, P.R.C., 2022. The "Lamprophyre Clan" Revisited. J. Geol. Soc. India 98, 1205–1209. https://doi.org/10.1007/s12594-022-2153-4.

Kamvisis, I., Phani, P.R.C., 2024. Some notes on the IUGS classification of lamprophyric rocks. Mineralogia 55, 30–39. https://doi.org/10.2478/mipo-2024-0003.

Kargin, A., Bussweiler, Y., Nosova, A., Sazonova, L., Berndt, J., Klemme, S., 2021. Titanium-rich metasomatism in the lithospheric mantle beneath the Arkhangelsk Diamond Province, Russia: insights from ilmenite-bearing xenoliths and HP–HT reaction experiments. Contrib. Mineral. Petrol. 176, 101.

Kelley, S.P., Wartho, J.-A., 2000. Rapid Kimberlite Ascent and the significance of Ar-Ar Ages in Xenolith Phlogopites. Science 1979 (289), 609–611. https://doi.org/10.1126/science.289.5479.609.

Kerr, I.D., Jacuqes, A.L., Lucas, H., Sun, S.-S., Chappell, B.W., 1986. Diamond-Bearing Alkaline Intrusions from Wandagee, Carnarvon Basin, Western Australia, in: Fourth International Kimberlite Conference, 1986 - Perth, Australia. Geological Society of Australia by Blackwell Scientific Publications, Melbourne.

Khan, S., Dongre, A., Viljoen, F., Li, Q.L., Le Roux, P., 2019. Petrogenesis of lamprophyres synchronous to kimberlites from the Wajrakarur kimberlite field: implications for contrasting lithospheric mantle sources and geodynamic evolution of the eastern Dharwar Craton of southern India. Geol. J. 54, 2994–3016. https://doi.org/10.1002/gj.3394.

Khokhryakov, A.F., Kruk, A.N., Sokol, A.G., 2021. The effect of oxygen fugacity on diamond resorption in ascending kimberlite melt. Lithos 394–395, 106166. https://doi.org/10.1016/j.lithos.2021.106166.

Kiminami, K., Imaoka, T., Ogura, K., Kawabata, H., Ishizuka, H., Mori, Y., 2017. Tectonic implications of Early Miocene OIB magmatism in a near-trench setting: the Outer Zone of SW Japan and the northernmost Ryukyu Islands. J. Asian Earth Sci. 135, 291–302. https://doi.org/10.1016/j.jseaes.2016.12.033.

Kiseeva, E.S., Kamenetsky, V.S., Yaxley, G.M., Shee, S.R., 2017. Mantle melting versus mantle metasomatism – "the chicken or the egg" dilemma. Chem. Geol. 455, 120–130. https://doi.org/10.1016/j.chemgeo.2016.10.026.

Kjarsgaard, B.A., Levinson, A.A., 2002. Diamonds in Canada. Gems Gemol. 38, 208–238.

Kjarsgaard, B.A., Pearson, D.G., Tappe, S., Nowell, G.M., Dowall, D.P., 2009. Geochemistry of hypabyssal kimberlites from Lac de Gras, Canada: Comparisons to a global database and applications to the parent magma problem. Lithos 112, 236–248. https://doi.org/10.1016/j.lithos.2009.06.001.

Kjarsgaard, B.A., de Wit, M., Heaman, L.M., Pearson, D.G., Stiefenhofer, J., Janusczcak, N., Shirey, S.B., 2022. A Review of the Geology of Global Diamond Mines and deposits. Rev. Mineral. Geochem. 88, 1–118. https://doi.org/10.2138/rmg.2022.88.01.

Konzett, J., Ulmer, P., 1999. The stability of hydrous potassic phases in lherzolitic mantle and experimental study to 9.5 GPa in simplified and natural bulk compositions. J. Petrol. 40, 629e652.

Kopylova, M.G., Afanasiev, V.P., Bruce, L.F., Thurston, P.C., Ryder, J., 2011. Metaconglomerate preserves evidence for kimberlite, diamondiferous root and medium grade terrane of a pre-2.7 Ga Southern Superior protocraton. Earth Planet. Sci. Lett. 312, 213–225.

Kumar Giri, R., Chalapathi Rao, N.V., Rahaman, W., Kumar, A., Satyanarayanan, M., Keshav Krishna, A., 2021. Paleoproterozoic calc-alkaline lamprophyres from the Sidhi Gneissic complex, India: implications for plate tectonic evolution of the Central Indian Tectonic Zone. Precambrian Res. 362, 106316. https://doi.org/10.1016/j.precamres.2021.106316.

Larsen, L.M., Rex, D.C., 1992. A review of the 2500 Ma span of alkaline-ultramafic, potassic and carbonafitic magmatism in West Greenland. Lithos, 28, 367-402.

Le Maitre, R.W., 2002. Classification of igneous rocks and glossary of terms. In: Recommendations of the IUGS Subcommission on the Systematics of Igneous Rocks. Cambridge University Press, Cambridge.

Lefebvre, N., Kopylova, M., Kivi, K., 2005. Archean calc-alkaline lamprophyres of Wawa, Ontario, Canada: Unconventional diamondiferous volcaniclastic rocks. Precambrian Res. 138, 57–87. https://doi.org/10.1016/j.precamres.2005.04.005.

Letendre, J., McCandless, T.E., Eastoe, C.J., 1998. Morphology and carbon isotope composition of microdiamonds from Dachine, French Guiana. In: International Kimberlite Conference: Extended Abstracts, vol. 7, pp. 500–502.

Li, G., Zeng, L., Gao, L.-E., Yan, L., Zhao, L., Tian, Y., 2024. Late Eocene sodic calc-alkaline lamprophyre in Gangdese batholith, southern Tibet: Implications for mantle metasomatism by carbonatitic melt. Geol. Soc. Am. Bull. https://doi.org/10.1130/b37566.1.

Liu, B., Tang, Y.J., Xing, L.Y., Xu, Y., Zhao, S.Q., Sun, Y., Huang, J., 2022. Triassic calc-alkaline lamprophyre dykes from the North Qiangtang, central Tibetan Plateau: evidence for a subduction-modified lithospheric mantle. Geol. Mag. 159, 407–420. https://doi.org/10.1017/S001675682100100X.

Lloyd, F.E., 1981. Upper-mantle metasomatism beneath a continental rift: clinopyroxenes in alkali mafic lavas and nodules from Sruth West Uganda. Mineral. Mag. 44, 315–338.

Lustrino, M., Bonin, B., Doroshkevich, A., Guo, Z., Kerr, A., Heilborn, M., Irving, T., Ivanov, A., Mitchell, R., Nakagawa, M., Natland, J.H., Pearce, J.A., Smith, B.S., Srivastava, R.K., Tappe, S., Wilson, M., Zellmer, G., 2020. IUGS Task Group on Igneous Rocks TGIR.

Ma, L., Jiang, S.Y., Hou, M.L., Dai, B.Z., Jiang, Y.H., Yang, T., Zhao, K.-D., Pu, W., Zhu, Z.-Y., Xu, B., 2014. Geochemistry of Early Cretaceous calc-alkaline lamprophyres in the Jiaodong Peninsula: Implication for lithospheric evolution of the eastern North China Craton. Gondwana research 25 (2), 859–872.

Macrae, N.D., Armitage, A.E., Jones, A.L., Miller, A.R., 1995. A Diamondiferous Lamprophyre Dike, Gibson Lake Area, Northwest Territories. Int. Geol. Rev. 37, 212–229. https://doi.org/10.1080/00206819509465401.

Mandler, B.E., Grove, T.L., 2016. Controls on the stability and composition of amphibole in the Earth's mantle. Contributions to Mineralogy and Petrology 171 (8), 68.

Mareschal, J.-C., Jaupart, C., 2006. Archean thermal Regime and Stabilization of the Cratons. Geophys. Monogr. Ser. 164.

Marker, M., Knudsen, C., 1988. Middle Proterozoic Ultramafic Lamprophyre Dykes in the Archaean of the Atâ Area, Central West Greenland.

McCammon, C., Kopylova, M.G., 2004. A redox profile of the Slave mantle and oxygen fugacity control in the cratonic mantle. Contrib. Mineral. Petrol. 148, 55–68.

Michaut, C., Jaupart, C., 2007. Secular cooling and thermal structure of continental lithosphere. Earth Planet. Sci. Lett. 257, 83–96. https://doi.org/10.1016/j.epsl.2007.02.019.
Miller, C.E., Kopylova, M.G., Ryder, J., 2012. Vanished diamondiferous cratonic root beneath the Southern Superior province: evidence from diamond inclusions in the Wawa metaconglomerate. Contrib. Mineral. Petrol. 164, 697–714. https://doi.org/10.1007/s00410-012-0773-1.
Mitchell, R., Tappe, S., 2010. Discussion of "Kimberlites and aillikites as probes of the continental lithospheric mantle", by D. Francis and M. Patterson (Lithos v. 109, p. 72–80). Lithos 115, 288–292. https://doi.org/10.1016/j.lithos.2009.10.017.
Mitchell, R.H., 1994. Mineralogy anti Petrology the lamprophyre facies. Mineral. Petrol. 51, 137–146.
Mitchell, R.H., 2020. Igneous rock associations 26. Lamproites, exotic potassic alkaline rocks: a review of their nomenclature, characterization and origins. Geosci. Can. 47, 119–142. https://doi.org/10.12789/geocanj.2020.47.162.
Mitchell, R.H., Bergman, S.C., 1991. Petrology of Lamproites. Springer US, Boston, MA. https://doi.org/10.1007/978-1-4615-3788-5.
Mitchell, R.H., Scott-Smith, B.H., Larsen, L.M., 1999. Mineralogy of Ultramafic Dikes from the Sarfartoq, Sisimiut and Maniitsoq Areas, West Greenland, in: Proceedings of the VIIth International Kimberlite Conference (Red Roof Design Cape Town).
Mizukami, T., Wallis, S., Enami, M., Kagi, H., 2008. Forearc diamond from Japan. Geology 36, 219–222. https://doi.org/10.1130/G24350A.1.
Moorhead, J., Perreault, S., Berclaz, A., Sharma, K.N.M., Beaumier, M., Cadieux, A.-M., 2000. Kimberlites and Diamonds in Northern Quebec.
Muravyeva, N.S., Senin, V.G., 2018. Xenoliths from Bunyaruguru volcanic field: some insights into lithology of East African Rift upper mantle. Lithos 296–299, 17–36. https://doi.org/10.1016/j.lithos.2017.10.023.
Nasir, S., 2016. Petrology of late Jurassic allochthonous ultramafic lamprophyres within the Batain Nappes, Northeastern Oman. Int. Geol. Rev. 58, 913–928. https://doi.org/10.1080/00206814.2015.1136571.
Nasir, S., Al-Khirbash, S., Rollinson, H., Al-Harthy, A., Al-Sayigh, A., Al-Lazki, A., Theye, T., Massonne, H.-J., Belousova, E., 2011. Petrogenesis of early cretaceous carbonatite and ultramafic lamprophyres in a diatreme in the Batain Nappes, Eastern Oman continental margin. Contrib. Mineral. Petrol. 161, 47–74. https://doi.org/10.1007/s00410-010-0521-3.
Nielsen, T.F.D., Jensen, S.M., Secher, K., Sand, K.K., 2009. Distribution of kimberlite and aillikite in the Diamond Province of southern West Greenland: a regional perspective based on groundmass mineral chemistry and bulk compositions. Lithos 112, 358–371. https://doi.org/10.1016/j.lithos.2009.05.035.
Nimis, P., 2022. Pressure and Temperature Data for Diamonds. Rev. Mineral. Geochem. 88, 533–565. https://doi.org/10.2138/rmg.2022.88.10.
Nixon, P.H., 1987. Mantle xenoliths. Wiley, New York, NY.
Nosova, A.A., Sazonova, L.V., Kargin, A.V., Smirnova, M.D., Lapin, A.V., Shcherbakov, V. D., 2018. Olivine in ultramafic lamprophyres: chemistry, crystallisation, and melt sources of Siberian Pre-and post-trap aillikites. Contributions to Mineralogy and Petrology 173 (7), 55.
Novella, D., Frost, D.J., 2014. The Composition of Hydrous Partial Melts of Garnet Peridotite at 6 GPa: Implications for the Origin of Group II Kimberlites. J. Petrol. 55, 2097–2124. https://doi.org/10.1093/petrology/egu051.
Nugumanova, Y., Doroshkevich, A., Prokopyev, I., Starikova, A., 2021. Compositional variations of spinels from ultramafic lamprophyres of the chadobets complex (Siberian craton, Russia). Minerals 11, 456.
Ogilvie-Harris, R.C., Field, M., Sparks, R.S.J., Walter, M.J., 2009. Perovskite from Dutoitspan kimberlite, Kimberley, South Africa: implications for magmatic processes. Min. Mag. 73, 915–928.
O'Neill, C., Wyman, D.A., 2006. Geodynamic modeling of late Archean subduction: Pressure-temperature constraints from greenstone belt diamond deposits. In: Benn, K., Mareschal, J.-C., Condie, K.C. (Eds.), Geophysical Monograph Series, pp. 177–188. https://doi.org/10.1029/164GM12.
Olierook, H.K., Fougerouse, D., Doucet, L.S., Liu, Y., Rayner, M.J., Danišík, M., Condon, D.J., McInnes, B.I.A, Jaques, A.L., Evans, N.J., McDonald, B.J., Li, Z.-X., Kirkland, C.L., Mayers, C., Wingate, M.T., 2023. Emplacement of the Argyle diamond deposit into an ancient rift zone triggered by supercontinent breakup. Nature communications 14 (1), 5274.
O'Reilly, S.Y., Griffin, W.L., 2013. Mantle Metasomatism, pp. 471–533. https://doi.org/10.1007/978-3-642-28394-9_12.
Pandey, A., Chalapathi Rao, N.V., Chakrabarti, R., Pandit, D., Pankaj, P., Kumar, A., Sahoo, S., 2017. Petrogenesis of a Mesoproterozoic shoshonitic lamprophyre dyke from the Wajrakarur kimberlite field, eastern Dharwar craton, southern India: Geochemical and Sr-Nd isotopic evidence for a modified sub-continental lithospheric mantle source. Lithos 292–293, 218–233. https://doi.org/10.1016/j.lithos.2017.09.001.
Pandey, A., Chalapathi Rao, N.V., Chakrabarti, R., Pankaj, P., Pandit, D., Pandey, R., Sahoo, S., 2018. Post-collisional calc-alkaline lamprophyres from the Kadiri greenstone belt: evidence for the Neoaarchean convergence-related evolution of the Eastern Dharwar Craton and its schist belts. Lithos 320–321, 105–117. https://doi.org/10.1016/j.lithos.2018.09.005.
Pandey, R., Rao, N.V.C., Pandit, D., Sahoo, S., Dhote, P., 2018b. Imprints of modal metasomatism in the post-Deccan subcontinental lithospheric mantle: petrological evidence from an ultramafic xenolith in an Eocene lamprophyre, NW India. Geol. Soc. Lond. Spec. Publ. 463, 117–136. https://doi.org/10.1144/SP463.6.
Pandey, R., Pandey, A., Chalapathi Rao, N.V., Belyatsky, B., Choudhary, A.K., Lehmann, B., Pandit, D., Dhote, P., 2019. Petrogenesis of end-cretaceous/early Eocene lamprophyres from the Deccan large Igneous Province: Constraints on plume-lithosphere interaction and the post-Deccan lithosphere-asthenosphere boundary (LAB) beneath NW India. Lithos 346–347. https://doi.org/10.1016/j.lithos.2019.07.006.
Pearson, D.G., Brenker, F.E., Nestola, F., McNeill, J., Nasdala, L., Hutchison, M.T., Matveev, S., Mather, K., Silversmit, G., Schmitz, S., Vekemans, B., Vincze, L., 2014. Hydrous mantle transition zone indicated by ringwoodite included within diamond. Nature 507, 221–224. https://doi.org/10.1038/nature13080.
Pearson, D.G., Woodhead, J., Janney, P.E., 2019. Kimberlites as geochemical probes of earth's mantle. Elements 15, 387–392. https://doi.org/10.2138/GSELEMENTS.15.6.387.
Pearson, D.G., Scott, J.M., Liu, J., Schaeffer, A., Wang, L.H., van Hunen, J., Szilas, K., Chacko, T., Kelemen, P.B., 2021. Deep continental roots and cratons. Nature 596, 199–210. https://doi.org/10.1038/s41586-021-03600-5.
Pezzera, A., Li, L., Stern, R.A., Pearson, D.G., 2026. Modeling extreme nitrogen isotope variability in Neoarchean diamonds from Knee Lake, Superior Craton. Geosci. Front. 415, 181–195.
Pearson, D.G., Kublik, K., Scott, J.M., Schaeffer, A., 2024. A global look at cratons and the thermal properties that define their roots. In: In: 12th International Kimberlite Conference Extended Abstract. Yellowknife.
Pearson, D.G., Canil, D., Shirey, S.B., 2003. Mantle samples included in volcanic rocks: xenoliths and diamonds. In: Holland, H.D., Turekian, K.K. (Eds.), Treatise on Geochemistry. Elsevier, Amsterdam, p. 171275.
Peterson, T.D., Van Breemen, O., Sandeman, H., Cousens, B., 2002. Proterozoic (1.85-1.75 Ga) igneous suites of the Western Churchill Province: granitoid and ultrapotassic magmatism in a reworked Archean hinterland. Precambrian Res. 119, 73–100.
Pezzera, A., Nestola, F., Stachel, T., Stern, R.A., Grütter, H., Pearson, D.G., 2025. Cool transient lithospheric thermal conditions driven by subduction recorded by Neoarchean diamonds from knee Lake, northwestern Superior Craton. Mineral. Petrol. https://doi.org/10.1007/s00710-025-00927-z.
Pilbeam, L.H., Rasmussen, T.M., Waight, T.E., Nielsen, T.F.D., 2023. Inverse Modeling to Constrain Composition of CO2-Rich parental Melt of Kimberlite: Model Development and Application to the Majuagaa Dyke, Southern West Greenland. J. Petrol. 64, 1. https://doi.org/10.1093/petrology/egac127.
Phani, P.R.C., Kamvisis, I., 2026. A few thoughts on the diamondiferous nature of lamprophyres from Wajrakarur Kimberlite Field, Southern India. Mineralogia 57.
Pilbeam, L.H., Nielsen, T.F.D., Waight, T., Tappe, S., 2024. Links between Calcite Kimberlite, Aillikite and Carbonatite in West Greenland: Numeric Modeling of Compositional Relationships. J. Petrol. 65. https://doi.org/10.1093/petrology/egae059 egae059.
Pitcavage, E., Furman, T., Nelson, W., Kalegga, P.K., Barifaijo, E., 2021. Petrogenesis of primitive lavas from the Toro Ankole and Virunga Volcanic Provinces: Metasomatic mineralogy beneath East Africa's Western Rift. Lithos 106192.
Plank, T., 2014. The Chemical Composition of Subducting Sediments. In: *Treatise on Geochemistry*. Elsevier, pp. 607–629.
Plank, T., Langmuir, C.H., 1998. The chemical composition of subducting sediment and its consequences for the crust and mantle. Chem. Geol. 145, 325–394. https://doi.org/10.1016/S0009-2541(97)00150-2.
Podborodnikov, I.V., Shatskiy, A., Arefiev, A.V., Litasov, K.D., 2019. Phase relations in the system Na2CO3–CaCO3–MgCO3 at 3 GPa with implications for carbonatite genesis and evolution. Lithos 330–331, 74–89. https://doi.org/10.1016/j.lithos.2019.01.035.
Prelević, D., 2004. Origin of Minette by Mixing of Lamproite and Dacite Magmas in Veliki Majdan, Serbia. J. Petrol. 45, 759–792. https://doi.org/10.1093/petrology/egg109.
Prelević, D., Förster, M.W., Buhre, S., Gülmez, F., Grützner, T., Wang, Y., Foley, S.F., 2024. Recent advances made by reaction experiments on melting of heavily metasomatized hydrous mantle. Earth Sci. Rev. 256, 104881.
Prokopyev, I., Starikova, A., Doroshkevich, A., Nugumanova, Y., Potapov, V., 2020. Petrogenesis of ultramafic lamprophyres from the Terina complex (Chadobets upland, Russia): mineralogy and melt inclusion composition. Minerals 10, 419.
Ravi, S., Sufija, M., Patel, S.C., Gupta, T., Sridhar, M., Kaminsky, F.V., Khachatryan, G.K., Netravali, S.V., 2012. In: Diamonds from the eastern Dharwar Craton, India: their physical and infrared characteristics. 10th International Kimberlite Conference.
Regier, M.E., Smit, K.V., Chalk, T.B., Stachel, T., Stern, R.A., Smith, E.M., Foster, G.L., Bussweiler, Y., DeBuhr, C., Burnham, A.D., Harris, J.W., Pearson, D.G., 2023. Boron isotopes in blue diamond record seawater-derived fluids in the lower mantle. Earth and Planetary Science Letters 602, 117923.
Rinaldi, M., Mikhail, S., Sverjensky, D.A., Kalita, J., 2023. The importance of carbon to the formation and composition of silicates during mantle metasomatism. Geochim. Cosmochim. Acta 356, 105–115. https://doi.org/10.1016/j.gca.2023.06.025.
Rock, N., 1977. The nature and origin of lamprophyres: some definitions, distinctions, and derivations. Earth Sci. Rev. 13, 123–169.
Rock, N., 1979. Petrology and origin of the type monchiquites and associated lamprophyres of Serra de Monchique, Portugal. Trans. R Soc. Edinb. 70, 149–170.
Rock, N., 1986. The nature and origin of ultramafic lamprophyres: alnöites and allied rocks. J. Petrol. 27, 155–196.
Rock, N., 1990. Lamprophyres. Blackie, Glasgow, p. 285.
Rock, N., 1991. Lamprophyres. Thomson Litho Ltd, East Kilbride.
Rock, N.M.S., 1984. Nature and origin of calc-alkaline lamprophyres: minettes, vogesites, kersantites and spessartites. Earth Environ. Sci. Trans. R. Soc. Edinb. 74, 193–227.
Rock, N.M.S., 1987. The nature and origin of lamprophyres: an overview. Geol. Soc. Spec. Publ. 30, 191–226. https://doi.org/10.1144/GSL.SP.1987.030.01.09.
Roden, M.F., Murthy, V.R., 1985. Mantle metasomatism. Annu. Rev. Earth Planet. Sci. 13, 269–296.

Russell, J.K., Jones, T.J., 2023. Transport and eruption of mantle xenoliths creates a lagging problem. Commun. Earth Environ. 4, 177. https://doi.org/10.1038/s43247-023-00843-0.
Russell, J.K., Sparks, R.S.J., Kavanagh, J.L., 2019. Kimberlite volcanology: transport, ascent, and eruption. Elements 15, 405–410. https://doi.org/10.2138/gselements.15.6.405.
Sand, K.K., Waight, T.E., Pearson, D.G., Nielsen, T.F.D., Makovicky, E., Hutchison, M.T., 2009. The lithospheric mantle below southern West Greenland: a geothermobarometric approach to diamond potential and mantle stratigraphy. Lithos 112, 1155–1166. https://doi.org/10.1016/j.lithos.2009.05.012.
Sargazi, M., Bagheri, S., Ma, X., 2022. Oligocene calc-alkaline lamprophyres and K-rich association in the eastern Iranian ranges: Products of low-degree melting of subduction-modified lithospheric mantle in post-orogenic setting. Lithos 430–431, 106864. https://doi.org/10.1016/j.lithos.2022.106864.
Sarkar, S., Dalton, H., Giuliani, A., Phillips, D., Graham Pearson, D., Nowell, G.M., Woodhead, J.D., Hergt, J., Maas, R., Lynton Jaques, A., Chalapathi Rao, N.V., Weiss, Y., Ghosh, S., 2025. Extreme enriched-mantle (EM) compositions recorded by the Sr-Nd-Hf isotopes of global cratonic lamproites. Geochim. Cosmochim. Acta 394, 220–243. https://doi.org/10.1016/j.gca.2025.02.014.
Scott, B.H., 1982. Petrogenesis of kimberlites and associated potassic lamprophyres from central West Greenland. In: Meyer, H.O.A., Boyd, F.R. (Eds.), Kimberlites, Diatremes, and Diamonds: Their Geology, Petrology, and Geochemistry, 15, pp. 190–205.
Scott, H.P., Hemley, R.J., Mao, H., Herschbach, D.R., Fried, L.E., Howard, W.M., Bastea, S., 2004. Generation of methane in the Earth's mantle: in situ high pressure–temperature measurements of carbonate reduction. Proc. Natl. Acad. Sci. 101, 14023–14026. https://doi.org/10.1073/pnas.0405930101.
Scott Smith, B.H., Nowicki, T.E., Russell, J.K., Webb, K.J., Mitchell, R.H., Hetman, C.M., Harder, M., Skinner, E.M.W., Robey, Jv.A., 2013. In: Kimberlite Terminology and Classification. Proceedings of 10th International Kimberlite Conference. Springer India, New Delhi, pp. 1–17. https://doi.org/10.1007/978-81-322-1173-0_1.
Scott Smith, B.H., Nowicki, T.E., Russell, J.K., Webb, K.J., Mitchell, R.H., Hetman, C.M., Robey, J.vA., 2018. A Glossary of Kimberlite and Related Terms Part 1: Scott-Smith Petrology. Inc., North Vancouver, British Columbia, Canada, pp. 144–p.
Shaikh, A.M., Patel, S.C., Ravi, S., Behera, D., Pruseth, K.L., 2017. Mineralogy of the TK1 and TK4 'kimberlites' in the Timmasamudram cluster, Wajrakarur Kimberlite Field, India: Implications for lamproite magmatism in a field of kimberlites and ultramafic lamprophyres. Chem. Geol. 455, 208–230. https://doi.org/10.1016/j.chemgeo.2016.10.030.
Shu, C., Foley, S.F., Ezad, I.S., Daczko, N.R., Shcheka, S.S., 2024. Experimental Melting of Phlogopite Websterite in the Upper Mantle between 1.5 and 4.5 GPa. J. Petrol. 65. https://doi.org/10.1093/petrology/egae030.
Skinner, E.M.W., Clement, C.R., Gurney, J.J., Apter, D.B., Hatton, C.J., 1992. The distribution and tectonic setting of South African kimberlites. Russ. Geol. Geoph. 33, 26–31.
Smit, K.V., Shirey, S.B., Wang, W., 2016. Type Ib diamond formation and preservation in the West African lithospheric mantle: Re–Os age constraints from sulphide inclusions in Zimmi diamonds. Precambrian Res. 286, 152–166. https://doi.org/10.1016/j.precamres.2016.09.022.
Smith, C.B., 1983. Pb, Sr and Nd isotopic evidence for sources of southern African cretaceous kimberlites. Nature 304, 51–54. https://doi.org/10.1038/304051a0.
Smith, C.B., Haggerty, S.E., Chatterjee, B., Beard, A., Townend, R., 2013. Kimberlite, lamproite, ultramafic lamprophyre, and carbonatite relationships on the Dharwar Craton, India; an example from the Khaderpet pipe, a diamondiferous ultramafic with associated carbonatite intrusion. Lithos 182–183, 102–113. https://doi.org/10.1016/j.lithos.2013.10.006.
Smith, C.B., Walter, M.J., Bulanova, G.P., Mikhail, S., Burnham, A.D., Gobbo, L., Kohn, S.C., 2016. Diamonds from Dachine, French Guiana: a unique record of early Proterozoic subduction. Lithos 265, 82–95. https://doi.org/10.1016/j.lithos.2016.09.026.
Soltys, A., Giuliani, A., Phillips, D., 2018. A new approach to reconstructing the composition and evolution of kimberlite melts: a case study of the archetypal Bultfontein kimberlite (Kimberley, South Africa). Lithos 304–307, 1–15. https://doi.org/10.1016/j.lithos.2018.01.027.
Sparks, R.S.J., Baker, L., Brown, R.J., Field, M., Schumacher, J., Stripp, G., Walters, A., 2006. Dynamical constraints on kimberlite volcanism. J. Volcanol. Geotherm. Res. 155, 18–48. https://doi.org/10.1016/j.jvolgeores.2006.02.010.
Stachel, T., Harris, J.W., 2008. The origin of cratonic diamonds — Constraints from mineral inclusions. Ore Geol. Rev. 34, 5–32. https://doi.org/10.1016/j.oregeorev.2007.05.002.
Stachel, T., Blackburn, L., Kurszlaukis, S., Barton, E., Walker, E.C., 2004. Diamonds from the Cristal and Genesis volcanics, Wawa area, Ontario. In: Abstracts of the 32nd Annual Yellowknife Geoscience Forum. Yellowknife, NWT, Canada, pp. 74–75.
Stachel, T., Banas, A., Muehlenbachs, K., Kurszlaukis, S., Walker, E.C., 2006. Archean diamonds from Wawa (Canada): samples from deep cratonic roots predating cratonization of the Superior Province. Contrib. Mineral. Petrol. 151, 737–750. https://doi.org/10.1007/s00410-006-0090-7.
Stachel, T., Aulbach, S., Harris, J.W., 2022. Mineral Inclusions in Lithospheric Diamonds. Rev. Mineral. Geochem. 88, 307–391. https://doi.org/10.2138/rmg.2022.88.06.
Starikova, A., Prokopyev, I., Doroshkevich, A., Ragozin, A., Chervyakovsky, V., 2021. Polygenic nature of olivines from the ultramafic lamprophyres of the Terina complex (Chadobets upland, Siberian platform) based on trace element composition, crystalline, and melt inclusion data. Minerals 11, 408.
Steenfelt, A., Jensen, S.M., Nielsen, T.F.D., Sand, K.K., 2009. Provinces of ultramafic lamprophyre dykes, kimberlite dykes and carbonatite in West Greenland characterised by minerals and chemical components in surface media. Lithos 112, 116–123. https://doi.org/10.1016/j.lithos.2009.03.022.
Streckeisen, A., 1979. Classification and nomenclature of volcanic rocks, lamprophyres, carbonatites, and melilitic rocks. Neues Jb. Mineral. Abh. 134, 1–14.
Sudholz, Z.J., Reddicliffe, T.H., Jaques, A.L., Yaxley, G.M., Haynes, M., Gorbatov, A., Czarnota, K., Frigo, C., Maas, R., Knowles, B., 2023. Petrology, age, and rift origin of ultramafic lamprophyres (aillikites) at Mount Webb, a new alkaline province in Central Australia. Geochemistry, Geophysics, Geosystems 24 (10), e2023GC011120.
Sudo, A., Tatsumi, Y., 1990. Phlogopite and K-amphibole in the upper mantle: Implication for magma genesis in subduction zones. Geophys. Res. Lett. 17, 29–32. https://doi.org/10.1029/GL017i001p00029.
Sutherland, F.L., 1996. Alkaline rocks and gemstones, Australia: a review and synthesis. Aust. J. Earth Sci. 43, 323–343. https://doi.org/10.1080/08120099608728259.
Syracuse, E.M., van Keken, P.E., Abers, G.A., 2010. The global range of subduction zone thermal models. Phys. Earth Planet. Inter. 183, 73–90. https://doi.org/10.1016/j.pepi.2010.02.004.
Tappe, S., Jenner, G.A., Foley, S.F., Heaman, L., Besserer, D., Kjarsgaard, B.A., Ryan, B., 2004. Torngat ultramafic lamprophyres and their relation to the North Atlantic Alkaline Province. Lithos 76, 491–518. https://doi.org/10.1016/j.lithos.2004.03.040.
Tappe, S., Foley, S.F., Jenner, G.A., Kjarsgaard, B.A., 2005. Integrating ultramafic lamprophyres into the IUGS classification of igneous rocks: rationale and implications. J. Petrol. 46, 1893–1900. https://doi.org/10.1093/petrology/egi039.
Tappe, S., Foley, S.F., Jenner, G.A., Heaman, L.M., Kjarsgaard, B.A., Romer, R.L., Stracke, A., Joyce, N., Hoefs, J., 2006. Genesis of ultramafic lamprophyres and carbonatites at Aillik Bay, labrador: a consequence of incipient lithospheric thinning beneath the North Atlantic Craton. J. Petrol. 47, 1261–1315.
Tappe, S., Foley, S.F., Stracke, A., Romer, R.L., Kjarsgaard, B.A., Heaman, L.M., Joyce, N., 2007. Craton reactivation on the Labrador Sea margins: 40Ar/39Ar age and Sr-Nd-Hf-Pb isotope constraints from alkaline and carbonatite intrusives. Earth Planet. Sci. Lett. 256, 433–454. https://doi.org/10.1016/j.epsl.2007.01.036.
Tappe, S., Steenfelt, A., Heaman, L.M., Romer, R.L., Simonetti, A., Muehlenbachs, K., 2008b. The alleged carbonatitic-kimberlitic melt continuum: Contrary evidence from West Greenland. In: Geochimica et Cosmochimica Acta. Goldschmidt Conference. Vancouver, Canada.
Tappe, S., Steenfelt, A., Heaman, L.M., Simonetti, A., 2009. The newly discovered Jurassic Tikiusaaq carbonatite-aillikite occurrence, West Greenland, and some remarks on carbonatite-kimberlite relationships. Lithos 112, 385–399. https://doi.org/10.1016/j.lithos.2009.03.002.
Tappe, S., Pearson, D.G., Nowell, G., Nielsen, T., Milstead, P., Muehlenbachs, K., 2011. A fresh isotopic look at Greenland kimberlites: Cratonic mantle lithosphere imprint on deep source signal. Earth Planet. Sci. Lett. 305, 235–248. https://doi.org/10.1016/j.epsl.2011.03.005.
Tappe, S., Beard, C.D., Borst, A.M., Humphreys-Williams, E.R., Walter, B.F., Yaxley, G.M., 2025. Kimberlite, carbonatite and alkaline magmatic systems: definitions, origins, and strategic mineral resources. In: The Encyclopedia of Volcanoes.
Tappe, Sebastian, Foley, S.F., Kjarsgaard, B.A., Romer, R.L., Heaman, L.M., Stracke, A., Jenner, G.A., 2008a. Between carbonatite and lamproite-Diamondiferous Torngat ultramafic lamprophyres formed by carbonate-fluxed melting of cratonic MARID-type metasomes. Geochim. Cosmochim. Acta 72, 3258–3286. https://doi.org/10.1016/j.gca.2008.03.008.
Tappert, R., Tappert, M.C., 2011. The Origin of Diamonds. In: Diamonds in Nature. Springer, Berlin Heidelberg, Berlin, Heidelberg, pp. 1–14. https://doi.org/10.1007/978-3-642-12572-0_1.
Tappert, R., Foden, J., Stachel, T., Muehlenbachs, K., Tappert, M., Wills, K., 2009a. The diamonds of South Australia. Lithos 112, 806–821.
Tappert, R., Foden, J., Stachel, T., Muehlenbachs, K., Tappert, M., Wills, K., 2009b. Deep mantle diamonds from South Australia: a record of Pacific subduction at the Gondwanan margin. Geology 37, 43–46.
Timmerman, S., Reimink, J.R., Vezinet, A., Nestola, F., Kublik, K., Banas, A., Stachel, T., Stern, R.A., Luo, Y., Sarkar, C., Ielpi, A., Currie, C.A., Mircea, C., Jackson, V., Pearson, D.G., 2022. Mesoarchean diamonds formed in thickened lithosphere, caused by slab-stacking. Earth Planet. Sci. Lett. 592, 117633. https://doi.org/10.1016/j.epsl.2022.117633.
Timmerman, S., Stachel, T., Koornneef, J.M., Smit, K.V., Harlou, R., Nowell, G.M., Thomson, A.R., Kohn, S.C., Davies, J.H.F.L., Davies, G.R., Krebs, M.Y., Zhang, Q., Milne, S.E.M., Harris, J.W., Kaminsky, F., Zedgenizov, D., Bulanova, G., Smith, C.B., Cabral Neto, I., Silveira, F.V., Burnham, A.D., Nestola, F., Shirey, S.B., Walter, M.J., Steele, A., Pearson, D.G., 2023. Sublithospheric diamond ages and the supercontinent cycle. Nature 623, 752–756. https://doi.org/10.1038/s41586-023-06662-9.
Torsvik, TH, Burke, K, Steinberger, B, Webb, SJ, Ashwal, LD, 2010. Diamonds sampled by plumes from the core-mantle boundary. Nature 466, 352–355.
Trønnes, R.G., 2002. Stability range and decomposition of potassic richterite and phlogopite end members at 5-15 GPa. Mineral. Petrol. 74, 129–148. https://doi.org/10.1007/s007100200001.
Ulrych, J., Dostal, J., Adamovič, J., Jelínek, E., Špaček, P., Hegner, E., Balogh, K., 2011. Recurrent Cenozoic volcanic activity in the Bohemian Massif (Czech Republic). Lithos 123, 133–144. https://doi.org/10.1016/j.lithos.2010.12.008.
Uto, K., Hirai, H., Goto, K., Arai, S., 1987. Uto et al., 1987. Geochem. J. 283–290. https://doi.org/10.2343/geochemj.21.283.
Wang, C., Zhang, Z., Giuliani, A., Bo, H., Krmíček, L., Li, X., 2023. Water contents and hydrogen isotope compositions of amphibole in aillikites from the Tarim large igneous province, NW China: Insight into Earth's Deepwater cycle. Geol. Soc. Am. Bull. 2097. https://doi.org/10.1130/B36906.1.
Wardle, R.J., Bridgwater, D., Mengel, F., Campbell, L., Van Kranendonk, M.J., Hauman, A., Churchill, R., Reid, L., 1994. Mapping in the Torngat Orogen, northernmost Labrador: Report 3. The Nain Craton (including a note on ultramafic

dyke occurrences in northernmost Labrador. In: Current research. Newfoundland Department of Mines and Energy, Geological Survey Branch, Report 94-1, pp. 399–407.
Wilson, L., Head, J.W., 2007. An integrated model of kimberlite ascent and eruption. Nature 447, 53–57. https://doi.org/10.1038/nature05692.
Wittig, N., Pearson, D.G., Webb, M., Ottley, C.J., Irvine, G.J., Kopylova, M., Jensen, S.M., Nowell, G.M., 2008. Origin of cratonic lithospheric mantle roots: a geochemical study of peridotites from the North Atlantic Craton, West Greenland. Earth Planet. Sci. Lett. 274, 24–33. https://doi.org/10.1016/j.epsl.2008.06.034.
Woodland, A.B., Koch, M., 2003. Variation in oxygen fugacity with depth in the upper mantle beneath the Kaapvaal craton, Southern Africa. Earth Planet. Sci. Lett. 214, 295–310.
Wyman, D.A., Kerrich, R., 1993. Archean Shoshonitic Lamprophyres of the Abitibi Subprovince, Canada: Petrogenesis, Age, and Tectonic setting. J. Petrol. 34, 1067–1109.
Wyman, D.A., Ayer, J.A., Conceição, R.V., Sage, R.P., 2006. Mantle processes in an Archean orogen: evidence from 2.67 Ga diamond-bearing lamprophyres and xenoliths. Lithos 89, 300–328. https://doi.org/10.1016/j.lithos.2005.12.005.
Wyman, D.A., O'neill, C., Ayer, J.A., 2008. Evidence for Modern-Style Subduction to 3.1 Ga: A Plateau-Adakite-Gold (Diamond) Association. In: Condie, K.C., Pease, V. (Eds.), When Did Plate Tectonics Begin on Planet Earth? Geological Society of America, pp. 129–148.
Wyman, D.A., Hollings, P., Conceição, R.V., 2015. Geochemistry and radiogenic isotope characteristics of xenoliths in Archean diamondiferous lamprophyres: Implications for the Superior Province cratonic keel. Lithos 233, 111–130. https://doi.org/10.1016/j.lithos.2015.02.018.
Xu, X.-W., Zhang, B.-L., Qin, K.-Z., Mao, Q., Cai, X.-P., 2007. Origin of lamprophyres by the mixing of basic and alkaline melts in magma chamber in Beiya area, western Yunnan, China. Lithos 99, 339–362. https://doi.org/10.1016/j.lithos.2007.06.011.
Yagi, K., Ishikawa, H., Kojima, M., 1975. Petrology of a lamprophyre sheet in Tanegashima Island, Kagoshima prefecture, Japan. J. Japan. Assoc. Mineral. Petrol. Econ. Geol. 70, 213–224.
Yaxley, G.M., Crawford, A.J., Green, D.H., 1991. Evidence for carbonatite metasomatism in spinel peridotite xenoliths from western Victoria, Australia. Earth Planet. Sci. Lett. 107, 305–317.
Yaxley, G.M., Ghosh, S., Kiseeva, E.S., Mallik, A., Spandler, C., Thomson, A.R., Walter, M. J., 2019. CO2-Rich Melts in Earth. In: Deep Carbon: Past to Present. Cambridge University Press, pp. 129–162. https://doi.org/10.1017/9781108677950.006.
Zheng, Y.-F., 2019. Subduction zone geochemistry. Geosci. Front. 10, 1223–1254. https://doi.org/10.1016/j.gsf.2019.02.003.
Zindler, A., Hart, S., 1986. Chemical geodynamics. Annu. Rev. Earth Planet. Sci. 14, 493–571. https://doi.org/10.1146/annurev.ea.14.050186.002425.